Development of Electrochemical Sensors for the Detection of Different Dyes Used as Artificial Food Colorants

Thesis Submitted By

Samhita Dasgupta

Doctor of Philosophy (Engineering)

Department of Instrumentation and Electronics Engineering

Faculty Council of Engineering and Technology

Jadavpur University

Kolkata- 700032, India

2024

JADAVPUR UNIVERSITY

KOLKATA- 700032, INDIA

INDEX NO.-184/19/E

Title of the Thesis

Development of Electrochemical Sensors for the Detection of Different Dyes Used as Artificial Food Colorants

Name, Designation & Institution of the Supervisors

Prof. Bipan Tudu

Professor

Department of Instrumentation and Electronics Engineering

Jadavpur University, Salt Lake Campus, Sector III, Block LB,

Plot 8, Kolkata 700106, India

Publications

Paper published in International Journals

1. Samhita Dasgupta, Shreya Nag, Runu Banerjee Roy, Rajib Bandyopadhyay, Panchanan Pramanik, Deepak Kumar Das, Bipan Tudu, "Development and detailed performance study of a carbon paste electrode for the electrochemical detection of malachite green," ***Nano LIFE,*** vol. 13, no.2, 2350006, pp. 1-9 , 2023. [DOI: 10.1142/S179398442350006X].

2. Samhita Dasgupta, Shreya Nag, Debangana Das, Runu Banerjee Roy, Deepak kumar Das, Panchanan Pramanik, Rajib Bandyopadhyay, Bipan Tudu, "Electrochemical sensor based on CuO nanoparticles modified graphite electrode for the detection of malachite green," ***Nano LIFE,*** vol. 14, no.1, 2350015, pp. 1-12, 2024. [DOI: https://doi.org/10.1142/S1793984423500150].

3. Samhita Dasgupta, A.H.M. Toufique Ahmed, Ipshita Bhattacharjee, Shreya Firdoushi, Don Biswas, Sumani Mukherjee, Rajib Bandyopadhyay, Bipan Tudu, "Crafting a graphite electrode with embedded Y_2O_3 nanoparticles for the electrochemical detection of amaranth in candies," ***IEEE Sensors Journal,*** vol. 24, no.13, pp. 20750-20757, 2024. [DOI: 10.1109/JSEN.2024.3400317].

4. Samhita Dasgupta, A.H.M. Toufique Ahmed, Ipshita Bhattacharjee, Shreya Firdoushi, Don Biswas, Sumani Mukherjee, Bidya Mondal, Rajib Bandyopadhyay, Bipan Tudu, "Electrochemical detection of indigo carmine in candies using Y_2O_3 nanoparticles infused graphite electrode," ***Journal of Food Composition and Analysis***, vol. 135, 106626, pp. 1-9, 2024. [DOI: https://doi.org/10.1016/j.jfca.2024.106626]

Paper published in International Conferences

1. Samhita Dasgupta, Shreya Nag, Runu Banerjee Roy, Rajib Bandyopadhyay, Bipan Tudu, "Malachite green detection using carbon paste electrode based on voltammetry,"***2nd IEEE International Conference on Emerging Frontiers in Electrical and Electronic Technologies (ICEFEET – 2022),*** NIT Patna, 24-25 June, 2022.

2. Samhita Dasgupta, Shreya Nag, Runu Banerjee Roy, Rajib Bandyopadhyay, Panchanan Pramanik, Deepak Kumar Das, Bipan Tudu, "Development and detailed performance study of a carbon paste electrode for the electrochemical detection of malachite green,"***2nd International conference on Nano-architectures for Chemical, Biological and Therapeutic Applications (NCBTA-2022),*** GLA University, Mathura, UP, 25-27 November, 2022.

3. Samhita Dasgupta, Ipshita Bhattacharjee, Rajib Bandyopadhyay, Bipan Tudu, "A voltammetric study for amaranth detection using carbon paste electrode," ***2024 IEEE 3rd International Conference on Control, Instrumentation, Energy & Communication (CIEC),*** Department of Applied Physics, University of Calcutta, India, January 25-27, 2024.

Journal Publications other than thesis

1. Swatilekha Roy, Shreya Nag, Mahuya Bhattacharyya Banerjee, Samhita Dasgupta, Panchanan Pramanik, and Rajib Bandyopadhyay. "Detection of geraniol in palmarosa essential oil using silicone sealant as molecularly imprinted polymer in a QCM sensor." ***Journal of Materials Nano Science,*** vol. 9, no. 2, pp. 120-124, 2022

2. Deepam Gangopadhyay, Shreya Nag, Samhita Dasgupta, Mahuya Bhattacharyya Banerjee, Bipan Tudu, Dipak Das, Panchanan Pramanik, Rajib Bandyopadhyay, Runu Banerjee Roy, "A simple and efficient formaldehyde detection technique using poly ethylene glycol modified quartz crystal microbalance sensor," ***Nano LIFE***, vol. 13, no.2,2350005,pp. 1-9 , 2023. [DOI: 10.1142/S1793984423500058].

3. Ipshita Bhattacharjee, Samhita Dasgupta, Shreya Firdoushi, Rajib Bandyopadhyay, Deepak Kumar Das, Bipan Tudu, "Electrochemical detection of nicotine in green tea using carbon paste electrode," ***Innovation and Emerging Technologies***, vol. 11, 2450004, pp. 1-6, 2024. [https://doi.org/10.1142/S273759942450004X].

4. Sumani Mukherjee, Samhita Dasgupta, Hemanta Naskar, Shreya Firdoushi, Ipshita Bhattacharya, A.H.M. Toufique Ahmed, Deepak Kumar Das, Rajib Bandyopadhyay, Bipan Tudu, "Development of an easy and economical carbon paste electrode for fisetin detection," ***Innovation and Emerging Technologies***, vol. 11, 2450005, pp. 1-7, 2024. [https://doi.org/10.1142/S2737599424500051].

5. Ipshita Bhattacharjee, Samhita Dasgupta, Shreya Firdoushi, Don Biswas, AHM Toufique Ahmed, Sumani Mukherjee, Rajib Bandyopadhyay, Bipan Tudu. "A Simple Nano $NiMn_2O_4$ Functionalized Graphite Electrode for Electrochemical Detection of Cinnamic Acid in Cinnamon Bark." ***IEEE Sensors Journal,*** vol. xx, no. xx, pp. xx-xx, Month xx, 20xx. [DOI: 10.1109/JSEN.2024.3477255]. **[Article in Press].**

Statement of Originality

I, Samhita Dasgupta, registered on 26th June, 2019 do hereby declare that this thesis entitled "Development of Electrochemical Sensors for the Detection of Different Dyes Used as Artificial Food Colorants" contains literature survey and original research work done by the undersigned candidate as part of her Doctoral studies.

All information in this thesis have been obtained and presented according to the existing academic rules and ethical conduct. I declare that, as per the requirements of these rules and conduct, I have fully cited and referred all materials and results that are not original to this work.

I also declare that I have checked this thesis as per the "Policy on Anti Plagiarism, Jadavpur University, 2019", and the level of similarity as checked by iThenticate software is 9%.

Samhita Dasgupta.
22/05/2024

Samhita Dasgupta
Index No.184/19/E
Date: 22nd May, 2024

Bipan Tudu
22/05/2024

Prof. Bipan Tudu
Professor
Dept. of Instrumentation and Electronics Engineering
Jadavpur University, Salt Lake Campus, Kolkata-700106. India

Certificate from the Supervisor

Date: 22/05/2024

This to certify that the thesis entitled "Development of Electrochemical Sensors for the Detection of Different Dyes Used as Artificial Food Colorants," submitted by Samhita Dasgupta, who enrolled on 26th June 2019 for the Ph.D. (Engineering)degree of Jadavpur University, is absolutely based upon her own work under the supervision of Prof. Bipan Tudu, and that neither her thesis nor any part of the thesis has been submitted for any degree/diploma or any other academic award anywhere before.

Bipan Tudu
22/05/2024

Prof. Bipan Tudu

Professor
Dept. of Instrumentation and Electronics Engineering
Jadavpur University, Salt Lake Campus, Kolkata-700106. India

Dedicated

To my parents

Dr. Sumita Sinha and Dr. Subhas Dasgupta

and my husband

Dr. Shohan Banerjee

Acknowledgement

The joy that accompanies the successful completion of any task is incomplete without acknowledging the individuals instrumental in making it possible. Their unwavering guidance, invaluable suggestions, and ceaseless encouragement are the foundation on which every successful endeavour rests. PhD itself is an adventurous journey. In accordance with established conventions, I hereby extend my heartfelt gratitude to those persons who have played a crucial role in making my journey a success.

I would like to express my deepest sense of indebtedness to Prof. Bipan Tudu, my supervisor at Jadavpur University's Department of Instrumentation and Electronics Engineering, for his continuous guidance in achieving the objective of the thesis. I am deeply grateful to Prof. Rajib Bandyopadhyay for his unwavering support and valuable suggestions throughout the research program, and I will need his blessings for my future goal.

I am thankful to the Head of the Department of the Instrumentation and Electronics Engineering Department, Jadavpur University, for his support and providing all the facilities during this journey.

I owe a great deal to Prof. Panchanan Pramanik, Retired Professor, Department of Chemistry, IIT Kharagpur, for his effective advice during the vital stages of the thesis work.

I am indebted to Prof. Manoj Kumar Ghosh, Retired Professor, IIT Kharagpur, for his continuous encouragement and guidance since my Post Graduation days. During my PhD journey, a visit to him was enough to boost up my energy level whenever needed.

I want to express my thanks to my lab mates namely Miss Shreya Nag, Mr. Nilava Debabhuti, Mr. Hemanta Naskar, Mr. A.H.M. Toufique Ahmed, Miss Shreya Firdoushi, Miss Ipshita Bhattacharjee, Mrs. Madhurima Moulick, all faculty, technical and non-technical staff in the Department of the Instrumentation and Electronics Engineering at Jadavpur University.

Finally, I would like to take this opportunity to dedicate this thesis work to all members of my loving family. I would like to express immense gratitude to my father Dr. Subhas Dasgupta and mother Dr. Sumita Sinha who inculcated within me the urge of doing higher research since my

Graduation days and used to stand by me in the thick and thin of life. I am grateful to my husband, Dr. Shohan Banerjee for his continuous support and guidance throughout this journey. I am also thankful to my in-laws for being the most supportive ones I think I could ever have.

Most importantly, I am indebted to Rabindranath Tagore and the ocean of Bengali Literature for providing me the positive attitude whenever I needed during this journey. A word of thank is also due to Life itself, my India, and the Mother Earth without whom I could never be here to write this acknowledgement.

Samhita Dasgupta.
22/05/2024.

Samhita Dasgupta

Department of Instrumentation and Electronics Engineering

Jadavpur University, Salt Lake Campus

Sector –III, Block –LB, Kolkata –700 106

22nd May, 2024

Abstract

Food colorants play a crucial role in enhancing the visual appeal of food products, making them more attractive to consumers. These substances can be both natural or artificially synthesized, used to enhance the visual appeal and acceptability of food products. There are different types of natural colors originating from fruits, vegetables, and other botanic sources. Beet juice is one creating a red color, while turmeric is used to get yellow color. Carmine is another natural color derived from the cochineal insect generally used for creating red and pink hues. These natural food colors are comparatively less stable, being easily destroyed during the different stages of food processing and storage. On the flip side, synthetic colorants, created chemically, offer numerous advantages over the natural ones like sufficient stability to the exposure of light, oxygen and pH, maintaining color uniformity, water solubility, low pathogenic contamination and low cost. Artificial food colors are randomly applied in different processed and packaged foods, beverages, candies, cosmetics, medicines, and other products to achieve alluring and consistent coloration. However, consumption of too much of these artificial food colors via food products can adversely affect human physical conditions resulting in different diseases. The joint Food and agriculture organization of the United Nations (FAO) and the World health organization (WHO) expert committee on food additives (JECFA) have already set limits on the daily maximum intake of these food colors by human bodies. Some food colors even have been banned. But these food colors are used still in India in an unauthorized way beyond the allowed limit in a number of commercial foods. Hence, monitoring the level of the daily dose of these colorants in foods is compulsory, emphasizing the necessity for a speedy and smooth method of detecting the artificial food colorants in distinct samples. This thesis work was taken up for rapid detection of some artificial food colorants present in the Indian food products. In this thesis, the synthesis of different electrodes using the principle of nanoparticles-based modification of Carbon paste electrode (CPE) is presented elucidating the selective determination of green colored dye Malachite green (MG), dark red colored dye Amaranth (AMR), and blue colored dye Indigo carmine (ICN), respectively. The molecule size, and the morphological changes of the modified electrodes are characterized with the help of methods like Fourier transform infrared (FTIR) spectroscopy, Scanning electron microscopy (SEM), X-ray diffraction (XRD), X-ray photoelectron spectroscopy (XPS), and Energy dispersive spectroscopy (EDX).

First, a basic CPE has been developed and studied for the voltametric detection of MG. Then, this CPE is modified via copper oxide (CuO) nanoparticles (NPs). A Limit of detection (LOD) of 0.18 μM and a wide linear range of 1-1000μM are obtained. This modified electrode was studied thoroughly for detecting MG, in some food samples. Secondly, a basic CPE and then its modification with yttrium oxide (Y_2O_3) NPs are applied to detect AMR with a LOD of 3.6nM and a wide linear range of 0.05-100μM. This modified electrode is used in some candies consumed by the children mainly. Next, the voltametric detection of ICN also is done in candies using CPE and Y_2O_3 nanoparticles modified CPE. A linear range of 5-300μM and a LOD of 0.11 μM is achieved here. In each of these three cases, the selection of optimum modifier, selection of the ideal concentration of modifier, variation of buffer, pH, scan rates, and concentrations are discussed. Different analytical parameters like repeatability, reproducibility, selectivity, and stability are studied.

Contents

List of Figures

List of Tables

List of Abbreviations

ABS	Acetate buffered saline
ADHD	Attention-deficit/hyperactivity disorder
Ag/AgCl	Silver/ Silver chloride
Ag/Ag_2SO4	Silver/ Silver sulfate
AMR	Amaranth
BB	Brilliant blue
CA	Control amplifier
CB	Citrate buffered saline
CCBPE	conductive carbon black paste electrode
CE	Capillary electrophoresis
CE	Counter electrode
C.F.	Correlation factor
CF	Current follower
CNTs	Carbon nanotubes
CPE	Carbon paste electrode
CSV	Cathodic stripping voltammetry
CuO NPs	Copper oxide nanoparticles
CV	Cyclic voltammetry
CVD	Chemical vapour deposition
DPV	Differential pulse voltammetry
EDX	Energy dispersive spectroscopy
ELISA	Enzyme-linked immunosorbent assay
FTIR	Fourier transform infrared spectroscopy
GCE	Glassy carbon electrode
GO	Graphene oxide
GPE	Graphite paste electrode
HPLC	High performance liquid chromatography
ICN	Indigo carmine
JECFA	Joint FAO and WHO expert committee on food additives
LOD	Limit of detection
LOOCV	Leave one out cross validation
LOQ	Limit of quantification
LSV	Linear sweep voltammetry

LV	Latent variable
MIP	Molecularly imprinted polymer
MG	Malachite green
NPV	Normal pulse voltammetry
PBS	Phosphate buffered saline
PC	Principal component
PCA	Principal component analysis
PLSR	Partial least square regression
PTH	Phthalate buffer
PV	Pulse voltammetry
RE	Reference electrode
RMSEP	Root mean square error of prediction
RSD	Relative standard deviation
SEM	Scanning electron microscope
SI	Separability index
SWV	Square wave voltammetry
WE	Working electrode
XPS	X-ray photoelectron spectroscopy
XRD	X-ray diffraction

Chapter 1

Introduction and Scope of the Thesis

This chapter elucidates the objectives and illustrates the aims of this thesis endeavour. There are brief descriptions of various electrochemical methods. Different nanoparticles, their formation, incorporation to develop electrode, and required characterization methods are briefed for narrating the performance enhancement of carbon paste electrodes (CPEs) through nanoparticle modification. Some advantages and challenges related to these methods are included thereafter. Literature survey regarding the usage of nanoparticles modification for carbon electrode-based detection technique for various molecules has been done thoroughly. This has been followed by the objective and scope of the thesis, where the organization of chapters are briefed.

List of Sections

1.1. Introduction

The role of food color in different foods is not only mere aesthetics because it makes a food product more sellable by influencing the human perception and expectations. Vivid food hues intensify the aesthetic allure of dishes, while some specific colors may have links with distinct flavours or brands, being helpful in product identification. Beverage colors often correlate with their flavours. As for examples, orange juice is typically supposed to possess an orange color, while cola is anticipated to be deep brown colored. Consistency in color helps meet these expectations. There is use of different natural and artificial food colors. Natural colorants obtained from different plants and microbes were initially utilized to color the food products, but they were eventually supplanted by synthetic alternatives. Natural colorants are of two types like organic (derived from living sources like fruits, flowers, etc.) and inorganic (gold, silver). Synthetic food colorants are generally processed from coal tar compounds; most of them containing dyes from the azo group. Moreover, natural identical man-made colors like riboflavin are also available [1]. Though natural food colors are generally perceived as a healthier and more customer-friendly option, they do have some disadvantages as well. The natural colors are costly, not long lasting, and unstable in face of heat, light and pH change. Here comes the synthetic counterpart providing more stability in all senses. Synthetic food colors hold stability to light, oxygen, and pH; shows consistent color uniformity, nice water solubility, and low susceptibility to microbiological contamination. Considering all these phenomenon, use of different artificial food dies are now trending in Indian market places. Amaranth (AMR), Indigo carmine (ICN), Malachite green (MG), Erythrosine, Ponceau 4R, Allura red, Sunset yellow, Tartrazine, Brilliant blue, Azorubine are some important artificial food dies used now-a-days.

However, too much intake of these artificial colors through food causes adverse effect on human body. The extensive application of both authorized and unauthorized food colorants, along with their associated toxicities and potential adulterations, poses global concerns of varying severity across different countries. Diseases like irritations, diarrhoea, vomiting, tumours, permanent injury to cornea and conjunctiva, may take place if these synthetic food dies are consumed unlimitedly. Arnold et al. [2] demonstrated that artificial colorants considerably affect growing children, resulting in symptoms such as irritability, sleep disturbances, reduced attention span, impulsivity, and hyperactivity, commonly associated with Attention-deficit/hyperactivity disorder (ADHD). Application of combinations of Erythrosine, Ponceau 4R, Allura Red, Sunset Yellow, Tartrazine, Amaranth, Brilliant Blue, Azorubine, and

Indigotine on female rats and their offspring has been found to induce a decline in spatial working memory and gender-specific anti-depressive and anxiolytic behaviours [3]. Furthermore, there are recorded instances of synergistic effects between colorants and an increased prevalence of asthma and allergies [4]. Red 40, Yellow 5, and Yellow 6 are reported to be carcinogenic [5]. Concerns regarding genotoxicity following the ingestion of colorants such as titanium dioxide, erythrosine, and brilliant black warrant validation through in vivo studies [6] . Additionally, a number of organic dyes are recognized as micropollutants in aquatic environments because of their toxic impact on aquatic organisms and subsequent consumers within the food chain [7]. Numerous synthetic food colorants banned in the developed nations are still being used as food ingredients in India, such as the toxic azo dyes [8], characterized by one or more azo groups (–N=N–) in their chemical compositions. Tartrazine, a widely utilized azo dye, is documented to have adverse effects on liver function, renal function, lipid profiles, and behaviour [9]. Similarly, in vitro studies on sunset yellow in rodents resulted in the reduction of testicle size and altered lipid profiles. Moreover, indigo carmine is reported to demonstrate atrioventricular blocking capabilities [10]. A comprehensive analytical study was conducted to examine the utilization of synthetic food colorants in India and it was found that that samples of candyfloss, sugar toys, beverages, mouth fresheners, ice candy, and bakery products exceeded permissible limits of colorants. Besides, the widespread practice of blending colorants with non-permitted hues, such as azo dyes like sunset yellow and tartrazine, in large quantities was observed [11]. Similarly, elevated levels of these synthetic food colorants were detected in samples of colored crushed ice, surpassing permitted levels by 8–20%. Moreover, a variety of food products were found to contain non-permitted colorants such as rhodamine B, metanil yellow, orange II, malachite green, auramine, quinoline yellow, amaranth, and Sudan dyes [12]. The Joint Food and agriculture organization of the United Nations (FAO) and the World health organization (WHO) expert committee on food additives (JECFA) have already fixed the highest point of the admissible daily dose limit of these colors' intake. Some dies have been declared banned also [13]. Disappointingly, in many parts of India, sellers and vendors are using these artificial colors still now in an unauthorized way beyond the allowed limit in a number of commercial foods. Naturally, monitoring the level of the daily dose of these dies in foods is compulsory, emphasizing the necessity for a speedy and smooth method of detecting it in distinct samples. In this context, some conventional approaches are there like high performance liquid chromatography (HPLC) [14], [15], spectrophotometry [16], [17], and capillary electrophoresis [18]. These methods, though being highly accurate, are full of some serious shortcomings also, like long sample preparation time, need of skilled operators,

complex circuitries, etc [13]. In this manner, such strategies are not so easy to manage for regular and extensive use for the detection of artificial food colorants in foods.

The present thesis titled "Development of Electrochemical Sensors for the Detection of Different Dyes Used as Artificial Food Colorants" describes the development of some electrodes, specific for an individual synthetic food color. Among various artificial food colorants, three colors namely malachite green (MG), Amaranth (AMR), and indigo carmine (ICN) have been selected whose detection schemes are studied in this thesis. Some reasons for selecting these three dies among all other artificial food colorants are narrated below:

1. **Toxicity Concerns:** Being potentially harmful, MG has been banned for use in food products in many countries because of its carcinogenicity. Studying its presence in food items could provide insights into potential health risks associated with its intake.
2. **Regulatory Compliance:** Studying the presence and levels of AMR and ICN in different food items can help ensure regulatory compliance and monitor adherence to allowed usage limits.
3. **Consumer Safety:** Understanding the prevalence of these colorants in food products is essential for ensuring consumer safety. Identifying any instances of unauthorized dies or excessive use of these artificial food dies can help mitigate potential health risks for consumers.
4. **Comparative Analysis:** The selection of these three colorants may allow for a comparative analysis of their presence and levels in different food products, potentially revealing patterns or trends in their usage across various food categories.

Malachite green (MG) was considered first for this study. MG, found under the N-methylated diamino triphenylmethane group, is a noted water-soluble, synthetic, and commercial dye [19]. With the physical appearance of green-colored crystalline dust, MG is enormously used in the dyeing sectors of silk, leather, paper, cotton, wool, jute, and nylon, as well as in the coloration of cells. Since the time of 1930s, MG has found massive use in the global agroindustry and the food trade because of its reasonable cost and suitability for the sterilisation goal. Having antifungal, antiparasitic and anti-microbial characteristics, MG is effective in killing different parasites and mould identified on fish eggs along with skin flukes and gill flukes. Moreover, it plays a role also as a food staining agent, preservative, and antiseptic. Some vendors use synthetic colors like MG, and wax coating to make fruits and vegetables look shinier and greener. It's frequently used to give chillies, cucumbers, peas, ladyfinger, and spinach a vivid

green color. However, MG is found questionable because of the consequences it leaves. Since 1990, this azo dye has been established as toxic, carcinogenic, and mutagenic. MG is converted into leuco malachite green (LMG) through rapid metabolization. LMG, with similar types of degeneration pathways and longer half-life, is fat-soluble and more threatening to the animal kingdom. Consumption of these two virulent chemicals through the food chain causes human cancer, gene mutation as well as many other diseases like heinz body formation, jaundice, tetraplegia, abnormal heart rate, dizziness, tissue necrosis, and cyanosis. The receiving stream polluted with MG causes toxic effects in the liver, gill, kidney, intestine and gonads. Skin contacts with MG results in irritation, redness, and pain, while eye contact damages the eyes in humans and animals. The hepatic tumour is developed in rodents, and the reproductive systems of fish and rabbits face deformities due to MG contamination. Apart from all these health effects, even a very minor concentration of MG in the aqueous environment can color large water bodies and prevent light penetration which in turn decreases photosynthesis and inhibit the growth of aquatic flora and fauna. Based on the possibility of a negative effect on public health, MG was nominated by the U.S. Food and Drug Administration as a priority chemical for carcinogenicity testing by the National Toxicology Program in 1993. National Center for Toxicological Research, Jefferson, Ark, is currently performing these studies [20]. MG has already been banned [21], [22] in developed countries like China, the United States of America, Canada, and Europe. E.U. Act 2002/675/E.C. has prescribed the most acceptable amount of MG and LMG slag in foods to 2 µg/kg [23]. Unfortunately, illegal usage of MG is still found in some places. Besides being easy on the pocketbook, MG is the only definite drug reported [24] to combat the saprolegniaceae disease of fish and its eggs. This is also a reason for its illegal use in India even after being prohibited.

The next molecule selected for study was Amaranth (AMR). Amaranth (E-123) is a synthetic anionic azo dye. Being reddish or brownish in color, the term Amaranth originates from the amaranth plant which is reddish in color and high in eatable protein [25]. AMR is extensively used as a food color in different soft drinks as well as foodstuffs like ice creams, coffee, wines, salad toppings, and syrups [26], [27], [28] providing spellbinding red color. It finds its application in fields of artificial dyeing, medicines, paper, cosmetics, and wood also [29]. However, consumption of too much AMR via food products can adversely affect human physical conditions resulting in diseases like tumours, dizziness, nausea, allergies, asthma, hypersensitivity, liver and renal dysfunction [30]. This dye plays a threatening role in patients consuming aspirin and benzoic acid as part of their treatment. The admissible daily dose limit

of AMR intake is set to 0–1.5 mg/kg by the Joint FAO and WHO Expert Committee on Food Additives (JECFA) [31]. Disappointingly, AMR is used even now in an unauthorized way beyond the allowed limit in a number of commercial foods. Naturally, monitoring the level of the daily dose of AMR in foods is compulsory.

Finally, the third molecule considered was indigo carmine (ICN). ICN is a blue artificial food dye, widely known as a coloring object in beverages, foods, cosmetics industries and in the dyeing of denim and polyester fibres [32], [33]. ICN is used also in pharmacies and medicines for diagnosis purpose [34], [35]. It has been found from different reports that ICN is a severely toxic chemical. Unlimited consumption of ICN results in different health disasters in mass like irritations, diarrhoea, vomiting, tumours [36], [37], and permanent injury to eyes by affecting cornea and conjunctiva. ICN makes the condition of the genetically damaged cells worse, affects liver and then central nervous system, and proves to be mutagenic. Naturally, monitoring and controlling the quantity of ICN in various foodstuffs, biological samples, and natural environment is necessary. Maximum daily intake limit of ICN has been set to 5 mg/Kg of body mass [34]. Therefore, it is very much required to develop a sensitive and selective determination system for ICN.

The synthesis of electrodes for these three molecules is described in this thesis, utilising the method of modification of basic carbon paste electrode (CPE) by incorporating different nanoparticles. The associated nano molecule size, and morphological modifications were studied using a Fourier transform infrared (FTIR) spectroscope, a scanning electron microscope (SEM), x-ray diffraction (XRD), x-ray photoelectron spectroscopy (XPS), and energy dispersive spectroscopy (EDX), respectively. In this thesis, the analytical abilities of these electrodes have been scrutinised intensively. Fish fillets, pond water samples, and various candies have been analysed using voltammetry for precise data evaluation.

The upcoming section of this chapter in the thesis is structured as follows:
The electrochemical principles of sensing are briefly outlined, focusing on voltammetric techniques. The modification of CPE with various nanoparticles is covered. A comprehensive literature review is presented, followed by a synopsis of the objectives and scope of the thesis.

1.2. Electrochemical methods in brief

Electrochemical transduction mechanisms are fundamental in quantifying both volatile and non-volatile compounds by leveraging electrochemistry principles. These mechanisms involve redox reactions that enable the detection of current associated with the target species and the potential difference across electrodes. This process facilitates the quantitative analysis of samples by providing crucial information about the sample composition. The widespread adoption of electrochemical techniques is attributed to their cost-effectiveness, stability, high sensitivity, ease of sample retrieval, and minimal interference [38], [39] from external factors.

1.2.1. Different electrochemical techniques

There may remain numerous regulatory factors behind an electrochemical reaction. Some of them are potential, current, charge and time. Depending upon the excitation signal as well as the achieved response, the electrochemical techniques can be categorised into different types mentioned below.

a) Coulometry

This electroanalytical method works on the principle of quantifying the amount of electricity (coulombs) required for a substance to undergo a change in the oxidation state. The fundamental principle used here is Faraday's first law of electrolysis [40]. The weight of the produced or consumed substance (w) because of electrolysis can be calculated using the equation (1.1), considering the charge transfer of Q coulombs, the liberated or consumed material of M molecular mass, and the reacting electron number of n.

$$w = \frac{MQ}{96487n} \tag{1.1}$$

There are generally two techniques: potentiostatic (controlled potential) coulometry and amperostatic (controlled current) coulometry. In the first one, the electrode has a constant working potential. This allows the analyte to be oxidised or reduced without the interference of less reactive species in the sample or solvent. In case of the later, the respective signal is recorded in terms of current during the reaction. Furthermore, the quantity of output charge can be determined based on the magnitude and the duration of flow of the current.

b) Potentiometry

In potentiometry, the potential of an electrochemical cell without drawing a significant amount of current is the main point of attention. This is a two-electrode system with an indicator electrode (measuring electrode) and a reference electrode. The measuring electrode is dipped into the target solution and the potential signal is obtained with respect to a fixed reference electrode. Potentiometry can be further subdivided into direct potentiometry and potentiometric titrations. In the former, the cell potential is determined and correlated with the concentration of the active chemical species whereas the cell potential is used to determine the volume of reagent in case of the later [40].

c) Amperometry

In amperometry[40], the cell current is measured keeping the working electrode potential constant. The current varies in direct proportion with the target analyte concentration. This technique is useful to detect reactions over time or to detect endpoint in titrations.

d) Conductometry

Conductometry [40] is used to gauge the electrical conductivity of a solution. It assesses a solution's capacity for electricity conduction, correlating with the overall concentration of ions within the solution. Conductometry, despite being not as precise as other electrochemical techniques, serves as a valuable tool for tracking reactions leading to alterations in ionic concentration.

e) Voltammetry

The predominant electrochemical techniques primarily revolve around the principle of voltammetry, assessing the current across the electrode within a varying potential range [40], [41]. This method involves adjusting the potential within a specified range ensuring the presence of electroactive chemical species at the surface of the working electrode. Quantitative data then is acquired in terms of the peak current at the working electrode's surface. Figure 1.1. illustrates a three-electrode cell setup [42], [43], including a reference electrode (RE), a counter or auxiliary electrode (CE), and a working or measuring electrode (WE). Reference electrodes may be of different types like saturated calomel reference electrode (SCE), Ag/AgCl electrode, Ag/Ag_2SO_4 electrode etc. Depending upon aqueous or non-aqueous electrolyte solution or application in different temperature, the proper reference electrode is selected. There are

various types of counter electrodes as well. Platinum electrode, gold electrode, stainless steel electrodes are some of them.

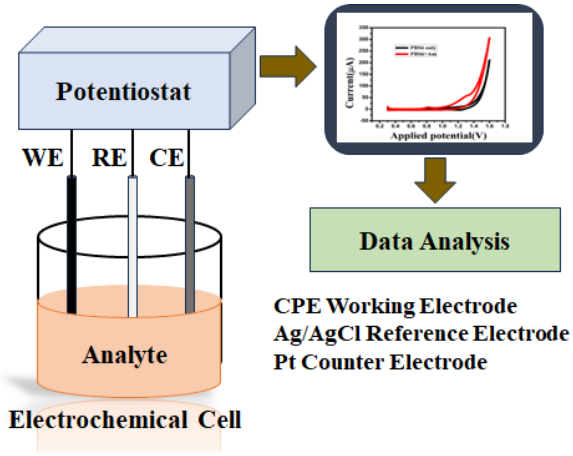

Fig. 1.1. Voltammetric arrangements for three electrode setups.

Unlike in potentiometry, where the reference electrode is not typically utilized, in voltammetry, the reference electrode is necessary to maintain a reference potential against the working electrode, facilitated by a power source or potentiostat. The potentiostat functions akin to a controlled voltage source in an electrical system, monitoring and adjusting the voltage applied across the working electrode to induce redox reactions at the electrode interface, thereby generating current. This generated current flows between the counter electrode and the working electrode, offering quantitative insights into the electrochemical properties and reaction kinetics of the system.

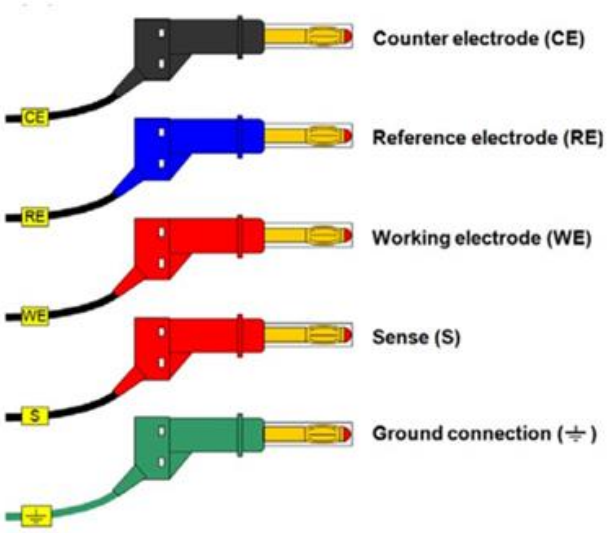

Fig. 1.2. The cell cables of the Autolab PGSTAT101 equipped with connections, each identified by its corresponding color code.

The possible configuration of these three electrodes is presented in Fig. 1.2., where the direction of current flow is between the CE and WE. The potential difference is controlled between the WE and CE and its measurement is done between the RE and sense (S) connections. It can be noted that the RE is placed very closely to the WE to prevent the solution resistance. With proper connection of WE with S, WE are kept at a fixed stable potential controlling the polarization of the CE. On the other hand, the developed potential between the RE and WE are time independent. The basic electrical circuitry of potentiostat [41] can be found in Fig. 1.3. Control amplifier (CA) block is connected to CE, hindering the current flow through the electrochemical cell. WE have connection with the current follower (Low CF) circuit. The corresponding value of the current can be measured using a low CF for low current and a shunt for high currents, respectively. A differential amplifier is used to measure the potential difference between RE and S. The resulting signal is fed to the summation point (Σ), where it combines with the waveform generated by the digital-to-analog converter (E_{in}), and then is utilized as an input to the CA. E_{out} is the output potential whereas I_{out} is the output current.

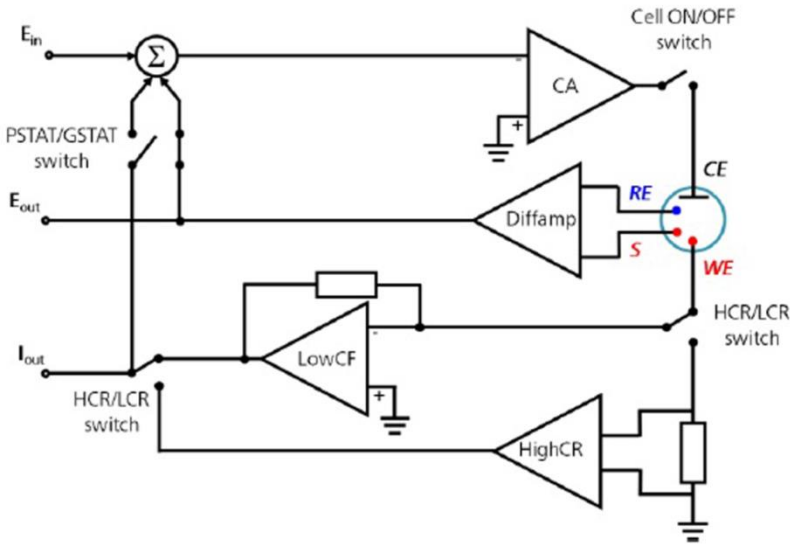

Fig. 1.3. Basic electrical circuit diagram of a potentiostat.

The traditional type of voltammetric measurements is found as follows:

i) Linear sweep voltammetry (LSV)

In this case, the current generated in an electrochemical cell is scanned with reference to the potential between the WE and RE which is varied linearly with time. Mainly the following characteristics are related to the LSV [40]:

- The rate of the ongoing electron transfer reactions
- The chemical reactivity of the electroactive species
- The voltage scan rate

The capacitive current surges with the escalation of the scan rate, beyond the scope of electrochemical compensation. Hence, it facilitates a lower detection threshold (mg/l) to be achieved.

ii) Square wave voltammetry (SWV)

In this case, symmetrical square wave pulses having an amplitude of E_{sw} are overlaid such that the forward pulse is in alignment with the staircase phase [40]. The study of disparity between the forward and reverse currents makes the resultant current to be gauged, and centred around the redox potential. The concentration of the electroactive species and the peak amplitude are in linear correlation, with a lower detection limit up to the order of 0.1 nM.

iii) Stripping voltammetry (SV)

SV technique [40]detects trace number of metals in a solution. The methodology follows the steps mentioned below:

•At first, certain potential is applied onto the electrode triggering the target metal ions to be deposited on its active surface. The solution is continuously stirred for maximizing the number of metal ions for deposition.

•Once the deposited ions are settled on the electrode surface, the stirring is stopped.

•Next, the deposited metal ions are stripped from the electrode by scanning the potential. This phase is known as the stripping state. The produced current is proportional to the amount of the metal present in the solution.

The stripping voltammetry is of two types based on the positive potential scan (anodic stripping voltammetry (ASV)) or negative potential scan of the stripping process (cathodic stripping voltammetry (CSV)).

iv) Cyclic voltammetry (CV)

Cyclic voltammetry (CV) is the most extensively applied potentiodynamic electrochemical measurement. Here the WE potential changes linearly with respect to time, and once the upper threshold voltage is reached, ramps in the opposite direction to reach its initial value again. In

Figure 1.4 (a) and (b), a typical cyclic voltammogram is illustrated, showing the anodic currents (I_{pa}) and cathodic currents (I_{pc}) associated to oxidation and reduction processes, respectively, at different time intervals. The triangular pulse indicates the initiation of the reaction as pictured in Fig. 1.4.

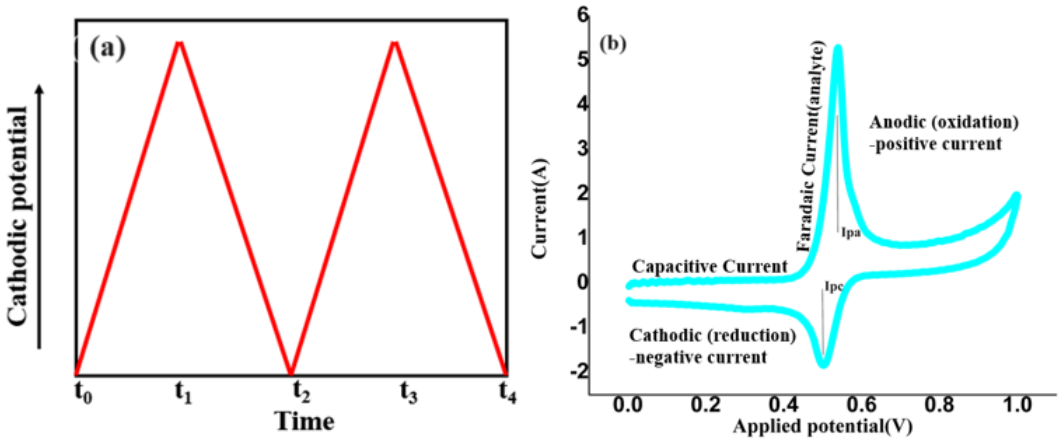

Fig. 1.4. (a) CV waveform; (b) Typical CV curve featuring various parameters for a reversible reaction.

The current increases with the increasing input potential in time of forward scan (t_0-t_1) and rapid oxidation takes place during this phase because of the presence of a significant number of reactants. Subsequently, once the voltage is applied again, the availability of these reactants becomes diffusion-limited, causing the current to reduce to a lower or sometimes constant level. On the reverse sweep (t_1 to t_2), the cathodic peak is observed with the reduction of the oxidized species. CV provides important information on electron transfer kinetics, mechanisms, and other electrochemical characteristics.

v) Pulse voltammetry (PV)

Pulse voltammetry relies on a potential pulse to discern differences in the decay rates of charging and Faradaic currents. Charging current diminishes exponentially or according to a function of $\frac{1}{\sqrt{time}}$. Faradaic current declines at a notably slower pace. This technique enables the detection of analytes at very low concentrations around 10^{-8} M. Classification of pulse voltammetry is based on the applied potential waveform and its corresponding current profile, as narrated below.

- ***Normal pulse voltammetry (NPV)***

In this setup, at the conclusion of each pulse, a train of steadily rising potential pulses initiates the output current providing an interval for the charging current to decay. The pulse duration

(t), in response to the potential (E_i), lasts for around 1 to 100 milliseconds, with corresponding intervals ranging from 0.1-5 seconds. The voltammogram illustrates a stepped pulse along the horizontal axis, while the sampled current is depicted on the vertical axis.

- ***Differential pulse voltammetry (DPV)***

A conventional DPV technique is shown in Fig. 1.5. [44]. DPV technique is to some extent similar to the NPV method mentioned earlier, except the shape of the applied potential with an amplitude rising in an incremental manner. The application of successive pulses is accompanied by maintaining a baseline potential for a fixed duration until the next pulse is applied. Sequential current readings are sampled both before and at the finishing of each pulse. The discrepancy between these two sampled current values is then recorded for quantitative analysis of the aimed analyte. As a result, DPV emerges as the most sensitive technique, offering a lower limit of detection compared to other types of pulse voltammetry.

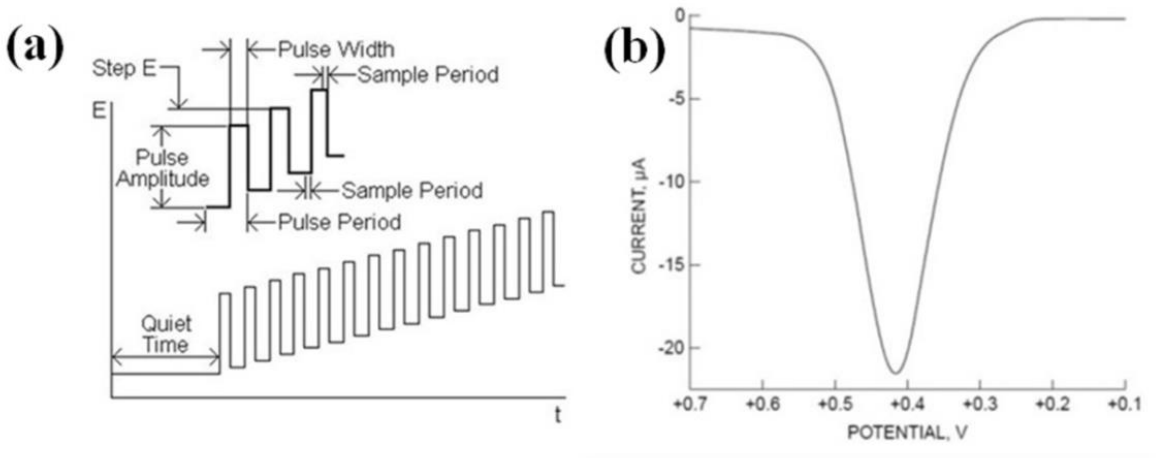

Fig. 1.5. (a) Excitation potential waveform for DPV; (b) A typical DPV curve.

1.3. Nanoparticles based modification of CPE

The enhancement of carbon paste electrodes (CPEs) through nanoparticle modification is a vastly researched domain in electrochemical studies. It provides superior characteristics and heightened functionality for diverse sensing and analytical uses. Nanoparticles are ingrained into the carbon paste structure boosting its conductivity, expanding its surface area, as well as delivering a catalytic capability. A comprehensive summary of the modification of carbon paste electrodes using nanoparticles is presented below:

1.3.1. Types of nanoparticles

a) ***Metal nanoparticles:*** Gold (Au), silver (Ag), platinum (Pt), and others, which are able to impart catalytic activity and improve the kinetics of electron transfer.

b) ***Carbon-based nanomaterials:*** Graphene, carbon nanotubes (CNTs), and carbon nanofibers. These are applicable for enhancing the electrical conductivity providing an increased surface area.

c) ***Metal oxide nanoparticles:*** Titanium dioxide (TiO_2), iron oxide (Fe_2O_3), or other metal oxides, which contribute to specific catalytic activities.

1.3.2. Preparation of modified CPEs

The preparation of nanoparticles embedded CPEs includes several steps mentioned below:

a) Material preparation

i. ***Nanoparticles:*** There are numerous methods for preparing the nanoparticles like sol-gel method [13], hydrothermal synthesis, sonochemical synthesis [45], ball milling, chemical vapour deposition (CVD) [46], physical vapour deposition (PVD), etc. The selection of the most suitable method depends on the desired type, size, and properties of nanoparticle material. Some methods are useful for offering greater control over size and uniformity, while others might be more scalable for larger production.

ii. ***Base CPE materials:*** The standard carbon paste mixture is prepared generally involving graphite powder and a binder like mineral oil or paraffin oil.

b) Nanoparticle incorporation

i. ***Mixing:*** The chosen nanoparticles are mixed with the graphite powder maintaining a weight ratio of nanoparticles to graphite powder dependent on the desired effect and the specific nanoparticles used.

ii. ***Homogenization:*** Grinding with a mortar and pestle or ultrasonicating the mixture to ensure the uniformity in dispersion of the nanoparticles throughout the graphite powder.

iii. ***Binder addition:*** Once the nanoparticles and graphite powder are well mixed, a binder material (mineral oil or paraffin oil) is added and again the mixing is continued towards the formation of a fine and homogeneous paste.

c) Electrode fabrication

i. ***Packing the paste:*** The resulting paste is inserted into a designated electrode tip that houses the working electrode.

ii. ***Polishing the electrode:*** The surface of the packed paste is polished to achieve a smooth and reproducible surface. This is a crucial step for obtaining consistent and reliable electrochemical measurements.

d) Additional considerations

i. ***Safety:*** As the nanoparticles can pose health risks, safety data sheets (SDS) should be consulted. The developed nanoparticles should be handled with appropriate personal protective equipment (PPE).

ii. ***Optimization:*** The specific ratios of nanoparticles, graphite powder, and binder might require to be optimized for a desired application.

By following these steps, nanoparticles modified CPEs with tailored properties may be achieved for the electrochemical experiments.

1.3.3. Characterization and analysis

a) Electrochemical techniques: Various electrochemical methods are there for characterizing the modified electrode, such as cyclic voltammetry, chronoamperometry, and impedance spectroscopy.

b) Surface analysis techniques: Techniques like scanning electron microscopy (SEM) and transmission electron microscopy (TEM) may be useful to visualize the morphology and distribution of nanoparticles on the electrode surface.

1.3.4. Applications of nanoparticle modified CPEs

Nanoparticle modified electrodes are applied in electrochemical sensing, biosensing, and electrocatalysis. Some specific examples are:

- Detection of various biomolecules-glucose, dopamine, and DNA [47], [48].
- Sensing of environmental pollutants as well as heavy metal ions [49].
- Developing non-enzymatic biosensors [50].
- Electrocatalytic applications in fuel cells and energy conversion devices [51].

In conclusion, nanoparticle modification is a promising strategy for enhancing the CPE performances. By incorporating nanoparticles with specific properties, tailoring of CPEs for various analytical and electrocatalytic applications is possible.

1.3.5. Advantages

- ***Enhanced sensitivity:*** The incorporation of nanoparticles often leads to improvement in sensitivity of electrochemical sensing.
- ***Catalytic activity:*** Certain nanoparticles speed up the electrochemical reactions acting as catalysts.
- ***Stability and reproducibility:*** Nanoparticle-modified electrodes exhibit better stability and reproducibility compared to bare carbon paste electrodes.

1.3.6. Challenges

- ***Cost:*** Expensive nanoparticles affect the overall cost of electrode preparation.
- ***Synthesis and dispersion:*** Uniform dispersion of nanoparticles and achievement of their stability are tough job.
- ***Analyte specificity:*** The choice of nanoparticles requires tailoring based on the specific analyte of interest.

Strategic incorporation of nanoparticles may be helpful for transforming the ordinary carbon paste electrodes into powerful tools. This approach unlocks a new level of control, making the field to tailor the electrode's properties for specific electrochemical applications. Thus, the choice of nanoparticle and its preparation method become the artist's brush and palette, enabling the creation of electrodes perfectly suited for the desired task.

1.4. Literature on nanoparticles modified CPE

This section presents an in-depth progress in nanoparticles-modified CPE based detection techniques tailored to specific target molecules and diverse application domains. Table 1.1 illustrates recent research endeavours employing the nanoparticles-based modification coupled with electrochemical transduction, followed by comprehensive descriptions of key research contributions in this domain.

Table 1.1. Literature survey indicating the development of nanoparticles modified electrode using electrochemical transduction.

Sl. no.	Target analyte	Modified electrode	Principle of operation	Ref.
1	MG	Conductive carbon black paste electrode (CCBPE)	CV, SWV	[52]
2	MG	Graphene oxide (GO) and ethylenediamine (En) composite film modified carbon paste electrode (CPE)	CV, DPV	[21]
3	MG	Multiwall carbon nanotube (MWNT) modified Glassy Carbon Electrode (GCE)	CV, DPV	[22]

4	MG	Multi-walled carbon nanotubes (MWCNTs)- polyethylenimine (PEI) composites modified GCE	CV, DPV	[53]
5	Formalin (FAL)	Nano Cerium Oxide Modified Graphite Paste Electrode	CV, DPV	[54]
6	Dopamine, Ascorbic acid	Carbon Nanoparticle Embedded Graphene	CV, DPV	[55]
7	Cu^{2+} ion	CuO Nanoparticles Intermixed with chemically modified MWCNTs as a novel electrode	Potentiometric	[56]
8	MG	Silica-modified GCE	SWASV	[57]
9	AMR	Graphene quantum Dots (GQDs)/ionic liquid modified CPE	CV, DPV	[58]
10	AMR	Manganese dioxide nanorods-electrochemically graphene oxide nanocomposites modified glassy carbon electrode (MnO_2NRs-ErGO/GCE)	CV, LSV	[31]
11	AMR	Ce^{3+}-doped CuO modified CPE	CV, LSV	[26]
12	Luteolin	In_2O_3 nanoparticles modified Glassy Carbon Paste Electrode (In_2O_3 NPs/GCPE)	CV, SWV	[59]
13	Alanine	Silica nanoparticles-imprinted polymer	CV, DPV	[60]
14	Quercetin	NiO/CNTs Nanocomposite Modified Ionic Liquid Carbon Paste Electrode (ILs/NiO/CNT/CPE)	CV, SWV	[61]
15	Tartrazine	Poly (p-amino benzene sulfonic acid)/zinc oxide nanoparticles in carbon paste electrode (Pp-ABSA/ZnO NPs-CPE)	CV, DPV	[62]
16	Tartrazine	Gold nanoparticles supported on carbon nanofibers (CNF/AuNP-CPE)	CV, DPV	[63]
17	Carmoisine	Mesoporous praseodymium oxide nanoparticles modified CPE (Pr_6O_{11})	CV, LSV	[64]
18	Metanil Yellow	Nano nickel cobalt oxide modified Graphite Paste Electrode ($NiCo_2O_4$@GP)	CV, DPV	[65]
19	Theophylline	Graphite electrode modified with samarium oxide nanoparticles (Sm_2O_3 NPs)	CV, DPV	[66]
20	Hydrogen Peroxide	Carbon Paste Electrode with $CuFe_2O_4$ nanoparticle (RGO/$CuFe_2O_4$/CPE)	CV, DPV	[67]
21	Ferulic Acid	TiO_2 nanoparticles-decorated, chemically-reduced graphene oxide (rGO-TiO_2)-modified glassy carbon electrode (GCE)	CV, DPV	[68]
22	P-coumaric acid	Carbon paste electrode modified by $NiZnFe_2O_4$ nanospinels	DPV	[69]

A conductive carbon black paste electrode (CCBPE) has been reported [52] to study the voltammetric response of MG. An ethylenediamine and graphene oxide-based [21] and novel self-assembly modified carbon paste electrode (CPE) proposed as a greatly sensitive and selective electrochemical sensor for detecting MG has the application of CV and electrochemical impedance spectroscopy (EIS) for the necessary characterization. Multiwall carbon nanotube (MWNT) film has been used [22] as the modifier for the electrode to detect

MG. A glassy carbon electrode, modified with CeO_2 and Nafion (referred to as GC/CeO_2/Nafion) [70], was prepared via drop casting and subsequently characterized using square wave anodic stripping voltammetry (SWASV), batch amperometry, and electrochemical impedance spectroscopy (EIS). Additionally, the impact of various anionic and cationic surfactants, utilized in the preparation of CeO_2 nanoparticles suspension in water, on the performance of GC/CeO_2/Nafion electrodes was investigated. The sensor demonstrating the most optimal response was employed for the detection of MG (malachite green) in a commercial product widely utilized as a biocide in aquaria for ornamental fish.

Javar et al. in their work [26] proposed a Ce^{3+} doped CuO based modified carbon paste electrode for detecting AMR in real soft drink samples. They conducted stability, reproducibility, and repeatability tests for this sensing. The linear response obtained was between 0.05 and 240.0 µM and the detection limit was found to be 10.2 nM. In another work, Jahani et al. [71] presented a graphite carbon nitride (g-C_3N_4) based electrode to detect AMR in samples of orange juice and tap water specimens. The developed electrode showed linear response for different concentrations of AMR in the range of 0.08 µM–340.0 µM, with limit of detection (LOD) of 0.02 µM using DPV under optimal circumstances. Akbari in [58] proposed a graphene quantum dots/ionic liquid modified CPE for sensing AMR in real samples with acceptable recoveries. Electroanalysis method chronoamperometry was used along with CV and DPV in the presence of blank phosphate buffer. Their approach yielded the lower detection limit of 0.03 µM in the linear range from 0.1 to 400.0 µM under optimal conditions. Wang et al. in [72] proposed a Co_3O_4-CeO_2/Gr nanocomposite modified electrode for electrochemical sensing of AMR in soft drinks. In this paper, they performed various electrochemical mechanisms in the linear concentration range of 2–96 µM and detected AMR with a sensitivity of 0.8642 µA μM^{-1} cm^{-2} and LOD of 0.1591 µM with good repeatability and anti-interference stability. Moradpour et al. in [73] introduced a rapid and sensitive electrochemical sensing of amaranth by glassy carbon electrode (GCE) modified through N-doped reduced graphene oxide. The developed sensor was applied to real samples such as tap water and fruit juices such as apple and orange juice with recovery rate ranging between 96.0% and 104.3%. The LOD was found to be 0.03 µM over a concentration range of 0.1–600.0 µM. Tajik et al. in a similar paper [74] developed a novel screen-printed electrode which was modified by a Pd/GO nanomaterial for the detection of amaranth in various real samples such as orange juice, apple juice and tap water. Their proposed

Pd/GO/SPE sensor provided low detection limit of 30.0 nM in the linear concentration range of 0.08 µM–360.0 µM with long term stability and satisfactory reproducibility.

Silva et al. [75] reported a cathodically pretreated boron-doped diamond (BDD) electrode with a LOD of 0.058 µmol L^{-1}, for detecting ICN in water. The electro-oxidation reaction of ICN on this electrode was stated to be dominated by diffusion, with minimum adsorption. Despite fair electroanalytical performance to determine ICN, the manufacturing steps involved here was costly and time taking. Arvand et al. [76] used an azo dye as a mediator for electron transfer for modifying the CPE to detect ICN in chocolates, jellies, and diazepam tablets with the LOD of 0.36 µmol L^{-1}. Low cost, quick response, and low background current were some key features achieved here. Manjunatha et al. [77] developed a poly (glycine) modified CPE to detect ICN to trace range with a LOD of 11x 10^{-8} M.

1.5. Objective and scope of the research

The present work throws light on the usage of the nanoparticles modified CPE for the measurement of a few synthetic food colors viz., Malachite Green (green color), Amaranth (red color) and Indigo Carmine (blue color), separately. With the advancement of the sensors, different exploratory parameters like, effect of pH, effect of buffer, effect of scan rate, and effect of concentration variation have been examined in thoroughly. The goals of this thesis work can be outlined as follows:

- Selection and synthesis of nanoparticles
- Characterization of the nanomaterials in terms of their dimensions, structural and morphological variations.
- Investigating different electrocatalytic properties of the electrodes (high conductivity, wide potential range, renewable surface, etc.) as well as optimizing the experimental conditions like buffer, pH, scan rate, concentration, etc.
- Studying various electro-analytical characteristics (selectivity, sensitivity, repeatability, reproducibility, etc.) of the developed electrodes.
- Application of the developed electrodes to the real samples.

Considering the stated objectives, the entire study has been segmented into five chapters. A succinct breakdown of the thesis organization by chapter is provided below.

Chapter 1 explains the basis of the issue and illustrates the objectives of this thesis work. The chapter then portrays the distinctive transduction systems. Further, it concentrates on the

various electrochemical procedures utilized as of recently for determination of artificial food colorants alongside their advantages and disadvantages. Followed by it, the nanoparticles based modified carbon paste electrode (CPE) systems have been described as a way to alleviate the impediments brought about by ordinary electrochemical identification procedures. Here, a presentation of this modification is followed by a short literature review on nanoparticles modified CPE based sensing. The chapter ends with the summarized objectives and scope of the work.

Chapter 2 discusses the basic CPE and then the nanoparticles embedded graphite paste electrode (GPE) synthesized for the determination of green colored dye named Malachite green (MG) in pond water and fish fillets. Also, the comparative study of MG determination with other research reports is presented in this chapter. The electrochemical characteristics of the developed electrode and the experimental parameters for the detection of MG are discussed here in detail followed by analysis of real samples.

Chapter 3 discusses the CPE and then the nanoparticles ingrained GPE for the determination of red colored Amaranth (AMR) dye in different children's consumable candies. Also, the comparative study of AMR determination with other research reports is presented in this chapter. The electrochemical characteristics of the developed electrode and the experimental parameters for the detection of AMR are discussed here in detail followed by analysis of real samples.

Chapter 4 discusses the CPE and then the modified GPE to determine blue colored Indigo carmine (ICN) in different candies. A comparative study of ICN determination with earlier research reports is presented. The electrochemical characteristics of the developed electrode and the experimental parameters for the detection of ICN are discussed here in detail followed by analysis of real samples.

Chapter 5 shows a general overview of the work done and highlights the concluding comments. The strengths as well as weaknesses of the proposed framework have been investigated here with certain suggestions and a few proposals are presented as future scopes of work.

References

[1] R. Varghese and S. Ramamoorthy, "Status of food colorants in India: conflicts and prospects," *Journal of Consumer Protection and Food Safety*, vol. 18, no. 2, pp. 107–118, 2023, doi: 10.1007/s00003-023-01427-y.

[2] L. E. Arnold, N. Lofthouse, and E. Hurt, "Artificial food colors and attention-deficit/hyperactivity symptoms: conclusions to dye for," *Neurotherapeutics*, vol. 9, no. 3, pp. 599–609, 2012, doi: 10.1007/s13311-012-0133-x.

[3] D. K. Doguc, F. Aylak, I. Ilhan, E. Kulac, and F. Gultekin, "Are there any remarkable effects of prenatal exposure to food colorings on neurobehaviour and learning process in rat offspring?" *Nutritional Neuroscience*, vol. 18, no. 1, pp. 12–21, 2015, doi: 10.1179/1476830513Y.0000000095.

[4] P. Amchova, H. Kotolova, and J. Ruda-Kucerova, "Health safety issues of synthetic food colorants," *Regulatory Toxicology and Pharmacology*, vol. 73, no. 3, pp. 914–922, 2015, doi: 10.1016/j.yrtph.2015.09.026.

[5] S. Dey and B. H. Nagababu, "Applications of food color and bio-preservatives in the food and its effect on the human health," *Food Chemistry Advances*, vol. 1, no. January, p. 100019, 2022, doi: 10.1016/j.focha.2022.100019.

[6] M. M. Silva, F. H. Reboredo, and F. C. Lidon, "Food color additives: a synoptical overview on their chemical properties, applications in food products, and health side effects," *Foods*, vol. 11, p. 379, 2022.

[7] A. Tkaczyk, K. Mitrowska, and A. Posyniak, "Synthetic organic dyes as contaminants of the aquatic environment and their implications for ecosystems: a review," *Science of the Total Environment*, vol. 717, p. 137222, 2020, doi: 10.1016/j.scitotenv.2020.137222.

[8] I. Pratt, J. C. Larsen, A. Mortensen, and I. Rietjens, "Re-evaluation of azo dyes as food additives: problems encountered," *Toxicology Letters*, vol. 221, p. S53, 2013, doi: 10.1016/j.toxlet.2013.06.194.

[9] K. A. Amin and F.S. Al-Shehri, "Toxicological and safety assessment of tartrazine as a synthetic food additive on health biomarkers: a review," *African Journal of Biotechnology*, vol. 17, no. 6, pp. 139–149, 2018, doi: 10.5897/ajb2017.16300.

[10] K. Takeyama, R. Sakamoto, M. Yoshikawa, and T. Suzuki, "A case of Wenckebach-type atrioventricular block caused by administration of indigo carmine," *Tokai Journal of Experimental and Clinical Medicine*, vol. 39, no. 1, pp. 10–13, 2014.

[11] S. Dixit, S.K. Purshottam, S. K. Khanna & M. Das "Usage pattern of synthetic food colors in different states of India and exposure assessment through commodities preferentially consumed by children," *Food Additives & Contaminants: Part A*, vol. 28, no. 8, 2011.

[12] M. Tripathi, S. K. Khanna, and M. Das, "Surveillance on use of synthetic colors in eatables vis a vis prevention of food adulteration act of India," *Food Control*, vol. 18, no. 3, pp. 211–219, 2007, doi: 10.1016/j.foodcont.2005.09.016.

[13] S. Dasgupta *et al.*, "Electrochemical sensor based on CuO nanoparticles-modified graphite electrode for the detection of malachite green," *Nano Life*, vol. 14, no. 1, pp. 1–12, 2024, doi: 10.1142/S1793984423500150.

[14] M. Iammarino, A. Mentana, D. Centonze, C. Palermo, M. Mangiacotti, and A. E. Chiaravalle, "Simultaneous determination of twelve dyes in meat products: Development and validation of an analytical method based on HPLC-UV-diode array detection," *Food Chemistry*, vol. 285, no. March 2018, pp. 1–9, 2019, doi: 10.1016/j.foodchem.2019.01.133.

[15] K. S. Minioti, C. F. Sakellariou, and N. S. Thomaidis, "Determination of 13 synthetic food colorants in water-soluble foods by reversed-phase high-performance liquid chromatography coupled with diode-array detector," *Analytica Chimica Acta*, vol. 583, no. 1, pp. 103–110, 2007, doi: 10.1016/j.aca.2006.10.002.

[16] N. Pourreza and S. Elhami, "Cloud point extraction and spectrophotometric determination of amaranth in food samples using nonionic surfactant Triton X-100 and tetrabutylammonium hydrogen sulfate," *Journal of the Iranian Chemical Society*, vol. 6, no. 4, pp. 784–788, 2009, doi: 10.1007/BF03246170.

[17] J. J. Berzas, J. R. Flores, M. J. V. Llerena, and N. R. Fariñas, "Spectrophotometric resolution of ternary mixtures of Tartrazine, Patent Blue V and Indigo Carmine in commercial products," *Analytica Chimica Acta*, vol. 391, no. 3, pp. 353–364, 1999, doi: 10.1016/S0003-2670(99)00215-9.

[18] M. Ryvolová, P. Táborský, P. Vrábel, P. Krásenský, and J. Preisler, "Sensitive determination of erythrosine and other red food colorants using capillary electrophoresis with laser-induced fluorescence detection," *Journal of Chromatography A*, vol. 1141, no. 2, pp. 206–211, 2007, doi: 10.1016/j.chroma.2006.12.018.

[19] S. Dasgupta, S. Nag, R. B. Roy, R. Bandyopadhyay, and B. Tudu, "Malachite Green detection using carbon paste electrode based on voltammetry,"*2nd International Conference on Emerging Frontiers in Electrical and Electronic Technologies, ICEFEET 2022*, pp. 1–5, 2022, doi: 10.1109/ICEFEET51821.2022.9847835.

[20] X. C. Guo, X. Cao, H. H. Wang, M. Yuan, X. J. Chen, W.-Y. Kang, and W. H. Zhou, "Graphene-gold nanoparticles nanohybrids for electrochemical detection of malachite green," *International Journal of Electrochemical Science*, vol. 12, no. 8, pp. 7557–7569, 2017, doi: 10.20964/2017.08.49.

[21] K. Zhang, G. Song, L. Yang, J. Zhou, and B. Ye, "A novel self-assembly voltammetric sensor for malachite green based on ethylenediamine and graphene oxide," *Analytical Methods*, vol. 4, no. 12, pp. 4257–4263, 2012, doi: 10.1039/c2ay26039e.

[22] H. Yi, W. Qu, and W. Huang, "Electrochemical determination of malachite green using a multi-wall carbon nanotube modified glassy carbon electrode," *Microchimica Acta*, vol. 160, no. 1–2, pp. 291–296, 2008, doi: 10.1007/s00604-007-0814-z.

[23] P. Deng, J. Feng, Y. Wei, J. Xiao, J. Li, and Q. He, "Fast and ultrasensitive trace malachite green detection in aquaculture and fisheries by using hexadecylpyridinium

bromide modified electrochemical sensor," *Journal of Food Composition and Analysis*, vol. 102, no. March, p. 104003, 2021, doi: 10.1016/j.jfca.2021.104003.

[24] Y. Xu, Z. Gao, W. Chen, E. Wang, and Y. Li, "Preparation and application of malachite green molecularly imprinted/gold nanoparticle composite film–modified glassy carbon electrode," *Ionics (Kiel)*, vol. 25, no. 3, pp. 1177–1185, 2019, doi: 10.1007/s11581-018-2778-x.

[25] M. Alizadeh *et al.*, "Recent advantages in electrochemical monitoring for the analysis of amaranth and carminic acid as food color," *Food and Chemical Toxicology*, vol. 163, no. January, p. 112929, 2022, doi: 10.1016/j.fct.2022.112929.

[26] H. A. Javar, H. M. Moghaddam, A. Rajabizadeh, S. Hamzeh, and E. Akbari, "Development of an electrochemical sensor based on Ce3+ and CuO for the determination of amaranth in soft drinks," *Microchemical Journal*, vol. 183, no. September, p. 108081, 2022, doi: 10.1016/j.microc.2022.108081.

[27] M. Bijad, H. K. Maleh, M. Farsi, and S. A. Shahidi, "Simultaneous determination of amaranth and nitrite in foodstuffs via electrochemical sensor based on carbon paste electrode modified with CuO/SWCNTs and room temperature ionic liquid," *Food Analytical Methods*, vol. 10, no. 11, pp. 3773–3780, 2017, doi: 10.1007/s12161-017-0933-z.

[28] G. Zhang and Y. Ma, "Mechanistic and conformational studies on the interaction of food dye amaranth with human serum albumin by multispectroscopic methods," *Food Chemistry*, vol. 136, no. 2, pp. 442–449, 2013, doi: 10.1016/j.foodchem.2012.09.026.

[29] J. A. Buledi *et al.*, "Selective oxidation of amaranth dye in soft drinks through tin oxide decorated reduced graphene oxide nanocomposite based electrochemical sensor," *Food and Chemical Toxicology*, vol. 165, no. February, p. 113177, 2022, doi: 10.1016/j.fct.2022.113177.

[30] P. Mpountoukas *et al.*, "Cytogenetic evaluation and DNA interaction studies of the food colorants amaranth, erythrosine and tartrazine," *Food and Chemical Toxicology*, vol. 48, no. 10, pp. 2934–2944, 2010, doi: 10.1016/j.fct.2010.07.030.

[31] Q. He, J. Liu, X. Liu, G. Li, P. Deng, and J. Liang, "Manganese dioxide Nanorods/electrochemically reduced graphene oxide nanocomposites modified electrodes for cost-effective and ultrasensitive detection of Amaranth," *Colloids and Surfaces B: Biointerfaces*, vol. 172, no. September, pp. 565–572, 2018, doi: 10.1016/j.colsurfb.2018.09.005.

[32] E. G. Segura, M. S. Ríos, and A. C. Cruz, "Sorption of indigo carmine by a Fe-zeolitic tuff and carbonaceous material from pyrolyzed sewage sludge," *Journal of Hazardous Material*, vol. 170, no. 2–3, pp. 1227–1235, 2009, doi: 10.1016/j.jhazmat.2009.05.102.

[33] U. R. Lakshmi, V. C. Srivastava, I. D. Mall, and D. H. Lataye, "Rice husk ash as an effective adsorbent: Evaluation of adsorptive characteristics for Indigo Carmine dye," *Journal of Environmental Management*, vol. 90, no. 2, pp. 710–720, 2009, doi: 10.1016/j.jenvman.2008.01.002.

[34] L. Kavieva and G. Ziyatdinova, "Voltammetric sensor based on SeO_2 nanoparticles and surfactants for indigo carmine determination," *sensors*, vol. 22, p. 3224, 2022.

[35] "Scientific Opinion on the re-evaluation of Indigo Carmine (E 132) as a food additive," *European Food Safety Authority (EFSA) Journal*, vol. 12, no. 7. 2014. doi: 10.2903/j.efsa.2014.3768.

[36] M. S. Secula, I. Creżescu, and S. Petrescu, "An experimental study of indigo carmine removal from aqueous solution by electrocoagulation," *Desalination*, vol. 277, no. 1–3, pp. 227–235, 2011, doi: 10.1016/j.desal.2011.04.031.

[37] A. Mittal, J. Mittal, and L. Kurup, "Batch and bulk removal of hazardous dye, indigo carmine from wastewater through adsorption," *Journal of Hazardous Material*, vol. 137, no. 1, pp. 591–602, 2006, doi: 10.1016/j.jhazmat.2006.02.047.

[38] M. Palit *et al.*, "Classification of black tea taste and correlation with tea taster's mark using voltammetric electronic tongue," *IEEE Transactions on Instrumentation and Measurement*, vol. 59, no. 8, pp. 2230–2239, 2010, doi: 10.1109/TIM.2009.2032883.

[39] B. J. Privett, J. H. Shin, and M. H. Schoenfisch, "Electrochemical sensors," *Analytical Chemistry*, vol. 80, no. 12, pp. 4499–4517, 2008, doi: 10.1016/B978-0-12-813886-1.00004-8.

[40] F. Scholz, "Voltammetric techniques of analysis: the essentials," *ChemTexts*, vol. 1, no. 4, pp. 1–24, 2015, doi: 10.1007/s40828-015-0016-y.

[41] Autolab Application Note EC08, "Basic overview of the working principle of a potentiostat/galvanostat (PGSTAT) – Electrochemical cell setup," *Metrohm Autolab.B.V*, pp. 1–3, 2011.

[42] Y. Xie, Y. Ju, Y. Toku, and Y. Morita, "Fabrication of Fe_2O_3 nanowire arrays based on oxidation-assisted stress-induced atomic-diffusion and their photovoltaic properties for solar water splitting," *RSC Advances*, vol. 7, no. 49, pp. 30548–30553, 2017, doi: 10.1039/c7ra03298f.

[43] P. T. Kissinger and W. R. Heineman, "Cyclic voltammetry," *Journal of chemical education*, vol. 60, no. 9, pp. 702–706, 1983, doi: 10.1021/ed060p702.

[44] P. V. Techniques, "Pulse Voltammetric Techniques," pp. 1–10, 2010.

[45] K. Okitsu, A. Yue, S. Tanabe, and H. Matsumoto, "Sonochemical preparation and catalytic behavior of highly dispersed palladium nanoparticles on alumina," *Chemistry of Materials*, vol. 12, no. 10, pp. 3006–3011, 2000, doi: 10.1021/cm0001915.

[46] S. Meltzer *et al.*, "Fabrication of nanostructures by hydroxylamine seeding of gold nanoparticle templates," *Langmuir*, vol. 17, no. 5, pp. 1713–1718, 2001, doi: 10.1021/la001170s.

[47] C. Erdem, D. K. Zeybek, G. Aydoğdu, B. Zeybek, Ş. Pekyardimci, and E. Kiliç, "Electrochemical glucose biosensor based on nickel oxide nanoparticle-modified carbon paste electrode," *Artificial Cells, Nanomedicine, and Biotechnology*, vol. 42, no. 4, pp. 237–244, 2014, doi: 10.3109/21691401.2013.808649.

[48] Y. Z. Keteklahijani, F. Sharif, E. P. L. Roberts, and U. Sundararaj, "Enhanced Sensitivity of Dopamine Biosensors: An Electrochemical Approach Based on Nanocomposite Electrodes Comprising Polyaniline, Nitrogen-Doped Graphene, and DNA-Functionalized Carbon Nanotubes," *J Electrochem Soc*, vol. 166, no. 15, pp. B1415–B1425, 2019, doi: 10.1149/2.0361915jes.

[49] M. D. Shirsat and T. Hianik, "Electrochemical Detection of Heavy Metal Ions Based on Nanocomposite Materials," *Journal of Composites Science*, vol. 7, no. 11, 2023, doi: 10.3390/jcs7110473.

[50] A. Mohammadpour-Haratbar, S. Mohammadpour-Haratbar, Y. Zare, K. Y. Rhee, and S. J. Park, "A Review on Non-Enzymatic Electrochemical Biosensors of Glucose Using Carbon Nanofiber Nanocomposites," *Biosensors (Basel)*, vol. 12, no. 11, 2022, doi: 10.3390/bios12111004.

[51] S. A. A. Gawad and A. M. Fekry, "A novel environmental nano-catalyst of zeolite amended with carbon nanotube/silver nanoparticles decorated carbon paste electrode for electro-oxidation of propylene glycol," *Scientific Reports*, vol. 12, no. 1, pp. 1–11, 2022, doi: 10.1038/s41598-022-12268-4.

[52] K. Qu *et al.*, "Simultaneous detection of diethylstilbestrol and malachite green using conductive carbon black paste electrode," *International Journal of Electrochemical Science,* vol. 7, no. 3, pp. 1827–1839, 2012, doi: 10.1016/s1452-3981(23)13843-0.

[53] Y. Luo, and Z. Li, "A sensitive electrochemical sensor manufactured from multi-wall carbon nanotubes-polyethylenimine nanocomposite for malachite green detection," *Journal of Alloys and Compounds*, vol. 897, p. 163216, 2022, doi: 10.1016/j.jallcom.2021.163216.

[54] S. Nag *et al.*, "A simple nano cerium oxide modified graphite electrode for electrochemical detection of formaldehyde in mushroom," *IEEE Sensors Journal*, vol. 21, no. 10, pp. 12019–12026, 2021, doi: 10.1109/JSEN.2021.3066113.

[55] S. Biswas, R. Das, M. Basu, R. Bandyopadhyay, and P. Pramanik, "Synthesis of carbon nanoparticle embedded graphene for sensitive and selective determination of dopamine and ascorbic acid in biological fluids," *RSC Advances*, vol. 6, no. 103, pp. 100723–100731, 2016, doi: 10.1039/c6ra16774h.

[56] M. Ghaedi *et al.*, "CuO nanoparticles intermixed with chemically modified multiwalled carbon nanotubes as a novel electrode for Cu^{2+} ion determination," *IEEE Sensors Journal*, vol. 15, no. 5, pp. 2882–2890, 2015.

[57] A. M. Sacara, V. Nairi, A. Salis, G. L. Turdean and L. M. Muresan, "Silica-modified Electrodes for electrochemical detection of malachite green," *Electroanalysis*, vol. 29, no. 11, pp. 2602–2609, 2017, doi: 10.1002/elan.201700400.

[58] S. Akbari, "A new voltammetric sensor according to graphene quantum dots/ionic liquid modified carbon paste electrode for amaranth sensitive determination," *International Journal of Environmental Analytical Chemistry,* vol. 102, no. 3, pp. 789–803, 2022, doi: 10.1080/03067319.2020.1726338.

[59] H. Ibrahim and Y. Temerk, "Novel sensor for sensitive electrochemical determination of luteolin based on In_2O_3 nanoparticles modified glassy carbon paste electrode," *Sensors and Actuators B Chemical*, vol. 206, pp. 744–752, 2015, doi: 10.1016/j.snb.2014.09.011.

[60] Z. Aryan, H. R. Rajabi, H. Khajehsharifi, and O. Sheydaei, "Highly selective determination of alanine in urine sample using a modified electrochemical sensor based on silica nanoparticles-imprinted polymer," *Journal of the Iranian Chemical Society*, vol. 19, no. 10, pp. 4139–4148, 2022, doi: 10.1007/s13738-022-02589-6.

[61] V. K. Gupta, F. Golestani, S. Ahmadzadeh, H. Karimi-Maleh, G. Fazli, and S. Khosravi, "NiO/CNTs nanocomposite modified ionic liquid carbon paste electrode as a voltammetric sensor for determination of quercetin," *International Journal of Electrochemical Science*, vol. 10, no. 4, pp. 3657–3667, 2015, doi: 10.1016/s1452-3981(23)06569-0.

[62] G. Karim-Nezhad, Z. Khorablou, M. Zamani, P. Seyed Dorraji, and M. Alamgholiloo, "Voltammetric sensor for tartrazine determination in soft drinks using poly (p-aminobenzene sulfonic acid)/zinc oxide nanoparticles in carbon paste electrode," *Journal of Food and Drug Analysis*, vol. 25, no. 2, pp. 293–301, 2017, doi: 10.1016/j.jfda.2016.10.002.

[63] A. A. Cardenas-Riojas, S. L. Calderon-Zavaleta, U. Quiroz-Aguinaga, E. O. López, M. Ponce-Vargas, and A. M. Baena-Moncada, "Evaluation of an electrochemical sensor based on gold nanoparticles supported on carbon nanofibers for detection of tartrazine dye," *Journal of Solid State Electrochemistry*, vol. 27, no. 8, pp. 1969–1982, 2023, doi: 10.1007/s10008-023-05438-5.

[64] S. Hamzeh, H. Mahmoudi-Moghaddam, S. Zinatloo-Ajabshir, M. Amiri, and S. A. Razavi Nasab, "Eco-friendly synthesis of mesoporous praseodymium oxide nanoparticles for highly efficient electrochemical sensing of carmoisine in food samples," *Food Chemistry*, vol. 433, no. May 2023, p. 137363, 2024, doi: 10.1016/j.foodchem.2023.137363.

[65] S. Nag, D. Das, H. Naskar, B. Tudu, R. Bandyopadhyay, and R. Banerjee Roy, "Detection of metanil yellow adulteration in turmeric powder using nano nickel cobalt oxide modified graphite electrode," *IEEE Sensors Journal*, vol. 22, no. 13, pp. 12515–12521, 2022, doi: 10.1109/JSEN.2022.3178768.

[66] M. Moulick *et al.*, "Detection of theophylline using samarium oxide nanoparticles ingrained graphite electrode," *Nano Life*, vol. 13, no. 2, pp. 1–7, 2023, doi: 10.1142/S1793984423500071.

[67] A. Benvidi, M. T. Nafar, S. Jahanbani, M. D. Tezerjani, M. Rezaeinasab, and S. Dalirnasab, "Developing an electrochemical sensor based on a carbon paste electrode modified with nano-composite of reduced graphene oxide and $CuFe_2O_4$ nanoparticles for determination of hydrogen peroxide," *Materials Science and Engineering C*, vol. 75, pp. 1435–1447, 2017, doi: 10.1016/j.msec.2017.03.062.

[68] T. Di. Bharathi, S. Prem Anandh, and M. Rangarajan, "Differential pulse voltammetric detection of ferulic acid using RGO-TiO_2 electrodes," *INDICON 2018 - 15th IEEE India*

Council International Conference, no. 5, pp. 1–6, 2018, doi: 10.1109/INDICON45594.2018.8986994.

[69] Z. N. Khoveis, E. M. Khaledi, H. A. R. Pour, and M. Farhadpour, "Novel electrochemical sensor based on $NiZnFe_2O_4$/CPE for measurement of p-coumaric acid in honey," *Arabian Journal of Chemistry*, vol. 17, no. 2, 2024, doi: 10.1016/j.arabjc.2023.105472.

[70] A. M. Sacara, C. Cristea, and L. M. Muresan, "Electrochemical detection of Malachite Green using glassy carbon electrodes modified with CeO_2 nanoparticles and Nafion," *Journal of Electroanalytical Chemistry*, vol. 792, pp. 23–30, 2017, doi: 10.1016/j.jelechem.2017.03.030.

[71] P. M. Jahani, M. R. Aflatoonian, R. A. Rayeni, A. D. Bartolomeo, and S. Z. Mohammadi, "Graphite carbon nitride-modified screen-printed electrode as a highly sensitive and selective sensor for detection of amaranth," *Food and Chemical Toxicology*, vol. 163, no. February, p. 112962, 2022, doi: 10.1016/j.fct.2022.112962.

[72] H. Wang *et al.*, "Co_3O_4-CeO_2/graphene composite as a novel sensor for amaranth detection," *Journal of The Electrochemical Society*, vol. 168, no. 2, p. 027513, 2021, doi: 10.1149/1945-7111/abe3a3.

[73] H. Moradpour, H. Beitollahi, F. G. Nejad, and A. D. Bartolomeo, "Glassy carbon electrode modified with n-doped reduced graphene oxide sheets as an effective electrochemical sensor for amaranth detection," *Materials*, vol. 15, no. 9, 2022, doi: 10.3390/ma15093011.

[74] S. Tajik, H. Beitollahi, H. W. Jang, and M. Shokouhimehr, "A simple and sensitive approach for the electrochemical determination of amaranth by a Pd/GO nanomaterial-modified screen-printed electrode," *RSC Advances*, vol. 11, no. 1, pp. 278–287, 2020, doi: 10.1039/d0ra08723h.

[75] T. A. Silva, G. F. Pereira, O. F. Filho, K. I. B. Eguiluz, and G. R. Salazar-Banda, "Electroanalytical sensing of indigo carmine dye in water samples using a cathodically pretreated boron-doped diamond electrode," *Journal of Electroanalytical Chemistry*, vol. 769, pp. 28–34, 2016, doi: 10.1016/j.jelechem.2016.03.015.

[76] M. Arvand, M. Saberi, M. S. Ardaki, and A. Mohammadi, "Mediated electrochemical method for the determination of indigo carmine levels in food products," *Talanta*, vol. 173, no. February, pp. 60–68, 2017, doi: 10.1016/j.talanta.2017.05.062.

[77] J. G. G. Manjunatha, "A novel poly (glycine) biosensor towards the detection of indigo carmine: A voltammetric study," *Journal of Food and Drug Analysis*, vol. 26, no. 1, pp. 292–299, 2018, doi: 10.1016/j.jfda.2017.05.002.

Chapter 2

Detection of Malachite Green (MG) using Carbon Paste Electrode (CPE), and CuO Nanoparticles Modified Graphite Paste Electrode (CuO@GPE)

This chapter explores the fabrication and utilization of a carbon paste electrode (CPE), and then the graphite electrode modified with CuO nanoparticles for the detection of Malachite Green (MG) in fish flesh and pond water. It includes a comparative analysis of MG detection with prior studies. Detailed discussions are provided on the electrochemical properties of the developed electrode, experimental parameters for MG detection, and thorough analysis of real sample data.

List of Sections

Contents of this chapter are based on mentioned publications:

Samhita Dasgupta, Shreya Nag, Runu Banerjee Roy, Rajib Bandyopadhyay, Panchanan Pramanik, Deepak Kumar Das, Bipan Tudu, "Development and detailed performance study of a carbon paste electrode for the electrochemical detection of malachite green," *Nano LIFE,* vol. 13, no.2, 2350006, pp. 1-9, 2023. [DOI: 10.1142/S179398442350006X].

Samhita Dasgupta, Shreya Nag, Debangana Das, Runu Banerjee Roy, Deepak Kumar Das, Panchanan Pramanik, Rajib Bandyopadhyay, Bipan Tudu. "Electrochemical sensor based on CuO nanoparticles modified graphite electrode for the detection of malachite green." *Nano LIFE,* vol. 14, no. 1, 2350015, pp. 1-12, 2024. [DOI: https://doi.org/10.1142/S1793984423500150].

2.1. Introduction

Malachite green (MG) (MG: N-[4-[[4-(dimethylamino) phenyl] phenylmethylene]-2,5-cyclohexadien-1-ylidene]-N-methylmethaminium chloride, CAS nr. 569-64-2) [1], classified in the coloring industry as a triarylmethane dye, generally is found as the chloride salt $[C_6H_5C(C_6H_4N(CH_3)_2)_2]Cl$, in which the color is contributed mainly by the cationic part. It is an important dyeing agent, food-additive, preservative, and fish-drug [2]. The literature survey of MG is already discussed in Chapter 1, Section 1.1. and Section 1.4. The chemical structure of MG is shown in Fig.2.1.

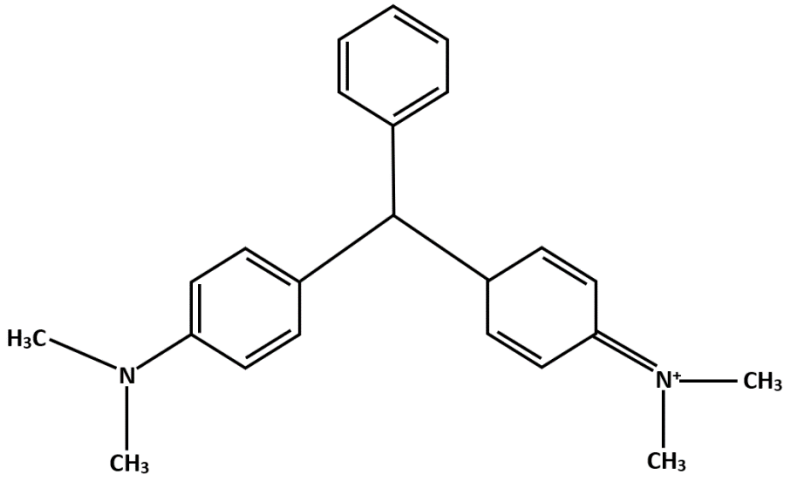

Fig. 2.1. Chemical structure of malachite green (MG).

Some established techniques for determining MG include high-performance liquid chromatography (HPLC) [3] or its mass spectrometry variant (HPLC-MS) [4], [5], [6] , enzyme-linked immunosorbent assay (ELISA) [7], [8], fluorescence spectrometry [9] , and capillary electrophoresis [10]. Despite their efficacy, these methods are hindered by expensive equipment, extended sampling times, the need for skilled operators, and slow response rates. In contrast, electrochemical approaches offer a compelling alternative: they are cost-effective, sensitive, selective, and rapid. For instance, voltammetric detection of MG using electrochemical methods has shown promise, as evidenced by several studies cited in references [11], [12], [13], [14] and [15].

A highly sensitive and selective sensor for MG detection is always in demand. Previous applications of CPE and different modified CPE have demonstrated its versatility in detecting various molecules [16], [17], [18]. In our research, we proposed the development of a straightforward carbon paste electrode (CPE) for voltammetric MG detection. We further optimized this newly developed CPE for MG detection, including parameter adjustments and

optimization techniques. To enhance its performance, we modified the CPE with copper oxide (CuO) nanoparticles, resulting in a new graphite paste electrode (CuO@GPE) composite. Subsequent testing of this composite electrode showed improved MG detection in real-life samples such as pond water and fish flesh.

Graphite, being highly electrically conductive, is suitable for use in electrodes for electrochemical measurements[19], [20] . Its chemical inertness makes it resistant to corrosion and degradation once exposed to various electrolytes and chemicals commonly used in electrochemical experiments. This property ensures the stability and longevity of the electrode made by graphite. Besides, Graphite has enough mechanical strength and stability to withstand the pressure and manipulation involved in the fabrication of CPEs. Graphite is available in the form of fine powder to be mixed with suitable binding agents to the formation of a smooth paste. This simplicity in fabrication makes it convenient for preparing CPEs in various shapes and sizes perfect for different experimental setups.

Nanoparticles have a high surface area to volume ratio compared to bulk materials. Incorporating nanoparticles into the carbon paste matrix increases the effective surface area of the electrode available for electrochemical reactions. This enhanced surface area allows for greater interaction between the analyte and the electrode surface, leading to improved sensitivity and detection limits. Certain nanoparticles exhibit intrinsic catalytic activity towards specific electrochemical reactions. By incorporating these nanoparticles into the CPE, the catalytic activity of the electrode can be enhanced, resulting in faster reaction kinetics and improved performance in terms of response time and sensitivity. Metal oxide nanoparticles are highly conductive. Incorporating these nanoparticles into the CPE can improve the overall conductivity of the electrode, reducing resistance and improving electron transfer kinetics at the electrode-electrolyte interface. Nanoparticle modification can impart selectivity to the CPE by facilitating selective adsorption or recognition of target analytes. Functionalized nanoparticles can be designed to selectively bind to specific analytes, thereby enhancing the electrode's selectivity towards target molecules in complex sample matrices. Stability and longevity also of the CPE increase after incorporating nanoparticles modifier.

Utilizing techniques such as principal component analysis (PCA) enabled qualitative discrimination among different MG concentrations. Additionally, Partial Least Square Regression (PLSR) algorithms were employed for precise quantitative evaluation of MG content. Our findings demonstrate a significant enhancement in detection efficiency following

the modification of the CPE with CuO nanoparticles. The flowchart shown in Fig. 2.2. narrates the electrochemical studies attempted so as to optimize the properties of the incorporated electrodes.

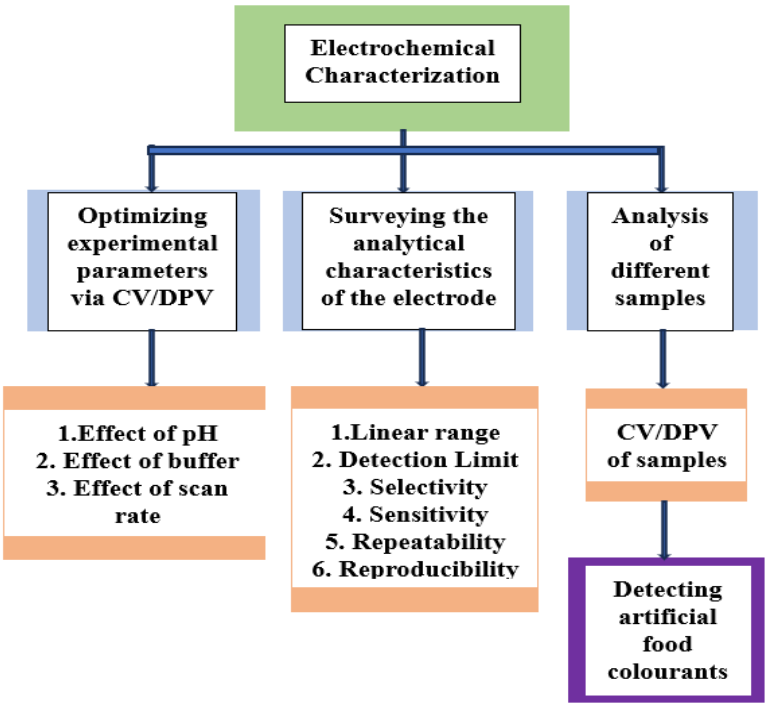

Fig. 2.2. Flowchart presenting the electrochemical characterization of the CPE and nanoparticles modified GPE followed all over the thesis work.

2.2. Experimentation with carbon paste electrode (CPE)

2.2.1. Reagents and chemicals

SISCO CHEM, India supplied MG and Sigma Aldrich, India supplied the Graphite powder. Merck & Co, India supplied the paraffin oil. Phosphate buffered saline (PBS), acetate buffered saline (ABS), and citrate buffered saline (CBS) (0.1 M concentration each) were prepared in the research lab to be used along with the MG solution as supporting electrolytes. All the chemicals were of pure analytical status without extra refinement. Millipore water (resistance 18MΩ) was used to make every required experimental solution. The whole experiment was performed at ambient temperature. During the experiments, between two consecutive data recordings, Millipore water was used to wash the working electrode for surface regeneration.

2.2.2. Apparatus and instrumentation

The electrochemical analysis was executed using a three-electrode arrangement and a potentiostat PGSTAT101 (Metrohom Autolab, Netherlands). The three-electrode system

consisted of a reference electrode (Ag/AgCl) and a counter electrode (platinum), while the developed CPE played the role of a working electrode. NOVA software of Metrohom Autolab showcased the CV and DPV results graphically. Labman scientific instruments ultrasonicator was used to blend the solutes and solvents appropriately.

2.2.3. Experimental setup

The previously described three-electrode system is connected with the potentiostat PGSTAT101 combined with a laboratory computer. The schematic diagram of the whole experimental assembly is depicted in Fig.2.3.

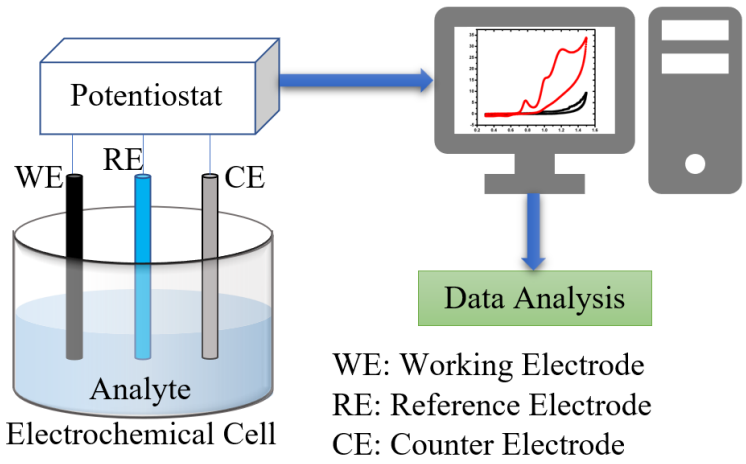

Fig. 2.3. Experimental setup-an illustration.

2.2.4. Preparing CPE- the working electrode

300 mg of graphite powder is measured in a weighing balance for making the CPE [17]. A mortar and pestle are applied for grinding this powder. This grinding process is continued for 40 mins by adding 0.15 ml paraffin oil in the form of 2 or 3 droplets to achieve a fine paste. This paste is then placed into a capillary glass tube with a 1mm inner radius. A copper wire is inserted into the glass tube to establish electrical contact with the substance. The pictorial presentation of this developed CPE is shown in Fig.2.4.

2.2.5. Data analysis

MATLAB 2017 version is used to analyse the obtained electrochemical data. PCA tool is applied to examine the CPE performance. For each of the mentioned concentrations (50 µM, 300 µM, 600 µM, 800 µM, and 1000 µM) of MG, three sets of repetitions are considered. The prediction accuracies of recorded data are further estimated by PLSR tools.

2.2.6. Precautionary measures regarding safety

Eyes, throat and nose may feel a scorching sensation after a long-term chemical exposure to a carcinogenic agent like MG. Hence, all the precautionary measures are taken during the experimentation. There is a strict prohibition on direct inhalation or oral consumption of MG. Laboratory aprons, gloves, respiratory masks, safety goggles, and exhaust fans are used for safety. After the experiment, the MG solution is disposed of carefully. Keeping this solution in a cool and dry place is advised, away from heat, for proper storage for further use.

Fig. 2.4. CPE- the working electrode (WE).

2.3. Results and discussions for carbon paste electrode (CPE)

2.3.1. Electrochemical behavior of working electrode CPE

The voltammetry technique is applied to examine the electrochemical behavior of the CPE. The CV response of CPE within the 0.3 V to 1.5 V range is recorded with only 0.1M PBS-6 solutions, at a scan rate of 50mV/sec. Next, 100 µM of the MG solution is added to the PBS solution, and the CV response is monitored once again, the potential range and the scan rate remaining identical. Figure 2.5. depicts the appearance of an oxidation peak in the presence of the target analyte, whereas no peak is found in the absence of the same. The electrochemical reaction is noticeable at the CPE surface as the oxidation peak is achieved at 1.2 V with a peak current of 28.67 µA in the presence of the target molecule. A scan rate of 50mV/sec and a concentration of 100 µM is generally considered as a standard for the parameters optimization and basic checking. A scan rate of 50 mV/sec is a good understanding between achieving a reasonable time resolution and obtaining meaningful data. It allows for a relatively quick scan while still providing sufficient time for electrochemical processes to occur.

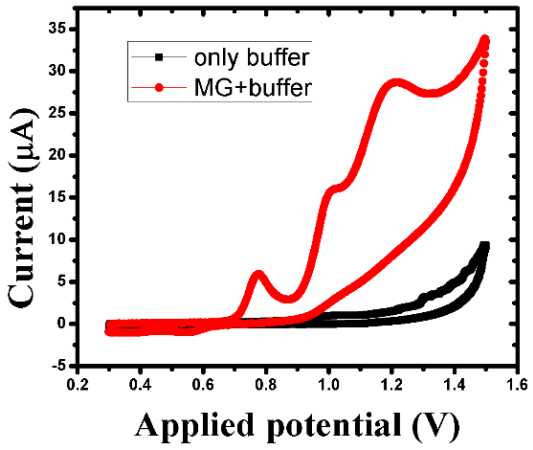

Fig. 2.5. CV response of CPE with and without MG molecule.

Higher scan rates can lead to increased noise in the recorded voltammogram. At 50 mV/s, the signal-to-noise ratio is often adequate, allowing for clear and reliable interpretation of the electrochemical response. Rapid changes in potential, especially at high scan rates, may lead to instability and distortion of the electrode surface. A moderate scan rate like 50 mV/s is less likely to cause electrode damage or instability. The choice of scan rate affects the separation and resolution of peaks in the cyclic voltammogram. A scan rate of 50 mV/s is often suitable for resolving different electrochemical processes while maintaining a manageable experimental time.

A concentration of 100 µM is often chosen as it provides a balance between having a detectable signal and avoiding excessive concentrations that increases the complications such as mass transport limitations or overlapping electrochemical reactions. This concentration allows for a measurable current response while maintaining favorable experimental conditions.

2.3.2. Effect of buffer variation

To find the optimum buffer solution, an investigation is carried out with various buffered saline (pH 6) named ABS, PBS, and CBS, respectively. From Fig.2.6. (a), it can be noticed that the oxidation Peak current (Ip) for CPE is the topmost (28.67 µA) for PBS. Hence PBS is finalized to get an optimum response using CPE for the detection of MG Next, PBS solutions with pH 5, 6, and 7 are accounted for to obtain the optimum pH. A maximum current of 28.67 µA is attained for PBS-6 (Fig.2.6. (b)); thus, pH is taken as 6 in this experiment.

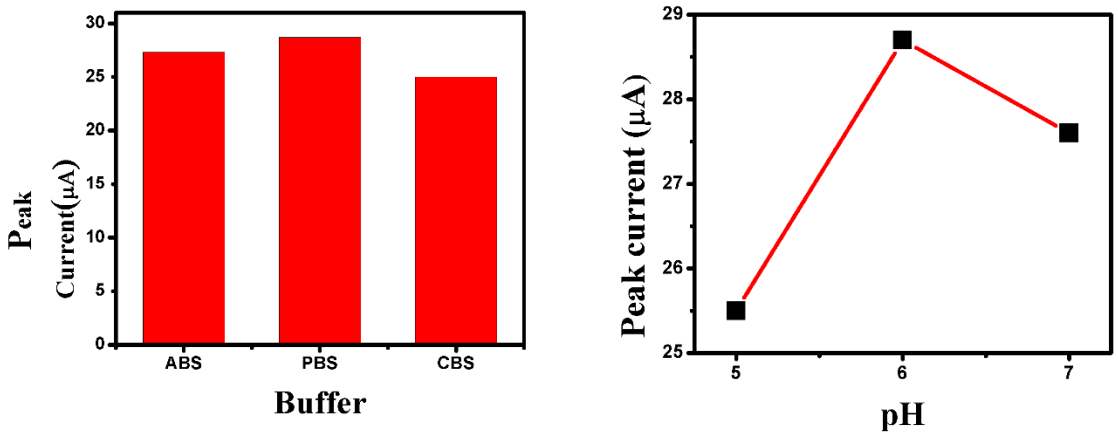

Fig. 2.6.(a) CPE response with MG for different types of buffer solutions; (b) CPE response with MG for different pH variations with optimised buffer PBS.

2.3.3 Outcome for different scan rate variation

The selection of the scan rate depends on the specific electrochemical system under observation and the goals of the experiment. Different scan rates may be employed for different studies, and experiments are often done at multiple scan rates to obtain a comprehensive understanding of the electrochemical behaviour.

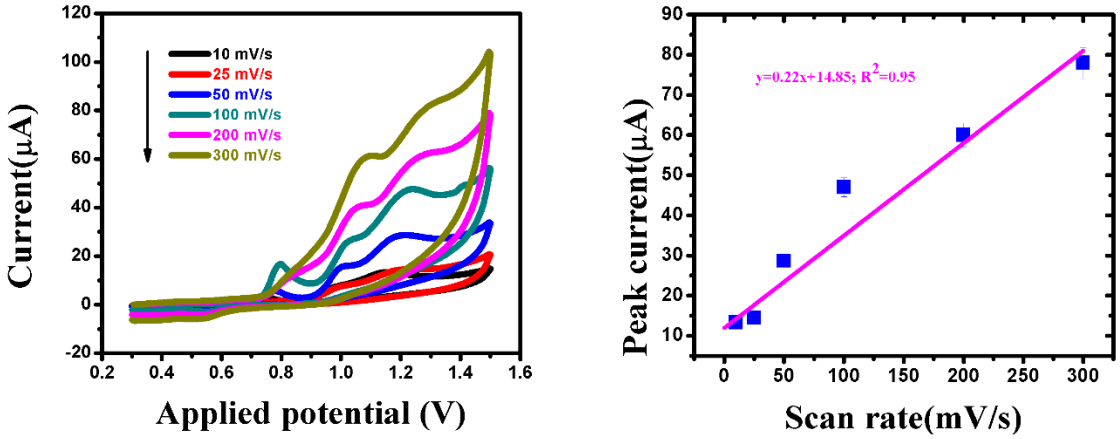

Fig. 2.7.(a) CV outcomes of changing peak current with various scan rates (10-300 mV/s); (b) linear regression of peak current vs scan rate in 0.1 M PBS.

In this study, different scan rates like 10 mV/sec, 25 mV/sec, 50 mV/sec, 100 mV/sec, 200 mV/sec, and 300 mV/sec are applied, and the impact on the peak current due to oxidation at the CPE is inspected for a better perception of the corresponding electrochemical mechanisms. The CV responses are obtained within the applied range from 0.3 V to 1.5 V for variation of scan rates. The CV plot in Fig.2.7. (a) shows that the oxidation peak current increases with a boost in the scan rate. A variation in scan rate is the reason behind the shifts in equilibrium at the electrode surface; hence, overvoltage drifts are prone to manifest, causing a reposition of

zenith potential. The regression equation for oxidation peak current derived from the linearity plot related to the scan rate variation is achieved as (2.1).

$$I_{MG} = 0.22v\ (mVs^{-1}) + 14.85;\ R^2 = 0.95 \quad (2.1)$$

which can be found in Fig.2.7. (b). The surge of peak current to its highest level with an escalation in scan rate validates an absorption-dominated mechanism.

2.3.4. Impact of various concentrations of MG

The DPV responses are monitored to study the effect of several MG concentrations at the CPE electrode surface within a potential range from 0.9 V to 1.5 V (buffer 0.1M PBS). The step-by-step increase in peak current with gradually raising MG concentrations (10µM, 50µM, 100µM, 300µM, 600µM, 800µM, and 1000µM) can be observed in Fig.2.8. (a). Figure 2.8. (b) indicates that the calibration plot has a linear pattern with the regression equation (2.2)

$$I_{MG} = 0.08C_{MG} + 2.66;\ R^2 = 0.98 \quad (2.2)$$

The LOD is achieved as 0.78µM through the equation (2.3), where σ stands for the standard deviation and m denotes the calibration curve slope, respectively.

$$LOD = 3\sigma/m \quad (2.3)$$

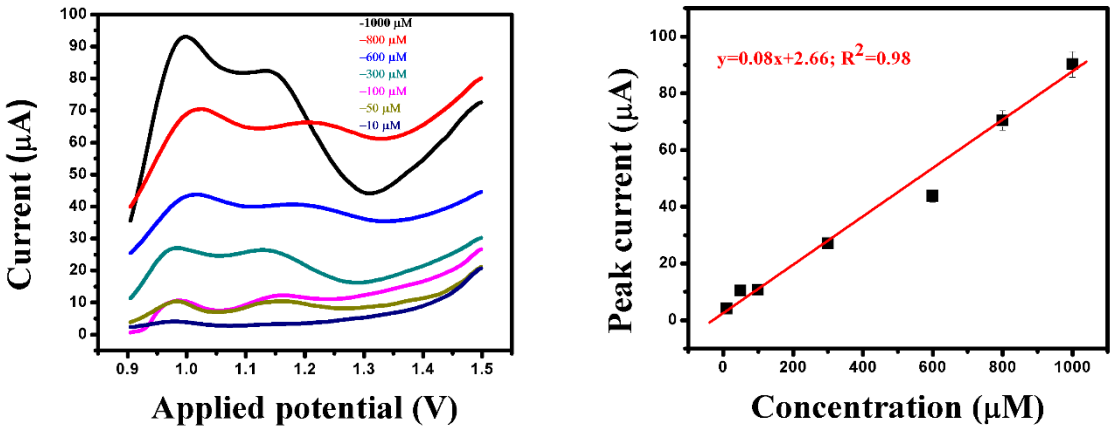

Fig. 2.8.(a) DPV measurements for MG detection using CPE in PBS solution for varying concentrations; (b) Linear plot of peak current vs concentration.

In Table 2.1, a comparative survey of the electrochemical performances with some of the formerly described works depicts that the proposed CPE offers a widely linear operative range with respect to our previous work [21] and other relevant studies.

Table 2.1. Comparison of the proposed method with other existing techniques.

Electrode	Technique	Linear range (µM)	Ref.
MWNTs/GCE	DPV	0.05-8	[14]
GQDs–Au/GCE	DPV	0.4-10	[22]
Grph-GNPs/GCE	DPV	0.1-800	[23]
CPE	DPV	10-75, 75-300	[21]
CPE	**DPV**	**10-1000**	**[This one]**

2.3.5. Repeatability, reproducibility, and stability study

A repeatability study involving three consecutive DPV responses, denoted as S1, S2, S3, demonstrates that the CPE exhibits high repeatability, with a percentage relative standard deviation (%RSD) of 2.27 (refer to Fig. 2.9.(a)).

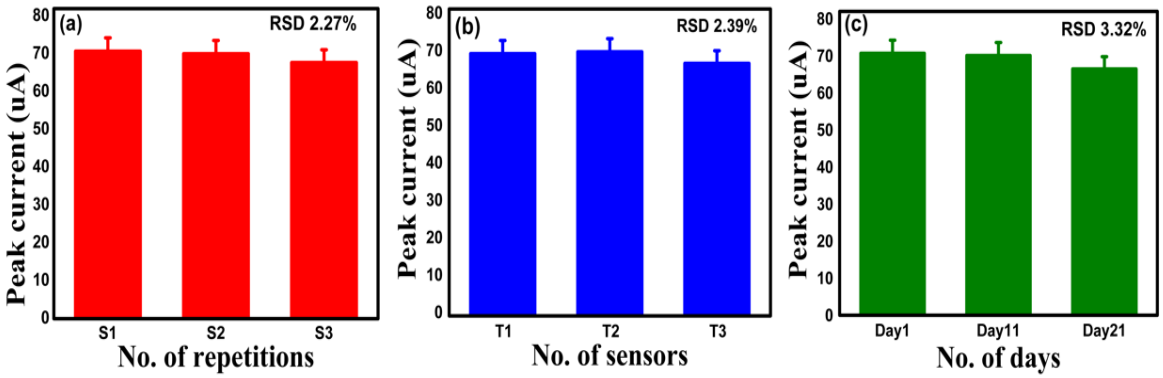

Fig. 2.9.(a)Repeatability plot; (b) Reproducibility plot; (c) Stability study.

Furthermore, the DPV responses of three identical CPEs, labelled as T1, T2, T3, are examined to assess reproducibility, yielding a satisfactory result with an RSD of 2.39% (as depicted in Fig. 2.9.(b)). In addition, a stability analysis is conducted by storing the same CPE at ambient temperature and performing the test at intervals of 10 days over a span of 21 days. The observed behaviour indicates satisfactory stability, with an RSD of 3.32% (refer to Fig. 2.9.(c)).

2.3.6. PCA plot for MG concentrations

PCA, a means of minimising dimensionality, orthogonally transforms a set of linear and correlated data into a set of non-correlated variables known as principal components (PCs) [24], [25]. The first principal component captures the maximum variability within the dataset, while subsequent components elucidate the remaining variability [26]. Utilizing PCA score plots enables swift differentiation between classes. Graphical representation of multivariate data analysis is facilitated by projecting the data onto the directions of the first two or three

principal components. The separability index (S.I.) provides a quantitative measure to discern various concentrations of MG. The ratio of trace between (S_b) to trace within (S_w) of the class scatter matrix is defined as this S.I., which is shown by (2.4) and (2.5).

$$S_b = \sum_{i=1}^{c} n_i (m_i - m)(m_i - m)^T \tag{2.4}$$

$$S_w = \sum_{i=1}^{2} \left(\sum_{j=1}^{n_i} (x_{i,j} - m_i)(X_{i,j} - m_i)^T \right) \tag{2.5}$$

Here the classes number, the samples number in the ith class, the average vector of the samples in the ith class, and the average vector of the samples are denoted by c, n_i, m_i, and m, respectively.

The DPV response curves obtained for distinct MG concentrations like 50 µM, 300 µM, 600 µM, 800 µM, and 1000 µM (C1, C2, C3, C4, and C5, respectively) using the developed CPE are analysed using PCA tool. Three repetitions are studied for each concentration. The PCA plot with successful data clustering is shown in Fig.2.10., where all the different concentrations are rightly discriminated. The PC1 and PC2 illustrate 85.80%, and 10.39% of total variances, respectively. A high value of the S.I. is calculated as 74.77, suggesting a clear separation of the classes in the dataset.

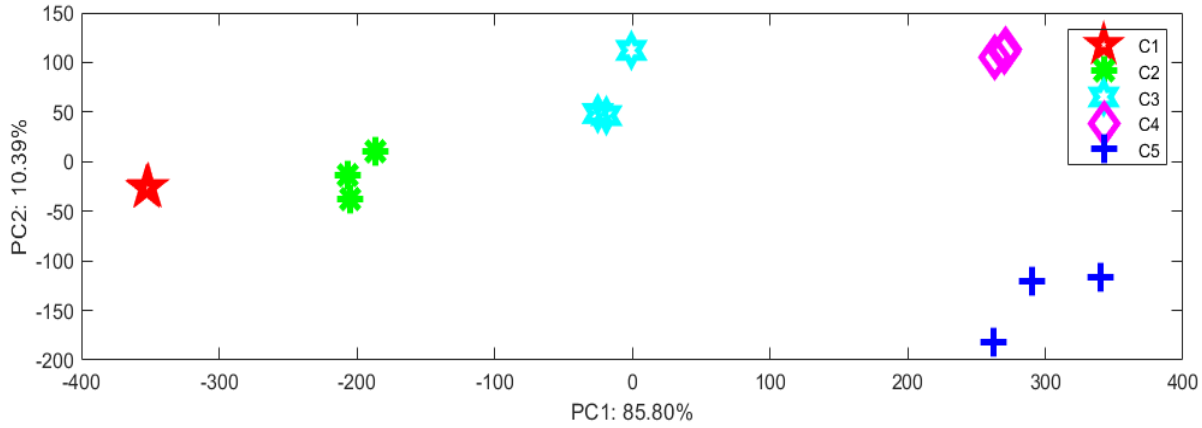

Fig. 2.10. DPV data analysis using PCA-a graphical representation.

2.3.7. PLSR for MG concentrations

PLSR algorithm draws the components out by the robust correlation between predictor variables and the quantity of the response variable, through which the predictors count is reduced [27]. In the current analysis, the 'leave one out' principle-based cross-validation technique is applied for the sensor to estimate MG concentration. The correlation level between the approximated and actual values can be represented by parameters like correlation factor

(C.F.), and root mean square error of prediction (RMSEP). In this presented research work, to estimate the prediction capability of CPE, different concentrations of MG (C1-C5) have been used. For each concentration, 75% of the data are treated for training purposes and 25% as the test set. A pretty prediction accuracy of 95.39% is achieved for the CPE using PLSR. The prediction parameters are summarised in Table 2.2 [27].

Table 2.2. Comparison of actual and predicted MG contents achieved via PLSR.

No. of samples	Actual MG contents (µM)	Predicted MG contents (µM)	Prediction accuracy (%)
1	50	52.63	94.74
2	300	316.91	94.36
3	600	604.70	99.22
4	800	867.23	91.6
5	1000	1029.78	97.02
Average prediction accuracy 95.39%			

Table 2.3. Different parameters of PLSR.

C.F. (training)	C.F. (prediction)	RMSEP
0.99	0.99	12.1

In Table 2.3, the correlation factor found after prediction is indicative of a nicely performing model in terms of accurate prediction of the response variable based on the predictor variables.

2.3.8. Real sample analysis

The diluted MG solution is exposed to measurements by the standard addition method. No preprocessing technique is applied before in this case. Various concentrations (10µM and 20µM) of MG solutions are added by spiking to the water, and the DPV technique is applied for the corresponding analysis purpose [27].

Table 2.4. Determination of MG in an aqueous sample using CPE

Sample	Spiking (µM)	Detected (µM)	Recovery [a] (%)	± RSD [b] (%) (n=3)
Water pure	0	0	-	-
Water spiked	10	9.73	97.3	1.54
	20	18.97	94.85	1.61

[a] Recovery = [Detected (µM)-Diluted sample (µM)]/Spiking (µM)
[b] RSD (%) = [100x Standard deviation]/ Mean

The achieved observations summarised in Table 2.4. show that the spiked sample's recovery rate is 97.3% and 94.85%, with RSD values of 1.54% and 1.61%, respectively. These results suggest that this electrode is free from the matrix effect while detecting MG.

2.3.9. Discussion

This present study focuses on the quick electrochemical detection of malachite green using an optimised CPE. The system described a wide operational range with linearity within 10µM to 1000µM and a LOD of 0.78µM. The DPV responses obtained using this electrode for various concentrations of MG were analysed effectively via the PCA tool with fair discrimination of each concentration. Besides the data clustering, a high value of S.I. (74.77) is attained. Moreover, the regression model of PLSR shows prediction accuracy of 95.39%. The application of this CPE on actual aquatic samples containing MG showed excellent recovery rates of 94.85% to 97.3%. This suitable efficacy of the CPE-centred electrochemical system is used to detect various MG traces in pond water and fish in the next study, where the detailed cover up of a CuO nanoparticles modified GPE has been presented.

2.4. Experimentation with CuO nanoparticles modified graphite paste electrode (CuO@GPE)

2.4.1. Reagents and chemicals used

Copper chloride ($CuCl_2$), cetylpyridinium chloride ($C_{21}H_{38}NCl$), ethanol, and sodium hydroxide (NaOH) are procured from Merck & Co, India. All other reagents used are detailed earlier in the Section 2.2.1. of this chapter.

2.4.2. Synthesis of copper oxide (CuO) nanoparticles

The sol–gel method is applied [27], [28] to synthesize the copper oxide nanoparticles in the research lab. Concisely, 10 g of $CuCl_2$ is first dissolved in 500 ml ethanol via quick stirring. Surfactant cetylpyridinium chloride ($C_{21}H_{38}NCl$) is added to this solution and then appropriately mixed by stirring for 30 min. Next, the dropwise introduction of 1 N NaOH solution into the mentioned reaction mixture is continued until the pH of the solution becomes 8–9. After some time, green-colored precipitation is found. It is filtered and dried in the hot air oven at 50°C. After air-dehydration, the residue is combusted at 400°C for around 3 h to obtain a black-colored CuO powder. The resultant CuO is then utilized for characterizing and preparing the electrode. The total measurement steps from the synthesis of CuO nanoparticles to the data recording by 3-electrode cell including the formation of CuO@GPE have been shown in Fig.2.11.

2.4.3. Characterizations

A Bruker D8 Advance diffractometer is used to study the X-ray diffraction (XRD) pattern of the synthesized CuO NPs. X-ray photoelectron spectroscopy (XPS) analysis is done using a Thermo Scientific, K-Alpha spectrometer operated with a monochromatic Al Kα X-ray source (1486.7 eV). The surface morphology of the CuO NPs is studied using scanning electron microscopy (SEM) (CARL ZEISS EVO 18). A 15 kV accelerated voltage is applied to operate this SEM. A three-electrode system is used for the behavioural study of the electrode with Autolab Potentiostat/ Galvanostat 101 (Metrohom Autolab, Netherlands). The platinum (Pt) electrode and Ag/AgCl electrode are used as the counter electrode (CE) and reference electrode (RE), respectively. A voltage range of 0.3V to 1.5V is considered for CV and DPV analysis.

2.4.4. CuO@GPE fabrication

CuO NPs and graphite powder are taken 30 mg, and 270 mg, respectively (Weight ratio of 1:9), and thus, 300 mg of the material was entirely blended by a mortar pestle [27]. The mentioned ratio is chosen by a trial-and-error method as the best current response is achieved using the graphite and CuO NPS in this ratio. Paraffin oil (2-3 drops), the binder material, is added to the above mixture for the formation of a smooth paste. This material is used to stuff a 2 mm inner diameter glass capillary tube. For proper electric connection with the sensor material, a copper wire is fitted across the rear side of the capillary tube. The same process is followed for developing the bare graphite paste electrode (bare GP) using only 300 mg of graphite powder.

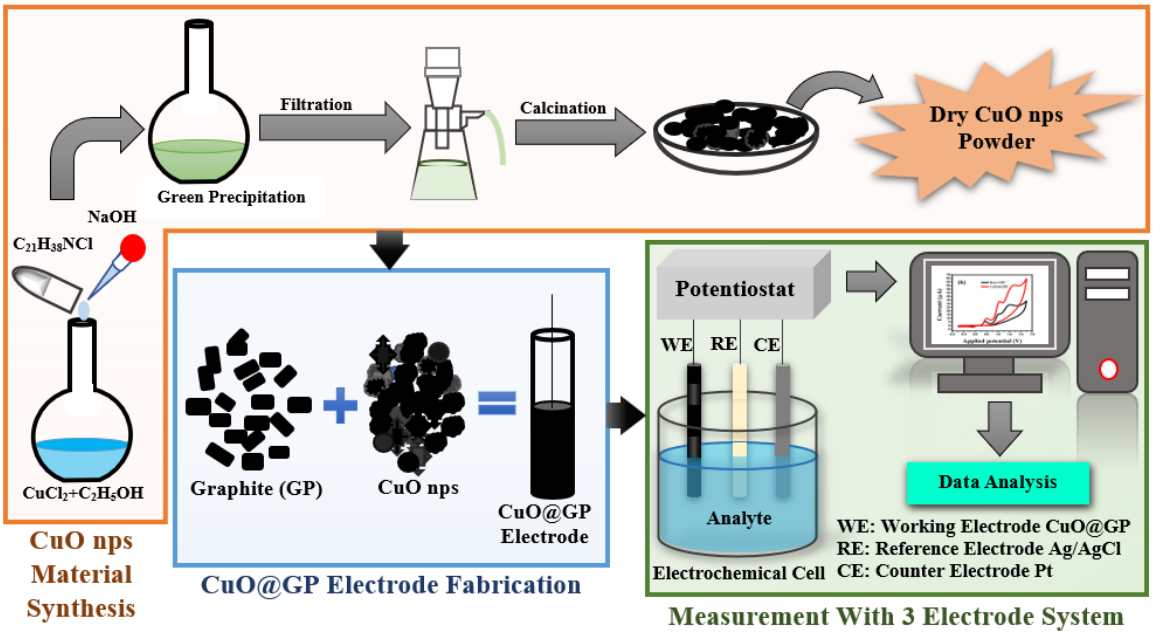

Fig. 2.11. Steps of measurement procedure for voltametric MG detection using CuO@GPE.

2.4.5. Real sample preparation

The carp are collected from the community market. After filleting the fish, the skin and bones are separated, and the muscles are minced. These fillets are kept deep-frozen before analysis. Around 20g weight, a piece of fish is blended with Millipore water and then put into an oven for some time. Once the fish fillet is boiled enough, the water is collected and used after filtration. For analysis of pond water, it is collected from a local pond and filtered before use for further research.

2.4.6. Safety features

As the molecule under study is MG here also, same type of safety features is followed as mentioned in the Section 2.2.6 of this chapter.

2.5. Results and Discussions for CuO@GPE

2.5.1. XRD characteristics of CuO nanoparticles

The X-ray diffraction (XRD) pattern of CuO NPs is illustrated in Fig. 2.12., displaying the monoclinic CuO structure. The XRD pattern resembles the standard JCPDS card no. 48-1548.

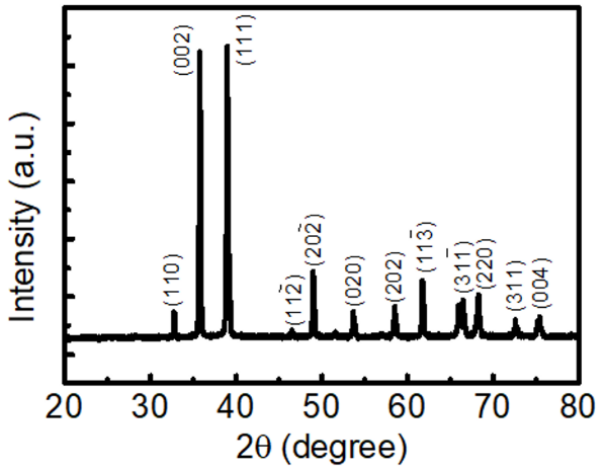

Fig. 2.12. XRD pattern of synthesized CuO nanoparticles.

The prominent diffraction peaks are observed at 32.73º, 35.77 º, 38.96 º, 46.47 º, 48.98 º, 53.66 º, 58.52 º, 61.73 º, 66.47 º, 68.29 º, 72.61 º, and 75.43 º, corresponding to the diffraction planes of (110), (002), (111), (11$\bar{2}$), (20$\bar{2}$), (0202), (202), (11$\bar{3}$), (3$\bar{1}$1), (220), (311) and (004), respectively. The lattice constants a, b, and c are 0.4688, 0.3423, and 0.5132 nm, respectively. No distinctive peak against other phases was discovered, indicating that the nanoparticles are constituted of purely monoclinic CuO and free from other impurities. This XRD response is comparable to [29].

2.5.2. SEM measurements

Scanning electron microscopy (SEM) graphs of CuO modified Graphite and CuO NPS are shown in Fig. 2.13.(a) and 2.13.(b), respectively. Via this SEM, the surface morphology of the CuO NPS can be studied where the particle size is found to be 194 nm by mean length. It reveals that the prepared materials contain nanoparticles.

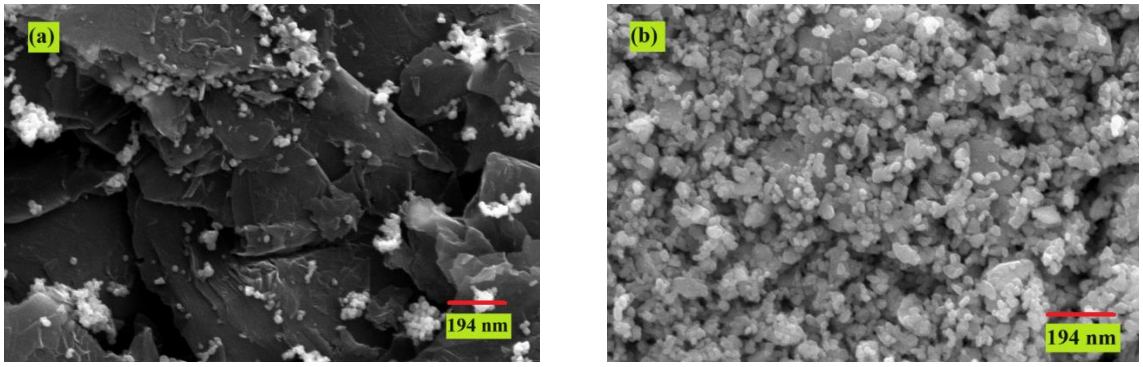

Fig. 2.13. SEM image of (a) CuO-modified graphite; and (b) CuO nanoparticles.

2.5.3. XPS analysis

XPS study is done to get information about the elemental compositions of CuO NPs. XPS survey scan in Fig.2.14. (a) reveals that CuO is constituted of Cu and O elements. There is also an adventitious C1s peak observed in the spectra due to environmental contaminations. In Fig. 2.14. (b), the high-resolution spectra of Cu 2p exhibit two peaks at 953.3 and 933.4 eV, corresponding to 2p 1/2 and 2p 3/2, respectively. Satellite peaks are also observed at 961.9, 943.5 and 941.1 eV. The Main Core level spectra of O 1s are observed at 529.3 eV, as found in Fig.2.14. (c). Adventitious oxygen species are also present due to environmental contaminations. This XPS response is comparable to [30], [31].

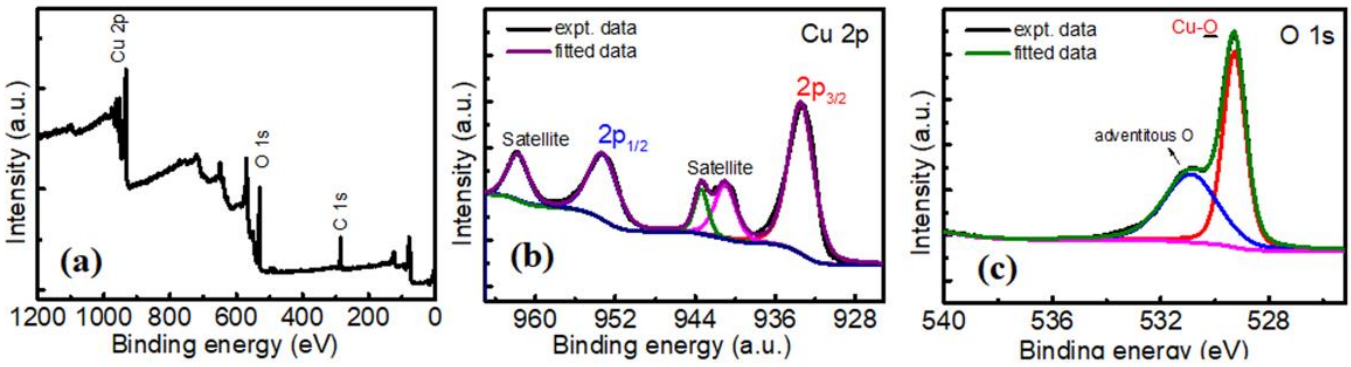

Fig. 2.14. XPS analysis. (a) XPS spectra of CuO nanoparticles showing complete scan survey; (b-c) High-resolution spectra for Cu 2p and O 1s from synthesized CuO nanoparticles, respectively.

2.5.4. Electrocatalytic behaviour of CuO@GPE

The voltammetry principle is applied to study the CuO@GPE along with its electrochemical behavior. Firstly, the CV response of the CuO@GPE is monitored in the presence of a supporting electrolyte PBS (0.1 M) in a voltage range of 0.3-1.5 V. In the absence of the analyte molecule, no oxidation peak is visible in the response, as shown in Fig.2.15. (a). Next, a specific MG concentration is added to the above solution, and the result is observed.

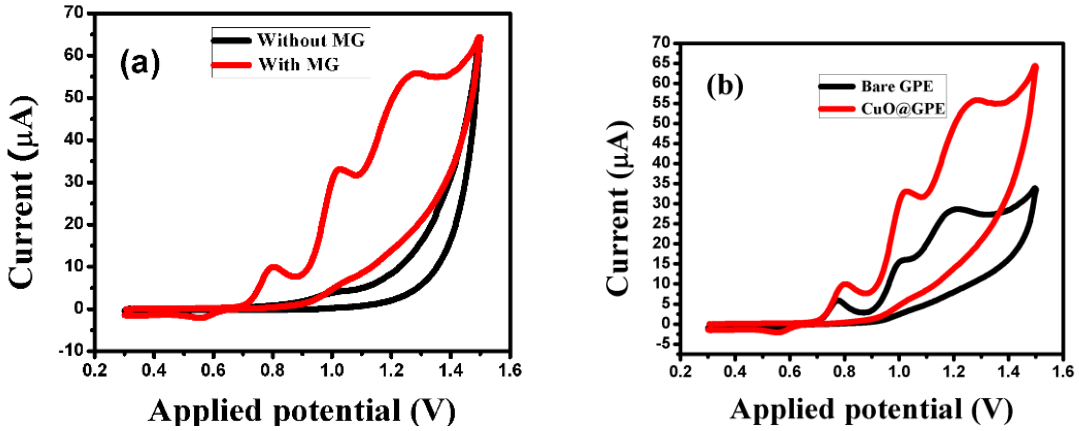

Fig. 2.15. CuO @GPE CV response in 0.1 M PBS (a) without and with MG; (b) performance comparison with bare GPE.

The appearance of the anodic oxidation peak at a potential of 1.28 V indicates the successful detection of the analyte molecule. A bare GPE replaces the CuO@GPE in the same solution, and a current of 28.67 µA is achieved. From Fig.2.15. (b), it is found that the maximum peak current of 55.8 µA is obtained using the CuO@GPE. Thus, it is proved that incorporating CuO nanoparticles into bare graphite powder amplifies the oxidation peak current of MG by more than 1.9 (almost 2) times and leads to advanced electron kinetics in the face of the molecule aimed at. This enhancement in the electrocatalytic activity of CuO@GPE may result from the inclusion of CuO nanoparticles which maximizes the electroactive surface area and thus leads to quicker electron transfer flow between the electrode surface and target molecule. Primarily the MG molecules from the aqueous solution adsorb onto the active sites of the CuO@GPE affected by the pH of the solution, temperature, and the presence of other ions or molecules. When the electrode is exposed to an applied potential, the adsorbed MG molecules are oxidized at its surface. The general representation of the oxidation reaction is:

$$MG\ (reduced\ form) \rightarrow MG\ (oxidized\ form) + e^-$$

The electrons (e-) produced during the oxidation of MG are transferred to the electrode, producing a current.

2.5.5. Effect of buffer and pH change

The CuO@GPE responses to CV depend on the nature of the buffer solution used and the pH of the medium. For finding the optimum buffer for the best current response, three different buffers, Phosphate (PBS), Phthalate (PHT), and Acetate (ABS), are used. From Fig.2.16. (a), it can be noticed that the electrode exhibits the highest peak current (55.8 µA) subjected to PBS solution with respect to PHT and ABS. Next, to find the optimum pH of the experimental system, the redox processes are performed using PBS in the pH ranges of 2,5,6 and 7.

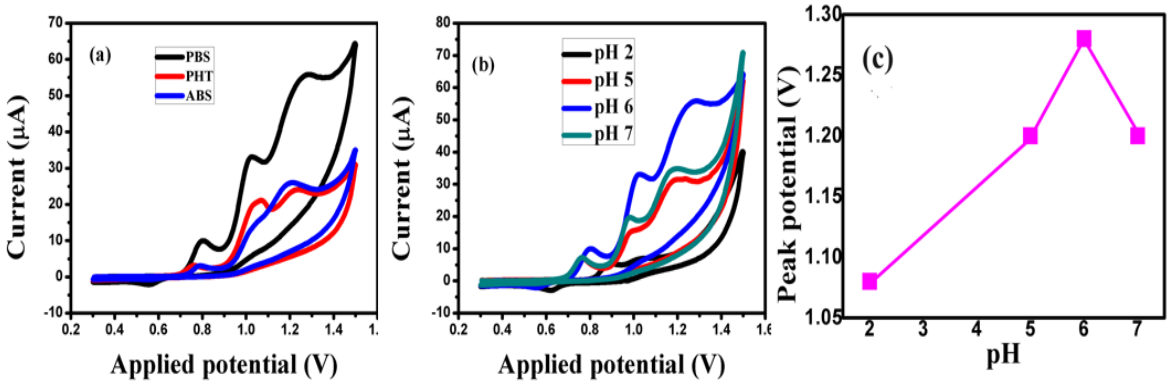

Fig. 2.16. CuO@GPE CV response to MG for (a) buffer optimization; and (b) pH optimization (I vs pH); (c) Plot for peak potential versus pH (2, 5, 6, 7).

In Fig.2.16. (b), it is observed that the maximum peak current occurs at pH 6. It falls again when the pH of the PBS solution further increases to 7 possibly because of weak adsorption of MG. Therefore, each experiment is done at pH 6 of PBS buffer. The plot for oxidation peak potential vs. pH can be found in Fig.2.16. (c).

2.5.6. Influence of scan rate variation

In the case of electrochemical sensors, scan rate optimization is mandatory. The impact of varying scan rates towards the electrochemical detection of MG molecule using CuO@GPE is tested using the CV technique within a range of 0.3 V-1.5 V. From Fig.2.17. (a); it is observed that the anodic peak current incremented linearly with an increasing scan rate from 5 to 400 mV/s. This observation suggests this oxidation of MG molecule to be an absorption-controlled phenomenon. The corresponding characteristic plot in Fig.2.17. (b) follows the linear regression equation (2.6)

$$I_{MG} = 0.63v\ (\mathrm{mVs^{-1}}) + 23.05;\ R^2 = 0.97 \quad (2.6)$$

The number of electrons-transfer during this process is obtained using Eq. (2.7)

$$Ip = \frac{nFQv}{4RT} = \frac{n^2F^2Av\Gamma_C}{4RT} \quad (2.7)$$

where Ip represents the peak current, n defines the number of electrons transmitted, F stands for Faraday's constant, R depicts the molar gas constant, T specifies the ambient temperature,

A the surface area of the electrode, Γ_C is the surface concentration of MG, Q is the charge consumed in time of the oxidation, and v denotes the scan rate [27]. The number of transferred electrons, n, is calculated to be 1.53 ~2, which may be compared with the study by [32], [33], and the surface concentration of MG, Γ_C is 1.3×10^{-8} mole /cm^2. The charge transfer coefficient α is found to be 0.5. It is calculated from the slope of the curve equal to $^{2.3RT}/_{(1-\alpha)nF}$ [27]. Next, the linear plot of peak potential (Ep) vs $logv$, as shown in Figure 2.16.(c), is considered to determine the electron transfer coefficient. The related regression equation is in (2.8),

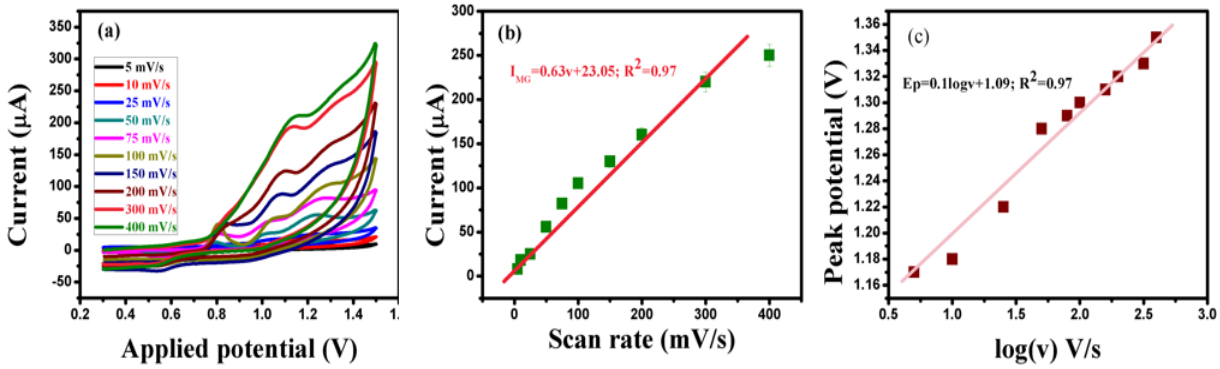

Fig. 2.17 a) CV outcome of peak current variation with various scan rates (5-400 mV/s); (b) Linear regression scheme-peak current vs. scan rate in 0.1 M PBS; (c) Linear plot of peak potential vs. log of scan rate.

$$Ep = 0.1logv + 1.09; R^2 = 0.97 \quad (2.8)$$

Laviron's equation, shown in Eq. (2.9), was applied to calculate k_s, the electron transfer rate.

$$logks = \alpha\, log(1-\alpha) + (1-\alpha)log\alpha - (logRT/nFv) - (nF\Delta Ep\alpha(1-\alpha)/2.3RT) \quad (2.9)$$

The k_s is found to be 0.016 s^{-1}. For an electrochemical mechanism, the degree of chemical reversibility depends on the rate of the chemical reaction. A higher value of the reaction rate constant may lead the response to the verge of chemical irreversibility [27]. The variation in scan rate may cause the shift in equilibrium at the electrode surface, resulting in overvoltage drifts, causing the peak potential to be repositioned.

2.5.7. Influence of concentration variation

Being capable of reducing non-faradic current, DPV is more current-sensitive than CV and provides better resolution. With the increase in the concentration of the MG molecule up to 1000µM (1µM, 10µM, 50µM, 100µM, 300µM, 400µM, 500µM, 600µM, 700µM, 800µM, and 1000µM), the corresponding current profile is observed via DPV analysis which is illustrated in Fig.2.18. (a). Figure 2.18. (b) simultaneously presents the linear relationship between the

oxidation peak currents with gradually increasing concentrations of the target analyte from 1µM to 1000µM. The linear range is found following the regression equation (2.10)

$$y = 0.08x + 5.61\ (R^2 = 0.99) \quad (2.10)$$

The results reveal that MG is detected with the best selectivity, sensitivity, and favourable resolution using CuO@GPE. With a fair dynamic linear range, MG's limit of detection (LOD) is achieved as 0.18µM with this newly developed electrode based on equation (2.3) mentioned in the Section 2.3.4. The reason behind the root of the oxidation potential is the Schottky barrier formed at the terminal of WE and MG. Various factors like the acidity of electrolyte, scan rate, and MG adsorption at different concentrations control this Schottky.

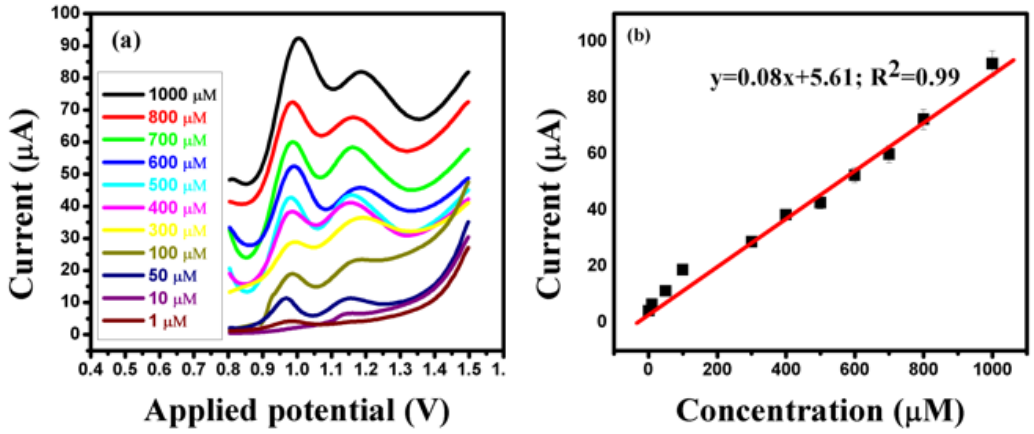

Fig. 2.18. (a) DPV measurement plots for MG detection using CuO@GPE in 0.1 M PBS solution for variable concentrations; (b) Linear plot of peak current vs. concentration.

Here, the oxidation potential moves after a specific concentration of MG because of the assertive adsorption property of MG into the WE surface. The analytical results matched with other related works are briefed in Table 2.5, showing that the LOD achieved here is less than those in earlier studies.

Table 2.5. Proposed CuO@GPE performance comparison for detecting MG with earlier reports.

Electrode material	Linear range (µM)	LOD (µM)	Ref.
Silica modified GCE	1-6	0.36	[34]
GCE/CeO_2/Nafion	1-100	1.025–7.880	[35]
CPE	10-1000	0.78	[2]
GCE/Graphene quantum dots/Gold	0.4-10	0.1	[22]
CuO@GPE	1-1000	**0.18**	**This work**

2.5.8. Repeatability, reproducibility, and stability

Four consecutive DPV readings are taken using the proposed electrode for repeatability study using 100µM and 500µM MG content (U1, U2, U3, U4, and U1', U2', U3', U4' respectively)

and corresponding Bar diagrams are presented in Fig.2.19. (a) and Fig.2.19. (b). No remarkable change is noticed in the peak current. Corresponding relative standard deviation (RSD) is found as 2.18% and 2.09%, respectively, indicating an excellent measure of repeatability. Next, four similar CuO@GP electrodes are developed to study this sensor's reproducibility. Figure 2.20. (a) and Fig. 2.20.(b) demonstrates the bar diagrams for the DPV response of these electrodes, namely V1, V2, V3, V4, and V1', V2', V3', V4', in 100µM and 500µM of MG solution respectively. The oxidation peak currents were almost similar, signifying a pleasant reproducibility where the corresponding RSD values are 2.21% and 2.03%, respectively. During the stability study of the proposed sensor, a single CuO@GPE is examined several times at room temperature for one month. The data is recorded at regular intervals of 10 days. Here also, the DPV data are recorded in 100µM and 500µM MG, with bar diagrams shown in Fig.2.21. (a) and Fig.2.21. (b), respectively. The RSD for the stability study is 3.14% and 2.36%, respectively. The gradual fall of the peak current may be due to the ageing effect of the electrode because of countless uses during the extended period.

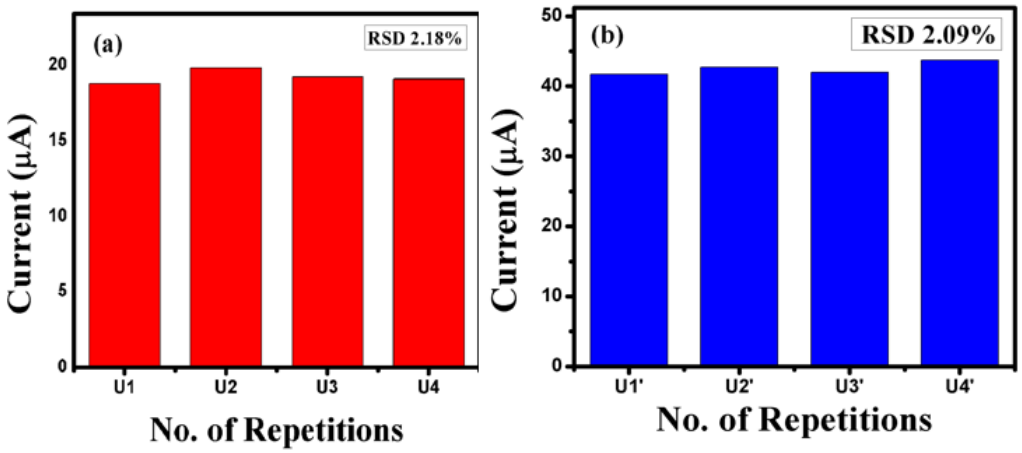

Fig. 2.19. Bar diagram for repeatability of CuO@GPE for (a)100µM MG; and (b) 500µM MG.

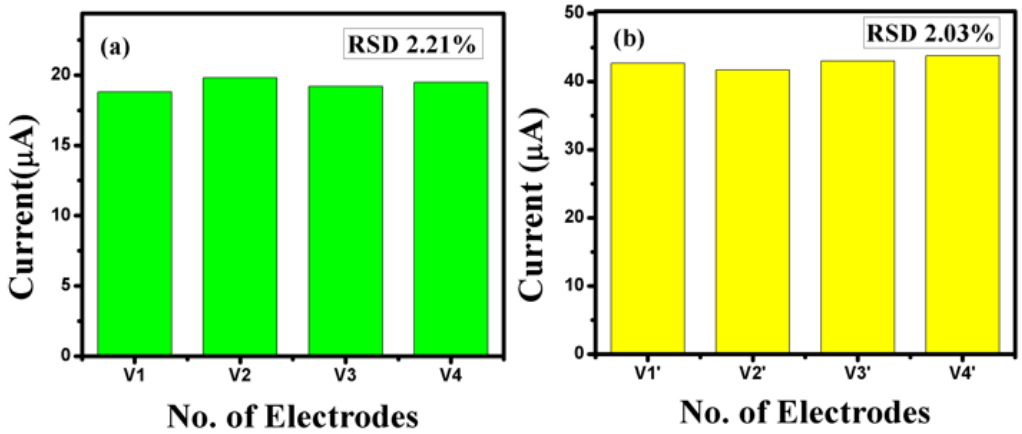

Fig. 2.20. Bar diagram for reproducibility of CuO@GPE for (a)100µM MG; and (b) 500µM MG.

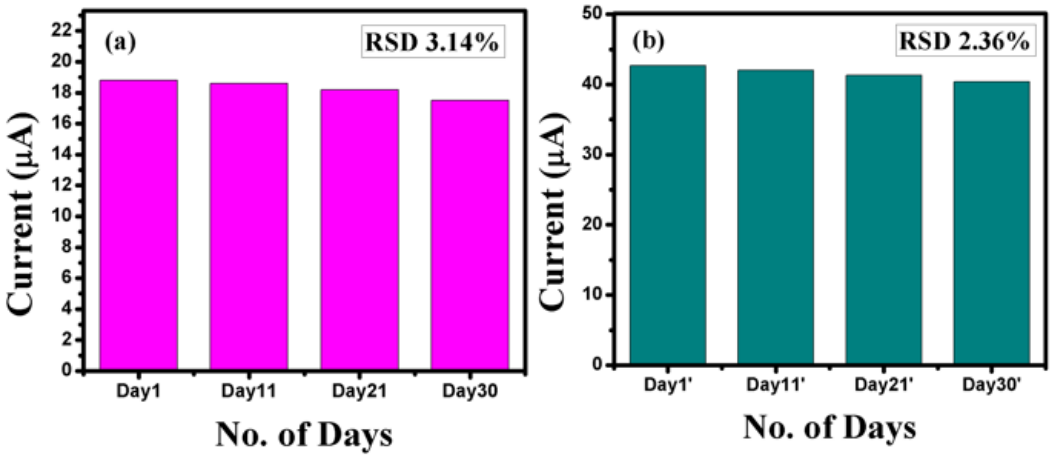

Fig. 2.21. Bar diagram for stability of CuO@GPE for (a)100μM MG; and (b) 500μM MG.

2.5.9. Interference and selectivity

CuO@GPE is subjected to multiple available interfering molecules like Dopamine (DA), Caffeine, Methyl Violet and inorganic ions like Na^+, K^+, and Cl^- to study its sensitivity. Figure 2.22. (a) depicts this profile where the plotting is done for the relative changes of signal affected by various interferences against the response obtained with target analyte only.

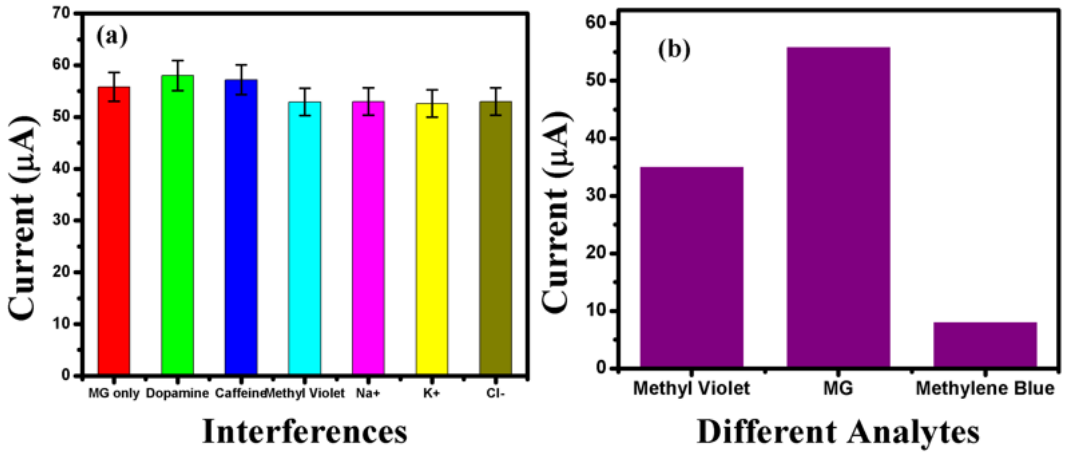

Fig. 2.22. Bar diagram for CuO@GPE in 100μM MG for (a) interference study; and (b) selectivity.

The presence of annoying materials over MG reveals no notable difference in oxidation peak current (±5% tolerance limit). The peak currents data are stored for the selectivity study by exposing the CuO@GPE to MG, Methyl Violet, and Methylene Blue. The highest current is achieved for MG solution compared to Methyl Violet and Methylene Blue solutions. This incident proves the selective nature of this electrode. The corresponding selectivity profile is shown in Fig.2.22. (b).

2.5.10. PCA plot for MG concentrations using CuO@GPE

PCA, the statistical procedure, allows the summarization of the information contained in large data tables by means of a comparatively small set of summary indices which is more convenient

to visualize and analyze. The PCA technique, already explained in the Section 2.3.6 of this chapter, has been applied here also for analyzing the data generated by CuO@GPE.

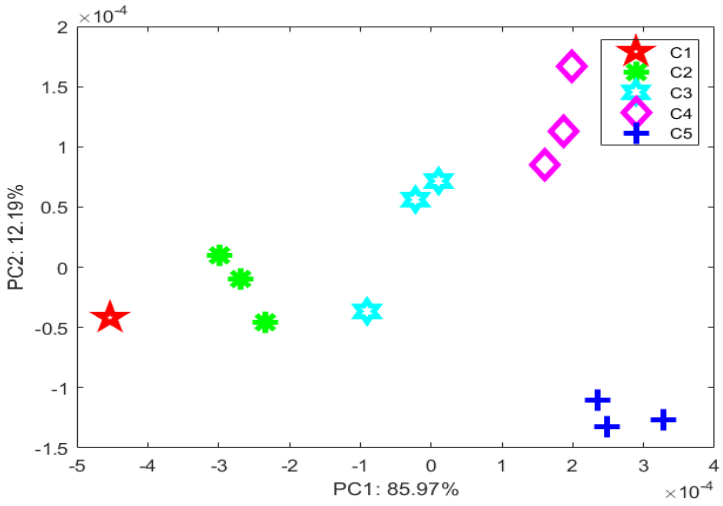

Fig. 2.23. DPV data analysis using PCA-a graphical representation.

The DPV response curves for MG concentrations (50 µM, 300 µM, 600 µM, 800 µM, and 1000 µM as C1, C2, C3, C4, and C5, respectively) using the developed CuO@GPE are studied using this PCA tool. Three repetitions are considered for each concentration. The PCA plot with successful data clustering is shown in Fig.2.23., where all the different concentrations are found to be rightly discriminated. The PC1 and PC2 illustrate 85.97%, and 12.19% of total variances, respectively. A high value of the S.I. is calculated as 80.99, suggesting a clear separation of the classes in the dataset. Besides, this S.I. value is higher than the S.I. obtained in case of CPE based detection of MG, indicating better separation and potentially more meaningful insights into the underlying data structure in case of the modified GPE, which probably may be because of the incorporation of CuO nanoparticles modifier.

2.5.11. PLSR analysis

Here, to estimate the prediction capability of CuO@GPE, different concentrations of MG (C1-C5) have been sent through the data analysis method called PLSR, which is described earlier in the section 2.3.7 of this chapter. For each concentration, training data and testing data were taken in a ratio of 3:1. The prediction parameters are summarised in Table 2.6 as follows. In Table 2.7, the higher correlation factor found after prediction indicates that the PLSR model has succeeded in enhancing the prediction accuracy compared to using the original independent variables alone. Thus, in case of CuO@GPE, PLSR model is able to explain more variance in the dependent variable and has better predictive power in comparison with the initial correlation before prediction. It suggests that the latent variables extracted by PLSR are more

effective in capturing the underlying structure of the data and predicting the dependent variable accurately.

Table 2.6. Comparison of actual and predicted MG contents achieved via PLSR for CuO@GPE.

No. of samples	Actual MG contents (µM)	Predicted MG contents (µM)	Prediction accuracy (%)
1	50	62.23	75.54
2	300	278.8	107.07
3	600	539.69	110.05
4	800	862.32	92.21
5	1000	1067.08	93.29
Average prediction accuracy 95.63%			

Table 2.7. Different parameters of PLSR for CuO@GPE.

C.F. (training)	C.F. (prediction)	RMSEP
0.9882	0.9934	17.3

The prediction accuracy has been increased in case of CuO@GPE with respect to the same for CPE for the voltammetric detection of MG.

2.5.12. Investigation of MG in real sample

Local pond water and fish flesh are considered to study the real-life application of this developed electrode. Water samples collected from local fish ponds are filtered through a grade 2 qualitative filter paper of 0.2 µM pore size. Rohu and Catla fish samples are purchased from a local fish market. Each fish is decapitated, gutted, peeled, sliced, crushed and homogenized. After washing correctly, the fish fillets are set to boiling in Millipore water for around 30 minutes. Once the fish flesh decomposes and mixes with the water, it is collected after proper filtration. The water and fish sample solutions are then kept in the voltammetric cell respectively, and the previously mentioned method is followed under optimum conditions to determine the presence of MG in the analysis of pond water samples; no MG signal is noticed, indicating the probability of no MG in water or the lower MG concentration than the detection limit. In the fish sample solutions analysis case, there is a trace of MG in some samples, while the other pieces are found free. The standard addition method was then undertaken. MG solution concentrations (10 µM and 20 µM) were mixed with the pond water and fish specimens for recovery analysis. The observations are exhibited in Table 2.8. The recoveries of the spiked samples are found to be good, indicating the ability of the system to determine MG in water and fish samples. The F test and student test are performed to check whether the reference (spiked data) was statistically similar to the detected data.

Table 2.8. Determination of MG in pond water and fish samples.

Sample	Spike (µM)	Detect (µM)	Recovery [a] (%)	RSD [b] (%) (n=2)
Pond water	0	0	-	-
	10	9.8	98	1.46
	20	22.77	113.85	2.1
Fish 1	0	0	-	-
	10	9.5	95	2.2
	20	18.97	94.85	1.22
Fish 2	0	1	-	-
	10	11.3	103	3.2
	20	21.7	103.5	2.66

[a] Recovery = [Detected (µM)-Diluted sample (µM)]/Spiking (µM)
[b] R.S.D (%) = [100x Standard deviation]/ Mean

F test is done to check the similarity in their standard deviation (SD). Here, the F-ratio (1.3, 1.11, and 1.07 for pond water, Fish 1, and Fish 2, respectively) and p-value (0.87,0.95, and 0.97, respectively) are found to be pretty hopeful. Student tests throw light on the similarity between the mean values of the data sets [36]. The output values for the student's t-test-related p-value are found to be 0.93, 0.95, and 0.88, respectively.

2.5.13. Comparative study for basic CPE and CuO@GPE: their performance parameters for detecting MG

Table 2.9 is presented here to summarize the performance indices of CPE and CuO@GPE for the voltametric detection of MG.

Table 2.9. Comparison between CPE and CuO@GPE performance to detect MG.

Sl. No.	Parameter	CPE	CuO@GPE
1	Maximum peak current	28.67µA	55.8µA
2	R^2 (Scan Rate)	0.95	0.97
3	R^2 (Concentration)	0.98	0.99
4	RSD(Repeatability)	2.27%	2.09%-2.18%
5	RSD(Reproducibility)	2.39%	2.03%-2.21%
6	RSD(Stability)	3.32%	2.36%-3.14%
7	Stability span	21 Days	30 Days
8	Separability index (S.I.)	74.77	80.99
9	Prediction accuracy	95.39%	95.63%
10	LOD	0.78µM	0.18µM

Different parameter values clearly indicate that the modification of CPE with the CuO nanoparticles undoubtedly improves its efficiency for the voltametric detection of MG. Though the RMSEP value increases little bit in case of the CuO@GPE, but it has been granted considering all other improvements in efficiency in case of CuO@GPE with respect to CPE performance. The Table 2.9 hence includes all the improved parameter values of CuO@GPE in comparison with the CPE parameter values.

2.6. Conclusion

In this chapter, the voltametric detection of MG using CPE and CuO@GPE has been narrated. the CuO nanoparticles modified graphite paste yielded an advanced electrochemical sensing platform for detecting Malachite Green in pond water along with Rohu and Catla fish fillet samples. CuO@GPE exhibited a superb electrochemical performance with a widely linear operating range of 1 µM to 1000 µM. The LOD is 0.18 µM, lower than 0.78 µM, the LOD of the CPE. The electrocatalytic behavior of the CuO@GPE was found to be an absorption-controlled process with a high electron transfer rate. The proposed CuO modified electrode was highly selective, repeatable, reproducible, and stable, with a fair enough recovery rate over countless uses for around a month. Thus, this newly developed electrode has demonstrated its power to be a field-deployable, pocket-friendly sensor for Malachite Green trace detections in fishes and aqueous solutions soon to achieve a much lower detection limit.

References

[1] A. Stammati *et al.,* "Effects of malachite green (MG) and its major metabolite, leucomalachite green (LMG), in two human cell lines," *Toxicology in Vitro*, vol. 19, no. 7, pp. 853–858, 2005, doi: 10.1016/j.tiv.2005.06.021.

[2] S. Dasgupta *et al.*, "Development and detailed performance study of a carbon paste electrode for the electrochemical detection of malachite green," *Nano Life*, vol. 13, no. 2, pp. 1–9, 2023, doi: 10.1142/s179398442350006x.

[3] K. Mitrowska, A. Posyniak, and J. Zmudzki, "Determination of malachite green and leucomalachite green in carp muscle by liquid chromatography with visible and fluorescence detection," *Journal of Chromatography A*, vol. 1089, no. 1–2, pp. 187–192, 2005, doi: 10.1016/j.chroma.2005.07.004.

[4] L. Valle, C. D´ıaz, A. L. Zanocco, and P. Richter, "Determination of the sum of malachite green and leucomalachite green in salmon muscle by liquid chromatography-atmospheric pressure chemical ionisation-mass spectrometry," *Journal of Chromatography A*, vol. 1067, no. 1–2, pp. 101–105, 2005, doi: 10.1016/j.chroma.2004.10.049.

[5] W. C. Andersen, S. B. Turnipseed, J. E. Roybal, "Quantitative and confirmatory analyses of malachite green and leucomalachite green residues in fish and shrimp," *Agricultural and Food Chemistry*, vol. 54, no. 13, pp. 4517–4523, 2006, doi: 10.1021/jf0532258.

[6] K. Halme, E. Lindfors, and K. Peltonen, "Determination of malachite green residues in rainbow trout muscle with liquid chromatography and liquid chromatography coupled with tandem mass spectrometry," *Food Additives and Contaminants*, vol. 21, no. 7, pp. 641–648, 2004, doi: 10.1080/02652030410001721457.

[7] W. Xing *et al.*, "Development of a sensitive and group-specific polyclonal antibody-based enzyme-linked immunosorbent assay (ELISA) for detection of malachite green and leucomalachite green in water and fish samples," *Journal of the Science of Food and Agriculture*, vol. 89, no. 13, pp. 2165–2173, 2009, doi: 10.1002/jsfa.3695.

[8] F. Wang *et al.*, "Bispecific monoclonal antibody-based multianalyte ELISA for furaltadone metabolite, malachite green, and leucomalachite green in aquatic products," *Journal of Agricultural and Food Chemistry*, vol. 64, no. 42, pp. 8054–8061, 2016, doi: 10.1021/acs.jafc.6b03233.

[9] W. Gui, H. Wang, Y. Liu, and Q. Ma, "Ratiometric fluorescent sensor with molecularly imprinted mesoporous microspheres for malachite green detection," *Sensors and Actuators B Chemical*, vol. 266, pp. 685–691, 2018, doi: 10.1016/j.snb.2018.03.176.

[10] T. A. Ferreira, I. S. Ibarra, M. L. S. Silva, J. M. Miranda, and J. A. Rodriguez,"Use of modified henequen fibers for the analysis of malachite green and leuco-malachite green in fish muscle by d-SPE followed by capillary electrophoresis," *Microchemical Journal*, vol. 157, no. February, p. 104941, 2020, doi: 10.1016/j.microc.2020.104941.

[11] S. J. Culp and F. A. Beland, "Malachite green: a toxicological review," *Journal of the Anierican College of Toxicology, 15(3):219-238, Lip*, vol. 15, no. 3, pp. 219–238, 1996, doi: 10.3109/10915819609008715.

[12] K. Qu, *et al.*, "Simultaneous detection of diethylstilbestrol and malachite green using conductive carbon black paste electrode," *International Journal of Electrochemical Science*, vol. 7, no. 3, pp. 1827–1839, 2012.

[13] K. Zhang, G. Song, L. Yang, J. Zhou, and B. Ye, "A novel self-assembly voltammetric sensor for malachite green based on ethylenediamine and graphene oxide," *Analytical Methods*, vol. 4, no. 12, pp. 4257–4263, 2012, doi: 10.1039/c2ay26039e.

[14] H. Yi, W. Qu, and W. Huang, "Electrochemical determination of malachite green using a multi-wall carbon nanotube modified glassy carbon electrode," *Microchimica Acta*, vol. 160, no. 1–2, pp. 291–296, 2008, doi: 10.1007/s00604-007-0814-z.

[15] W. Huang, C. Yang, W. Qu, and S. Zhang, "Voltammetric determination of malachite green in fish samples based on the enhancement effect of anionic surfactant," *Russian Journal of Electrochemistry*, vol. 44, no. 8, pp. 946–951, 2008, doi: 10.1134/S1023193508080107.

[16] N. S. Prinith, J. G. Manjunatha, and C. Raril, "Electrocatalytic analysis of dopamine, uric acid and ascorbic acid at poly(adenine) modified carbon nanotube paste electrode:

a cyclic voltammetric study," *Analytical & Bioanalytical Electrochemistry*, vol. 11, no. 6, pp. 742–756, 2019.

[17] S. Banerjee *et al.*, "Sensitive electrochemical detection of carvacrol using carbon paste electrode," *2022 2nd International Conference on Emerging Frontiers in Electrical and Electronic Technologies, ICEFEET 2022*, pp. 1–4, 2022, doi: 10.1109/ICEFEET51821.2022.9847722.

[18] M. M. Charithra, J. G. G. Manjunatha, and C. Raril, "Surfactant modified graphite paste electrode as an electrochemical sensor for the enhanced voltammetric detection of estriol with dopamine and uric acid," *Advanced Pharmaceutical Bulletin*, vol. 10, no. 2, pp. 247–253, 2020, doi: 10.34172/apb.2020.029.

[19] R. L. McCreery, "Advanced carbon electrode materials for molecular electrochemistry," *Chemical reviews*, vol. 108, no. 7, pp. 2646–2687, 2008, doi: 10.1021/cr068076m.

[20] I. G. David, D. E. Popa, and M. Buleandra, "Pencil graphite electrodes: A versatile tool in electroanalysis," *Journal of Analytical Methods in Chemistry*, vol. 2017, no. Cv, 2017, doi: 10.1155/2017/1905968.

[21] S. Dasgupta, S. Nag, R. B. Roy, R. Bandyopadhyay, and B. Tudu, "Malachite green detection using carbon paste electrode based on voltammetry," *2nd International Conference on Emerging Frontiers in Electrical and Electronic Technologies, ICEFEET 2022,* pp. 1–5, 2022, doi: 10.1109/icefeet51821.2022.9847835.

[22] J. Hou, F. Bei, M. Wang, and S. Ai, "Electrochemical determination of malachite green at graphene quantum dots-gold nanoparticles multilayers-modified glassy carbon electrode." *Journal of Applied Electrochemistry*, vol. 43, pp. 689–696, 2013.

[23] X. C. Guo *et al.*, "Graphene-gold nanoparticles nanohybrids for electrochemical detection of malachite green," *International Journal of Electrochemical Science*, vol. 12, no. 8, pp. 7557–7569, 2017, doi: 10.20964/2017.08.49.

[24] Y. Lu, C. Partridge, M. Meyyappan, and J. Li, "A carbon nanotube sensor array for sensitive gas discrimination using principal component analysis," *Journal of Electroanalytical Chemistry*, vol. 593, no. 1–2, pp. 105–110, 2006, doi: 10.1016/j.jelechem.2006.03.056.

[25] D. Das *et al.*, "Titanium oxide nanocubes embedded molecularly imprinted polymer-based electrode for selective detection of caffeine in green tea," *IEEE Sensors Journal*, vol. 20, no. 12, pp. 6240–6247, 2020, doi: 10.1109/JSEN.2020.2972773.

[26] P. B. Garcia-Allende, O. M. Conde, J. Mirapeix, A. M. Cubillas, and J. M. López-Higuera, "Data processing method applying principal component analysis and spectral angle mapper for imaging spectroscopic sensors," *IEEE Sensors Journal*, vol. 8, no. 7, pp. 1310–1316, 2008, doi: 10.1109/JSEN.2008.926923.

[27] S. Nag *et al.*, "A simple nano cerium oxide modified graphite electrode for electrochemical detection of formaldehyde in mushroom," *IEEE Sensors Journal*, vol. 21, no. 10, pp. 12019–12026, 2021, doi: 10.1109/JSEN.2021.3066113.

[28] D. Das *et al.*, "CuO nanoparticles decorated MIP-based electrode for sensitive determination of gallic acid in green tea," *IEEE Sensors Journal*, vol. 21, no. 5, pp. 5687–5694, 2021, doi: 10.1109/JSEN.2020.3036663.

[29] Z. Li *et al.*, "Room-temperature high-performance H_2S sensor based on porous CuO nanosheets prepared by hydrothermal method," *ACS Applied Materials and Interfaces*, vol. 8, no. 32, pp. 20962–20968, 2016, doi: 10.1021/acsami.6b02893.

[30] W. Lv, L. Li, Q. Meng, and X. Zhang, "Molybdenum-doped CuO nanosheets on Ni foams with extraordinary specific capacitance for advanced hybrid supercapacitors," *Journal of Material Science*, vol. 55, no. 6, pp. 2492–2502, 2020, doi: 10.1007/s10853-019-04129-9.

[31] M. A. Khan, N. Nayan, Shadiullah, M. K. Ahmad, and C. F. Soon, "Surface study of cuo nanopetals by advanced nanocharacterization techniques with enhanced optical and catalytic properties," *Nanomaterials*, vol. 10, no. 7, pp. 1–18, 2020, doi: 10.3390/nano10071298.

[32] P. Deng, J. Feng, Y. Wei, J. Xiao, J. Li, and Q. He, "Fast and ultrasensitive trace malachite green detection in aquaculture and fisheries by using hexadecylpyridinium bromide modified electrochemical sensor," *Journal of Food Composition and Analysis*, vol. 102, no. March, p. 104003, 2021, doi: 10.1016/j.jfca.2021.104003.

[33] Y. Luo and Z. Li, "A sensitive electrochemical sensor manufactured from multi-wall carbon nanotubes-polyethylenimine nanocomposite for malachite green detection," *Journal of Alloys and Compounds*, vol. 897, p. 163216, 2022, doi: 10.1016/j.jallcom.2021.163216.

[34] A. M. Sacara, V. Nairi, A. Salis, G. L. Turdean, and and L. M. Muresan, "Silica-modified Electrodes for Electrochemical Detection of Malachite Green," *Electroanalysis*, vol. 29, no. 11, pp. 2602–2609, 2017, doi: 10.1002/elan.201700400.

[35] A. M. Sacara, C. Cristea, and L. M. Muresan, "Electrochemical detection of malachite green using glassy carbon electrodes modified with CeO_2 nanoparticles and nafion," *Journal of Electroanalytical Chemistry*, vol. 792, pp. 23–30, 2017, doi: 10.1016/j.jelechem.2017.03.030.

[36] H. Naskar, S. Pradhan, B. Ghatak, S. Biswas, B. Tudu, and R. Bandyopadhyay, "Electrochemical detection of capsaicin in chili pepper using molecular imprinted poly β-cyclodextrin embedded graphite (MIP-β-CD@G) electrode," *IEEE Sensors Journal*, vol. 21, no. 16, pp. 17657–17664, 2021, doi: 10.1109/JSEN.2021.3083527.

Chapter 3

Detection of Amaranth (AMR) using Carbon Paste Electrode (CPE), and Y_2O_3 Nanoparticles modified Graphite Paste Electrode (Y_2O_3@GPE)

This chapter delves into the fabrication and utilization of a carbon paste electrode (CPE), succeeded by the modification of a graphite electrode with Y_2O_3 nanoparticles for the precise detection of Amaranth (AMR) in candies. It encompasses a detailed comparative analysis of AMR detection, juxtaposed against earlier studies. Elaborate discourse is presented on the electrochemical properties of the developed electrode, experimental parameters pertinent to AMR detection, and a meticulous analysis of real sample data.

List of Sections

Contents of this chapter are based on mentioned publication:

Samhita Dasgupta, A.H.M. Toufique Ahmed, Ipshita Bhattacharjee, Shreya Firdoushi, Don Biswas, Sumani Mukherjee, Rajib Bandyopadhyay, Bipan Tudu, "Crafting a graphite electrode with embedded Y_2O_3 nanoparticles for the electrochemical detection of amaranth in candies," *IEEE Sensors Journal*, vol. 24, no.13, pp. 20750-20757, 2024. [DOI: 10.1109/JSEN.2024.3400317].

3.1. Introduction

Amaranth (AMR) (Trisodium (4E)-3-oxo-4-[(4-sulfonate-1-naphthyl) hydrazono] naphthalene-2,7-disulfonate), the anionic dye, is hugely used as a food color in different soft drinks, hard drinks, as well as in desserts [1], [2], [3], [4]providing alluring red color. It finds its application in fields of artificial dyeing, medicines, paper, cosmetics, and wood also [2]. The chemical structure of AMR is in Fig. 3.1. The literature study of AMR is already discussed in Chapter 1, Section 1.1 and Section 1.4.

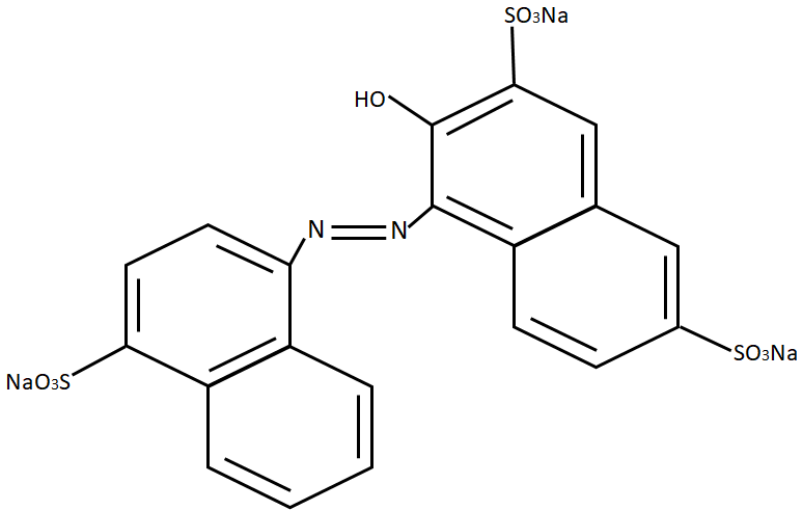

Fig. 3.1. Molecular structure of AMR.

High performance liquid chromatography (HPLC) [5], spectrophotometry [6], thin-layer chromatography [7], and capillary electrophoresis[8], are some of the conventional methods applied for detecting AMR in foods. Though these methods are accurate, but the unavoidable disadvantages of them enlarge the domain of application for the ground breaking substitute, the electrochemical approach, whose positive sides have already been discussed in Section 2.1. There are numerous methods reported for the electrochemical detection of AMR. A zinc oxide nanoparticles modified CPE has been used for the voltametric detection of AMR [9]. Many other nanoparticles like polypyrrole nanotubes[10] , Graphene/TiO_2-Ag based composites[11], single-walled carbon nanotube-Tin nanocomposites [12], and vanadium oxide nanoplates [13], have been applied as modifiers for enhancing the efficiency of carbon electrodes to detect AMR. However, still there remains a need for improvement in both the LOD and the detection range of all sensors. Additionally, the synthesis procedures entail intricate chemical steps, which are time-consuming and have the potential to impact the chemical stability of the sensor. This study finds a value-for-money route by developing a simple CPE for detecting AMR electrochemically in the laboratory. Different CV and DPV responses are noted for the

electrochemical study of this electrode. Next, Y_2O_3 nanoparticles are ingrained in the carbon paste to modify it for better efficiency. Reasons behind the use of graphite and Y_2O_3 nanoparticles for the electrode fabrication have already been discussed in the Section 2.1 of Chapter 2.

3.2. Experimentation with CPE to detect AMR

3.2.1. Materials

Amaranth extra pure, graphite powder (99%), and paraffin oil are procured from Loba Chemie Pvt. Ltd. (India), Sigma Aldrich (USA), and Merck (India) respectively. Millipore water with a resistance of 18 MΩ is used as solvent for preparing the standard solution of AMR as well as the other required solutions. Different buffer solutions like Phthalate (PHT), Acetate (ABS), and Phosphate (PBS) of 0.1 M each are prepared in the laboratory to be used as the supporting medium. No additional purification is required as each and all chemicals are of premium analytical status. Normal room temperature is preferred throughout the experimentation. Millipore water is also used to rinse the electrode surface after recording each data to clean and regenerate the CPE surface.

3.2.2. Apparatus and devices

Cyclic voltammetry (CV) and differential pulse voltammetry (DPV) measurements are performed using the potentiostat PGSTAT101 manufactured by Metrohom Autolab, Netherlands. A three-electrode cell is used to conduct the experiment wherein an Ag/AgCl reference electrode and a platinum counter electrode accompanied the developed CPE working electrode. Nova (2.1) electrochemistry software by Metrohom Autolab facilitates the CV and DPV to be graphically represented. The required blending of the solvents and solutes is confirmed by sonicating and homogenizing all solutions with the help of the ultrasonicator made by Labman scientific instruments.

3.2.3. Experimental setup

Figure 3.2. provides an insight into the measurement setup showing the mentioned three-electrode cell along with the potentiostat and data analysis units. For CV and DPV data, the scan rate of 50mV/sec is taken as a standard value wherever needed. In case of CV, as an example, for 0.3-1.6V range, the start potential, the lower vortex potential, and the stop potential are taken as 0.3V whereas the upper vortex potential is 1.6V. The number of scans is

1. In case of DPV analysis, the start potential, the stop potential, the step size, the modulation time, and the interval time is found as 0.8V, 1.6V, 0.025V, 0.05sec, and 0.5sec, respectively.

3.2.4. Preparing the working CPE

During the development process of a CPE, at first, 300 mg of graphite powder is measured in a weighing balance and then ground by a mortar and pestle. The grinding process is carried out adding 2 or 3 droplets (around 0.15ml) of paraffin oil for 45 mins and resulting in the formation of a fine paste. This paste is transferred into a glass capillary tube (2mm inner diameter) through a metal rod pressing and is followed by the insertion of a copper wire into that tube as an electrical connection with the paste. The formation of CPE by grinding graphite powder using a mortar and pestle is pictured in Fig. 3.3.

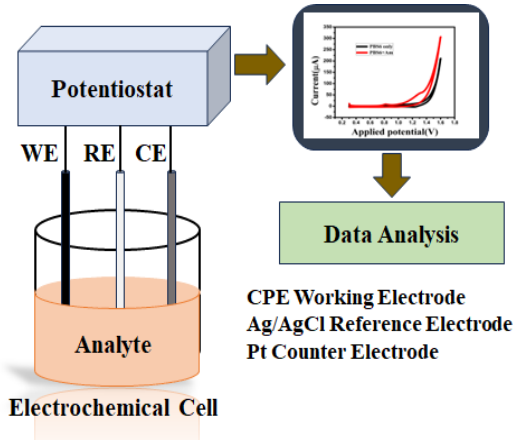

Fig. 3.2. Experimental setup diagram.

Fig. 3.3. Formation of CPE.

3.3. Results and discussions for CPE to detect AMR

3.3.1. Selection of buffer and relative study of CPE activity

The CPE is immersed in 100µM solution of AMR in a number of buffer solutions (each of pH 6 and 0.1 M) like PHT, ABS, and PBS one by one to investigate the effect of different buffer solutions. Once CV is conducted, in Fig. 3.4.(a), it is spotted that the oxidation peak current (Ip) is at its maximum (8.51µA) for PBS which leads to choose PBS to achieve the best response using CPE while detecting AMR. Next the electrochemical performance of the CPE is illustrated where a voltage range of 0.3 to 1.6V is considered for performing the CV analysis. First CV data recording is done for 0.1M PBS only using this CPE and no detectable peak is found. Some AMR solution is then introduced to this Phosphate buffer and the CV response is monitored again for same applied voltage range. Figure 3.4.(b) then shows the sensor identifying AMR molecule with a peak voltage of oxidation at 0.84V and 8.51µA peak current which is clearly because of the addition of AMR molecule.

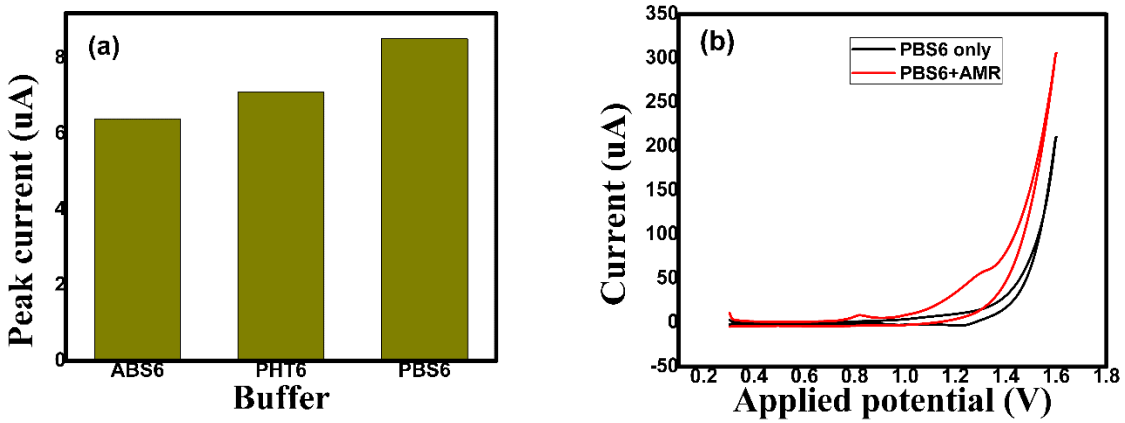

Fig. 3.4.(a) Bar plot for 100µM AMR in ABS, PHT, PBS solutions; (b) CV plot of CPE in presence and absence of AMR molecule.

3.3.2. Optimization of pH

Optimum pH of the PBS solution for CPE based AMR detection is studied by performing the redox process using CV with PBS of pH 5, 6 and 7. The highest current of 8.51µA is found for PBS6 and hence further readings are collected using this one. The corresponding graph can be found in Fig. 3.5. This figure shows that peak current I_p is reduced again when the related pH is raised to 7 which may be resulted by the slight AMR adsorption.

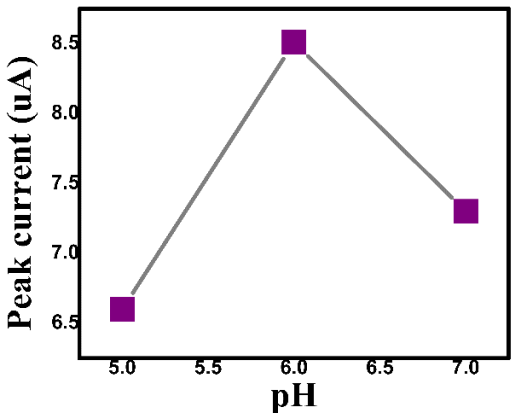

Fig. 3.5. pH optimization of PBS for CPE to detect AMR.

3.3.3. Effect of various scan rate

The impact of scan rate variation on I_p of AMR is observed by increasing the scan rate from 5mV/sec to 400mV/sec and recording the corresponding CV responses of CPE within the range of 0.7-1.6 V. The CV response in Fig. 3.6.(a) shows that the Ip increases with an increase in scan rate. The corresponding regression equation for I_p is shown below in (3.1), which is formulated from the linearity plot linked to the scan rate variation shown in Fig. 3.6.(b).

$$I_{AMR} = 0.17v\ (mVs^{-1}) + 2.91;\ R^2 = 0.96 \quad (3.1)$$

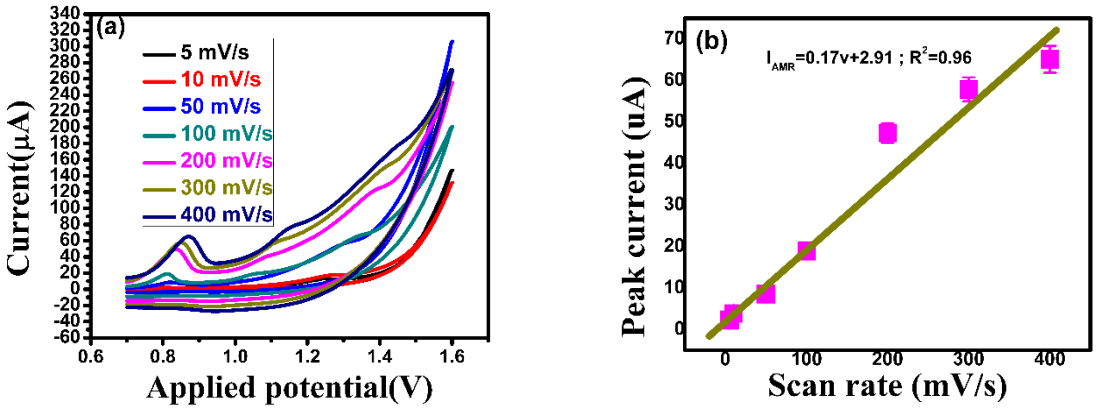

Fig. 3.6. (a) CV responses of I_p variation with scan rate (5-400 mV/sec); (b) Linear plot for I_p vs scan rate in 0.1 M PBS.

3.3.4. Impact of various concentration

Several AMR concentrations and their impacts at CPE surface are studied surveying the DPV responses within a range of 0.8-1.6V, with the 0.1 M PBS. The steady escalation in I_p with the rise in AMR concentrations (5-100µM) at a fixed scan rate of 50mV/s is shown in Fig. 3.7.(a) whereas Fig. 3.7.(b) demonstrates the calibration plot with the regression equation (3.2).

$$I_{AMR} = 0.17C_{AMR} + 21.03;\ R^2 = 0.98 \quad (3.2)$$

Signifying the standard deviation of I_p values at the lowest concentration reported(5µM) as σ and referring the slope of the characteristic plot as m, the LOD calculation is done as $LOD = (3\sigma)/m$ [9], [10], which has been shown earlier in an equation form in (2.3) of the section 2.3.4 of Chapter 2. Here a pleasing LOD value of 0.17µM is achieved. Table 3.1 has been prepared juxtaposing this study with formerly reported literature.

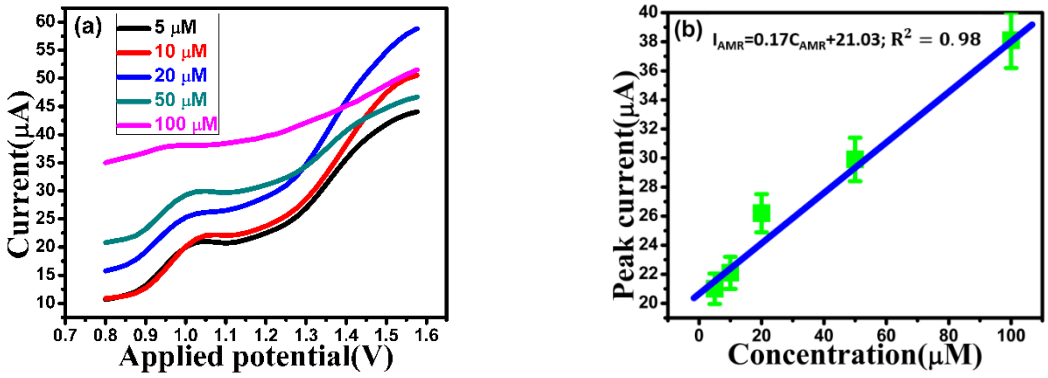

Fig. 3.7. (a) DPV responses for AMR by CPE in 0.1 M PBS; (a) concentration of 5-100 µM (b) Linear plot of I_p vs concentration.

3.3.5. Repeatability, reproducibility and stability assessment

Three successive DPV responses called S1, S2, and S3 are considered for repeatability analysis of this CPE and it is found enough repeatable with 1.3% RSD (Figure 3.8.(a)) whereas three identical electrode responses named T1, T2, and T3 were used to find it reproducible with %RSD of 2.8 (Figure 3.8.(b)). Maintaining same physical conditions, same test was performed with intervals of 10 days for stability study and a decent stability was achieved with %RSD of 2.6 (Figure 3.8.(c)).

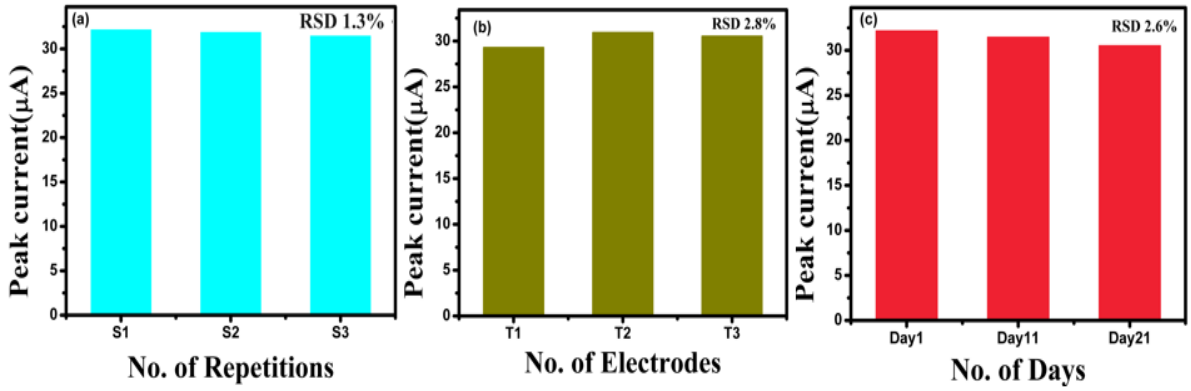

Fig. 3.8. (a) Repeatability graph; (b) Reproducibility study; (c) Stability plot;

Table 3.1. Comparison of the proposed method with other existing techniques.

Electrode	LOD(μM)	Ref.
Poly(L-arginine)–graphene modified glassy carbon electrode (GCE)	0.25 μM	[14]
Co_3O_4-CeO_2/graphene (Co_3O_4-CeO_2/Gr) composite modified electrode	0.16 μM	[15]
Carbon paste electrode (CPE)	0.17 μM	**[This study]**

3.3.6. PCA plot for AMR concentrations for CPE

The PCA technique, detailed in the Section 2.3.6 of Chapter 2, has been applied here also for analyzing the CPE generated data of AMR solution. The DPV response curves for AMR concentrations (5μM, 10μM, 20μM, 50μM, and 100μM as C1, C2, C3, C4, and C5, respectively) using CPE are analysed using this PCA tool. Three repetitions are considered for each concentration. The PCA plot with successful data clustering is shown in Fig.3.9., where all the different concentrations are found to be rightly discriminated. The PC1 and PC2 illustrate 90.26%, and 8.3% of total variances, respectively. The S.I. is calculated as 34.89, suggesting a clear separation of the classes in the dataset.

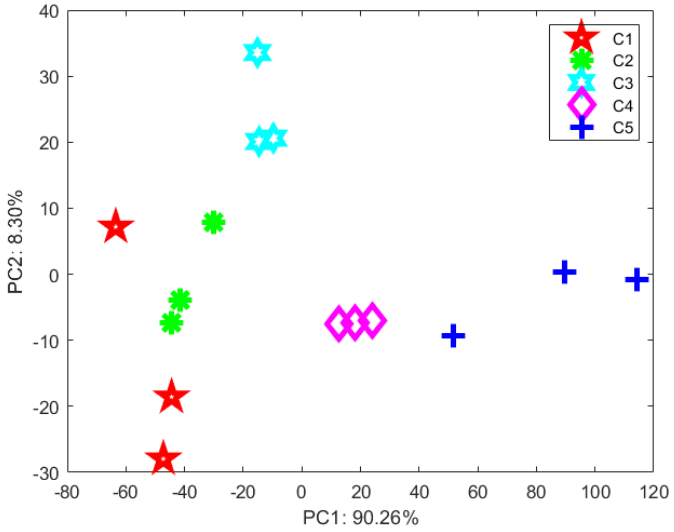

Fig. 3.9. DPV data (by CPE for AMR) analysis using PCA-a graphical representation.

3.3.7. PLSR for AMR concentrations

Different concentrations of AMR (C1-C5) have been assessed using PLSR analysis method, which is described previously in the Section 2.3.7 of Chapter 2. For each concentration, the ratio between training data and testing data was 3:1. The prediction parameters are listed in Table 3.2. In Table 3.3, the correlation factor found after prediction denotes a nicely performing model in terms of accurate prediction of the response variable based on the predictor variables.

Table 3.2. Comparison of actual and predicted AMR contents achieved via PLSR.

No. of samples	Actual AMR contents (µM)	Predicted AMR contents (µM)	Prediction accuracy (%)
1	5	4.1	82.16
2	10	9.39	93.88
3	20	13.98	69.88
4	50	45.63	91.26
5	100	131.45	131.45
Average prediction accuracy 93.73%			

Table 3.3. PLSR related Parameters

C.F. (training)	C.F. (prediction)	RMSEP
0.99	0.99	0.76

Results in Table 3.2. show that the average prediction accuracy using the PLSR tool for voltametric detection of AMR using CPE is pretty satisfactory as 93.73%. Though the prediction accuracy for 20µM has a disappointing result, it is granted in this case considering the overall result. In Table 3.3, the correlation factor found for prediction signifies a nicely

performing model in terms of accurate prediction of the response variable based on the predictor variables. The root means square error of prediction (RMSEP) has a good value of 0.76.

3.3.8. Discussion

The present study focuses on the rapid electrochemical detection of Amaranth using an optimised CPE. The system presents a wide operational range with linearity within 5µM to 100µM and a LOD of 0.17µM. The DPV responses obtained using this electrode for AMR were analysed effectively via the PCA tool with a nice value of SI as 34.89. Real sample data has not been recorded in this case. It has been done in the next study using a few types of candies where the detailed elucidation of a Y_2O_3 nanoparticles modified GPE has been presented.

3.4. Experimentation with Y_2O_3 nanoparticles modified graphite paste electrode (Y_2O_3@GPE)

3.4.1. Reagents and chemicals

Merck India supplied Y_2O_3, paraffin oil, Poly-ethylene glycol (PEG)-400, and Ammonia. All other reagents used are detailed earlier in the Section 3.2.1 of this chapter.

3.4.2. Preparation of Y_2O_3 nanoparticles

Y_2O_3 Nanoparticles are produced in the laboratory using the sol-gel technique [16]. At first, 10 ml of 20 (v/v) PEG-400 is mixed with a 0.2 (M) 100 ml Y_2O_3 solution. In this process, PEG-400 serves as a capping agent to regulate particle size. Subsequent to this, incremental introduction of liquid ammonia is performed to the mixture, resulting in the formation of a white gel that is allowed to age for 1 hour. This gel is then filtered and then rinsed again and again with Millipore water. Once air-dried, a white powder is the end result which is later calcined in a muffle furnace at 600˚C for 4 hours. Thus, the white colored Y_2O_3 nanoparticles are produced and are characterized later using XRD and SEM. The nanoparticles preparation and their application in forming the electrode are combined in a single picture shown in Fig.3.10.

3.4.3. Material assessment techniques

The XRD analysis is done using a PANalytical X'PERT PRO instrument, operating at 45 kV and 40 mA, with CuKα1 radiation (λ = 1.5406 Å). The developed Y_2O_3 nanoparticles are

characterized via XPS analysis technique utilizing a Thermo Scientific, K-Alpha spectrometer, which was operated with a monochromatic Al Kα X-ray source of 1486.7 eV. A SEM from CARL ZEISS (EVO 18 model) is employed, using an accelerated voltage of 15 KV for operation. ZEISS manufactured Energy dispersive spectroscopy (EDX) is used to observe the corresponding chemical composition. Fourier transform infra-red spectroscopic (FTIR) analysis is performed using a MAGNA 550 FTIR spectrometer (Nicolet, USA) of the powder samples with the KBr pellets. Electrochemical analysis incorporates a Potentiostat/Galvanostat interfaced three-electrode system. This Potentiostat/Galvanostat (PGSTAT101) is manufactured by Metrohom Autolab, Netherlands. The system involves a Pt counter electrode, an Ag/AgCl as reference electrode, and a Y_2O_3@GPE as the working electrode. Voltammetry analysis techniques are consistently used throughout the study.

3.4.4. Y_2O_3@GP electrode assembly

300 mg of a blended material is made as a mixture of Y_2O_3 nanoparticles and graphite powder in 1:9 weight ratio using a mortar and pestle. This particular ratio is decided through trial and error, as it provided the optimal current response combining graphite and Y_2O_3 nanoparticles.

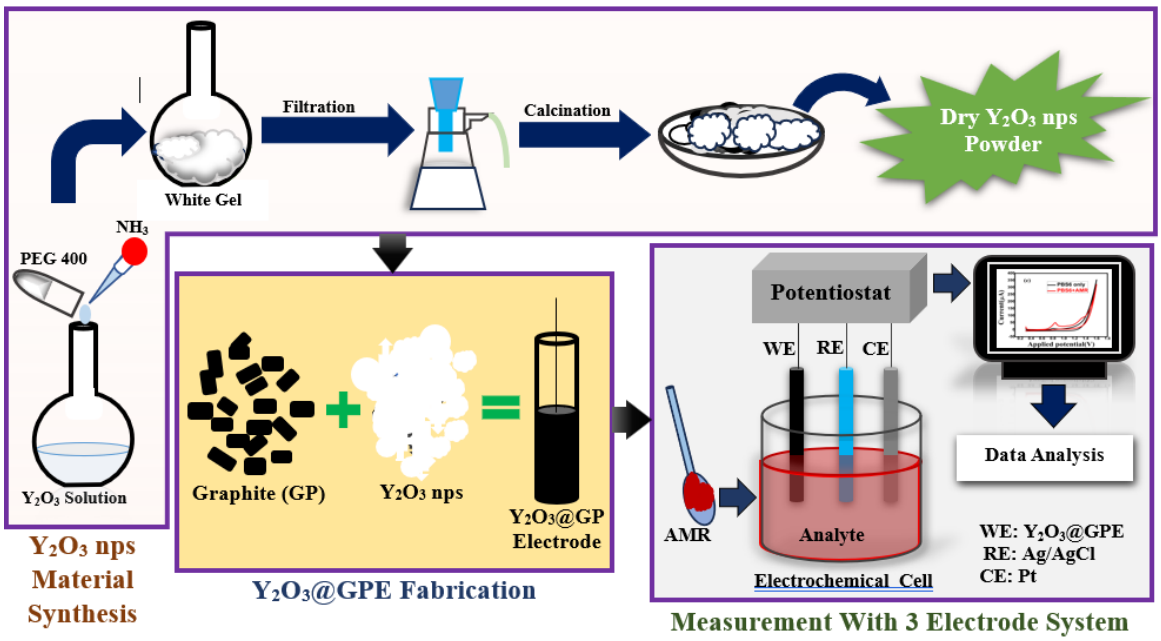

Fig. 3.10. Steps of measurement procedure for voltametric AMR detection using Y_2O_3@GPE.

A few drops (2-3) of paraffin oil, as a binder, are added to the mixture creating a consistent paste. This paste is then packed into a glass capillary tube of an inner diameter of 2mm. A copper wire is attached to the back end of the capillary tube to ensure a solid electrical connection with the sensing material. Likewise, a bare graphite paste electrode (bare GP) is crafted using only 300 mg of graphite powder.

3.5 Results and discussions for Y_2O_3@GPE to detect AMR

3.5.1. XRD properties of Y_2O_3 nanoparticles

The X-ray diffraction pattern is studied with the goal of confirming the phase purity as well as the crystallinity of the developed Y_2O_3 nanoparticles. This XRD pattern illustrated in Fig.3.11. resembles the ICSD Reference code: 01-079-1256 with a score of 96%. The data collection is done at a scan speed of 0.3s per step whereas the step size was 0.02º. The holding time is kept 5min for the XRD data collection. The measurement temperature is fixed at 25º C. The structure of the sample is cubic at room temperature. Crystallite size is estimated from the XRD data (406.15 nm). The 2θ angle range selected here was 15º-70º. The most intense peak found is at 2θ = 29.141º for (222) plane [17],[18] while the other prominent diffraction peaks are observed at 20.492º, 33.776º, 35.894º, 37.91º, 39.849º, 41.70º, 43.482º, 46.890º, 48.526º, 50.10º, 53.191º, 56.163º, 57.611º, 59.043º, 60.442º, and 64.549º, corresponding to different diffraction planes like (211), (400), (411), (420), (332), (422), (134), (125), (440), (433), (611), (541), (622), (136), (444), and (721), respectively. No secondary phase was detected suggesting the formation of Pure Y_2O_3.

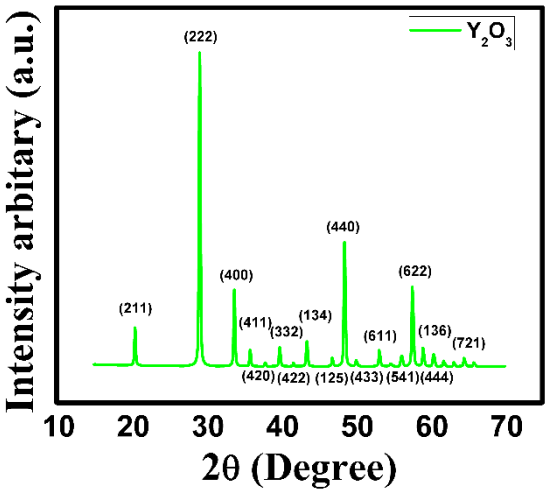

Fig.3.11. XRD pattern of synthesised Y_2O_3 nanoparticles.

3.5.2. XPS analysis of Y_2O_3 nanoparticles

The XPS survey spectra of Y_2O_3 nanoparticles in Fig.3.12. (a) shows that both the elements Y and O are present in the material. Detailed analysis of the high-resolution spectra of Y 3d in Fig.3.12. (b) shows that there exist two prominent peaks at 159.93 eV and 157.95 eV, representing the 3d3/2 and 3d5/2 states, respectively. Besides, in Fig.3.12. (c), the high-

resolution O 1s spectra exhibits a peak at 531.51 eV. This XPS response of Y_2O_3 nanoparticles can be compared to the spectra found in [19].

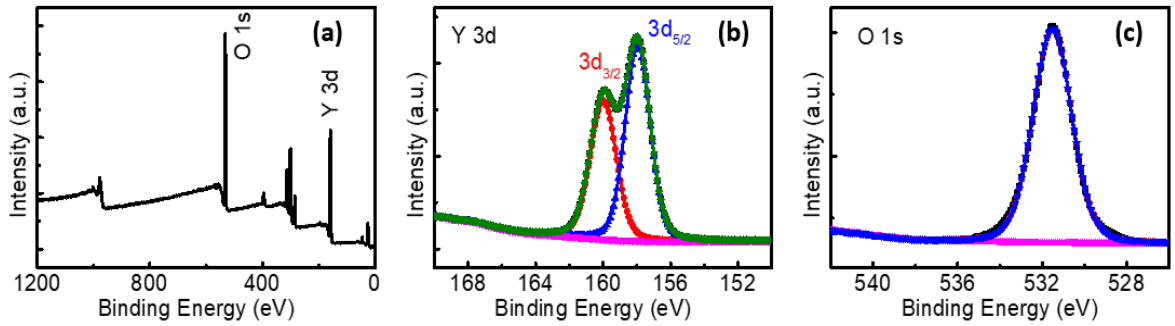

Fig.3.12. XPS analysis of Y_2O_3 nanoparticles (a) complete scan survey; (b) High-resolution spectra for Y 3d; (c) High-resolution O 1s spectra.

3.5.3. SEM analysis and EDX study of Y_2O_3 nanoparticles

SEM study is done for conducting a morphological analysis for both the developed Y_2O_3 nanoparticles and pure graphite. These SEM images presented in Fig. 3.13.(a-c) show the particles size to be around 500nm. EDX study is done for getting idea about the fundamental composition and purity of Y_2O_3 nanoparticles. This image is available in Fig. 3.13.(d).

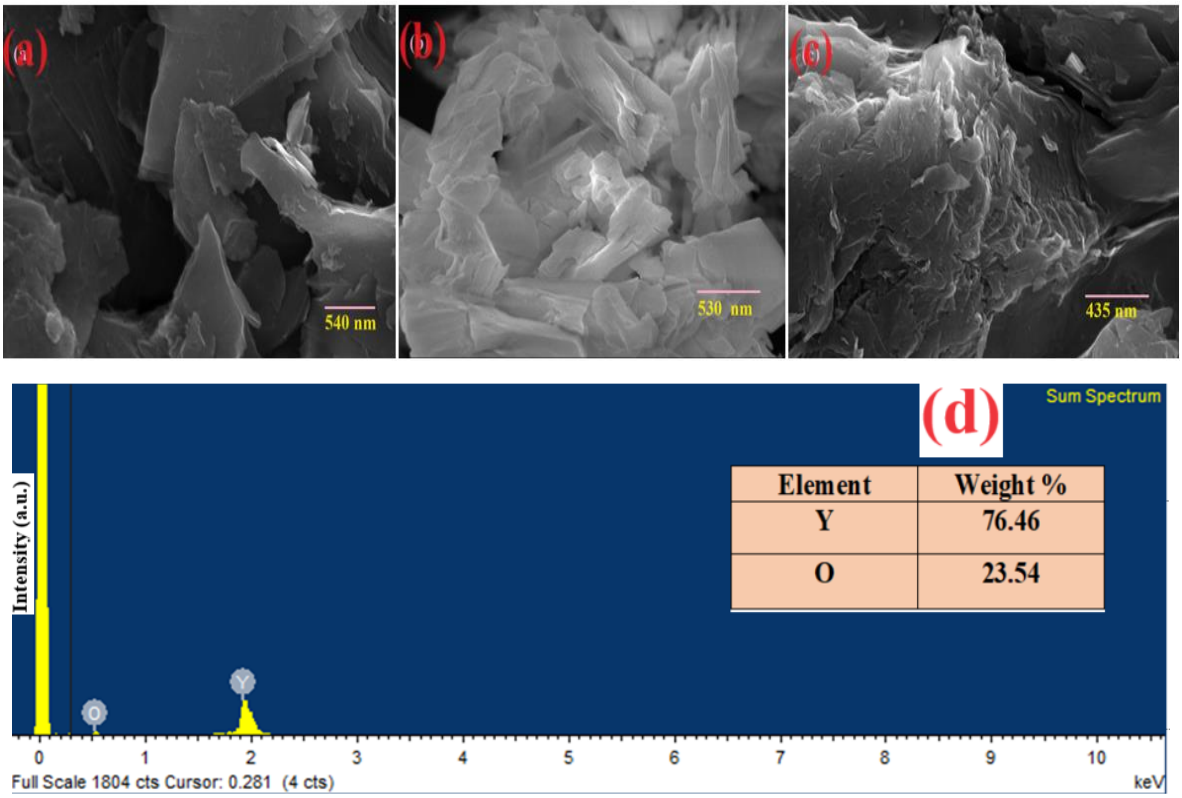

Fig.3.13. SEM image of (a)Pure graphite; (b)Fabricated Y_2O_3 nanoparticles; (c) Y_2O_3 nanoparticles ingrained graphite; (d) EDX spectrum-Y_2O_3 nanoparticles.

3.5.4. FTIR analysis of Y_2O_3 nanoparticles

The FTIR spectrum is employed for illuminating the bonding characteristics of the synthesized Y_2O_3 nanoparticles. Figure 3.14. provides the infrared spectra of Y_2O_3 nanoparticles subjected to a calcination temperature of 600º C. This spectral data is recorded within the mid-infrared range of 4000-400 cm^{-1}. The solitary broad peak found within 3536–2560 cm^{-1} is ascribed to the stretching vibrations of OH^- groups [20], [21], [22]. This phenomenon may be caused by the absorption of moisture, originating either from the atmosphere by Y_2O_3 nanoparticles or from the standard reference sample KBr pellet. In the next region, the peaks at around 1665 and 1551 cm^{-1} are representative of the asymmetric stretching of the C–O band, probably a result from the absorption of atmospheric CO_2. At last, the peaks around 731 cm^{-1} are found for the stretching frequency of Y–O molecule originating from Y_2O_3.

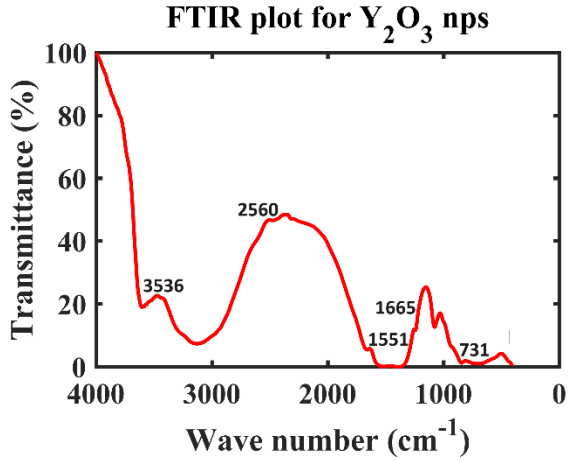

Fig.3.14. FTIR pattern of synthesized Y_2O_3 nanoparticles.

3.5.5. Electrocatalytic behavior of Y_2O_3@GPE for AMR detection

The newly developed Y_2O_3@GPE is examined through CV analysis for investigating its electrochemical behavior. CV responses are monitored for both the bare CPE and this nanoparticle modified GPE. It is found in Fig.3.15. (a), that the Y_2O_3@GPE is found to reveal a redox process with oxidation peaks at 0.84V and a hump around 1.3V. There may lie a number of reasons for the generation of this hump including side reactions, the state of the electrode surface, and any issues or artifacts related to the measurement setup. The peak (at 0.84V) is considered for further analytical purposes. The Y_2O_3@GPE is found to provide a significant increase in I_p (49.89 µA) compared to the I_p provided by the CPE (8.51 µA). This more than 5.8 times of elevation in I_p may be a result of the accelerated electron kinetics because of the modification of the graphite paste material with Y_2O_3 nanoparticles.

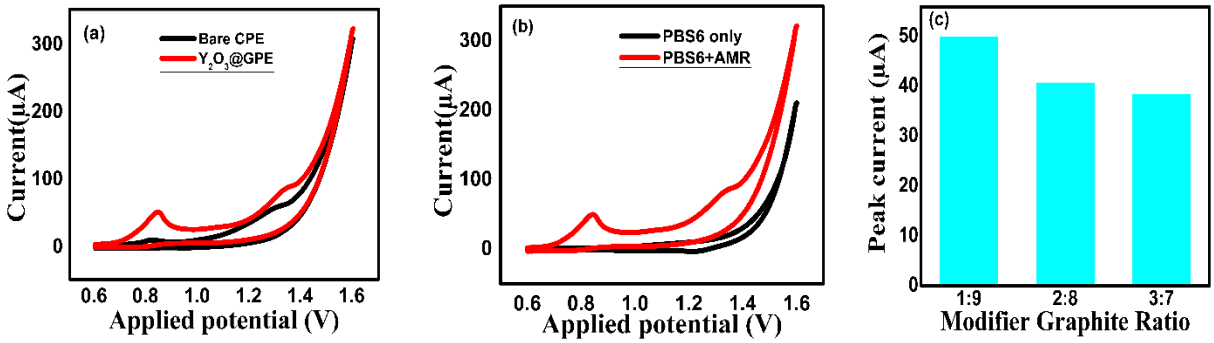

Fig.3.15. Performance comparison of Bare CPE and Y_2O_3@GPE; (b)Role of presence of AMR on CV plot; (c) Bar plot for modifier: graphite vs peak current.

This modification has enhanced the electrochemical performance of graphite electrodes, potentially facilitated by nano-crystallites with a larger surface area and electron levels that align well with analytes and nano-metallic oxides. Besides, in Fig.3.15. (b), the appearance of no peak in presence of buffer solution only clearly proves that the oxidation peaks occur because of the AMR molecules present in the 100 µM stock solution of AMR only. Determination of the ideal ratio of mixing for the modifier Y_2O_3 and the graphite powder is involved in the experimental optimization procedure. Three electrodes are developed alternating the ratios of Y_2O_3 nanoparticles to graphite as 1:9, 2:8, and 3:7, pictured in Fig. 3.15. (c). The highest Ip of 49.89µA was reached in case of 1:9 ratio.

3.5.6. Effect of buffer and pH change

The supporting buffer solution and the pH value of the medium notably influenced the CV response of the new Y_2O_3@GPE.

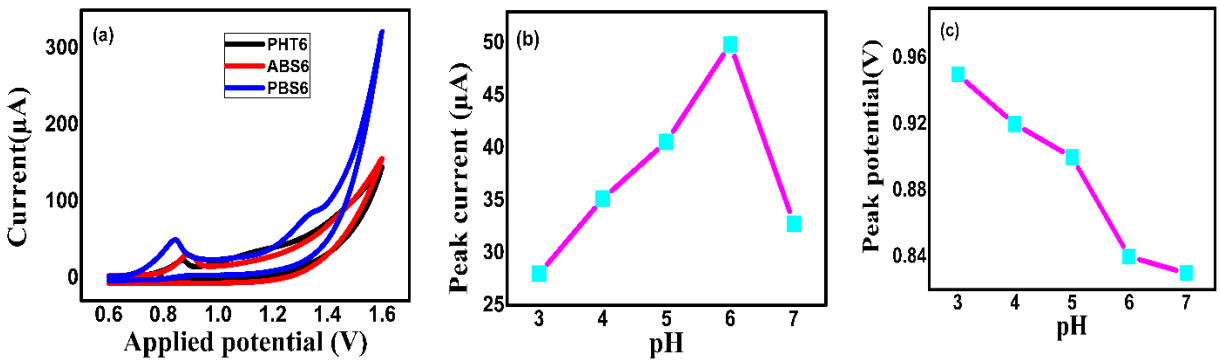

Fig.3.16. (a)Optimum buffer selection for Y2O3@GPE; (b)Plot for Peak current and pH (3,4,5,6,7); (c) Plot-Peak voltage vs pH (3,4,5,6,7).

The investigation of this impact is carried out by immersing the electrode in AMR solution supported by three distinct electrolyte buffers namely PBS, ABS, and PHT, each having a pH value of 6. Figure 3.16. (a) provides the CV diagrams corresponding to the responses of the AMR molecule in each buffer solution. Among all of these, the solution with PBS exhibits the highest I_p. As a result, the PBS is chosen for the further progress of experimentations. For the

fine-tuning of the pH of the experimental system, the redox processes are performed in PBS with pH ranges of 3,4,5,6, and 7 (refer to Fig.3.16. (b)). The results in Fig.3.16. (b) indicates the I_p to be maximum at pH 6. The I_p decreases as the pH of the PBS solution drops to 3 and also as it reaches 7, possibly associated to the weak adsorption of AMR. Consequently, all experiments are conducted at pH 6 of PBS. The plot for peak potential (E_p) vs pH is shown in Fig.3.16. (c). In case of E_P and pH, a linear relationship was found as:

$$E_P = -0.032pH + 1.05;\ R^2 = 0.96 \quad (3.3)$$

Here the slope is found as -0.032, displaying nice concordance with 50% of the theoretical value established by Nernst [1]. This investigation suggests the engagement of a number of electrons double the number of protons in this irreversible electrochemical reaction of AMR [15].

3.5.7. Influence of scan rate variation

CV method wis applied for investigating the role of variation in scan rates on the Y_2O_3@GPE based electrochemical determination of AMR molecule using PBS6 within a voltage range of 0.8-1.6 V. Figure 3.17. (a) displays the CV data showing increase in I_p with corresponding rise in scan rates from 5-400 mV/s whereas a linear plot of I_p against scan rate is depicted in Fig.3.17. (b). This observation indicates that the electrocatalytic oxidation of AMR using Y_2O_3@GPE follows a surface-controlled process [23]. The linear plot supported by Fig.3.17. (b) is like (3.4):

$$I_{AMR} = 0.56v + 15.5;\ R^2 = 0.99 \quad (3.4)$$

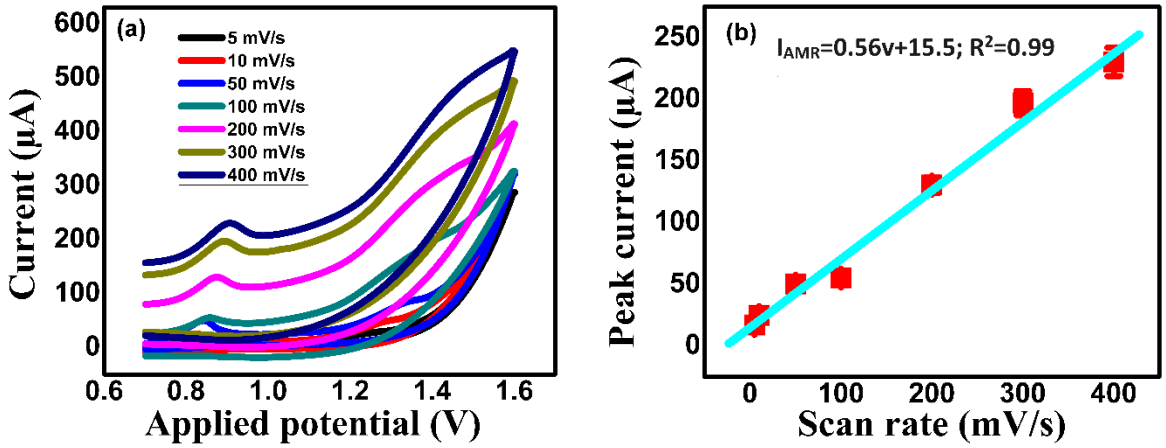

Fig.3.17. (a)Peak current variation vs scan rates variation (5 mV/s-400 mV/s); (b) Plot for linearity between peak current and scan rate.

The electrochemical oxidation pathway associated to AMR molecule on the electrode surface is shown in Fig.3.18, where the no. of transferred electrons in this process is shown as 2, which is similar to the value of transferred electrons number calculated mathematically later.

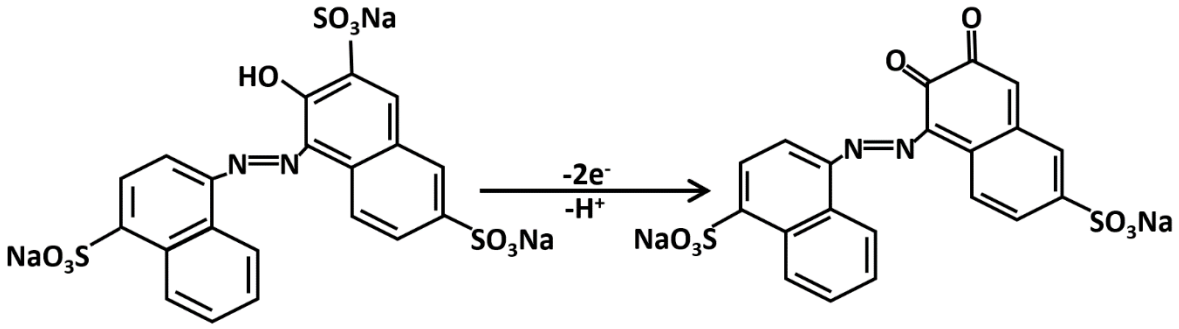

Fig.3.18. The oxidation pathway for AMR.

The equation applied for the calculation of the number of electrons transported amid the oxidation process [24], [25] is (2.7), mentioned earlier in the Section 2.5.6 of Chapter 2. The meaning of each and every symbol used there is also explained in Section 2.5.6. Using that equation, n is found 1.86, after calculation estimated as 2, comparable to the report presented by [1], [15]. The charge transfer coefficient α is got as 0.5, from the slope of the curve equal to $^{2.3RT}/_{(1-\alpha)nF}$ [24]. The surface concentration of AMR, Γ_C is calculated to be 0.85 × 10^{-8} mole /cm^2, using (2.7) again. In addition, heterogeneous rate constant Ks of the reaction is found to be 0.001 s^{-1} applying Laviron's equation [26], [27], expressed in Eq. (2.9) in the Section 2.5.6 of Chapter 2.

3.5.8. Influence of concentration variation

Because of its enhanced sensitivity and precision in quantitative analysis, DPV has gained preference over CV. DPV flaunts notable responses, yielding clearly defined peaks even at lower concentration levels [28], [29], [30]. In this work, the different parameters of DPV like the step size, the modulation time, and the interval time is set as 0.025V, 0.05sec, and 0.5sec, respectively for these measurements to examine the impact of different concentrations of AMR on Y_2O_3@GPE surface with PBS6. The DPV response of Y_2O_3@GPE reveals that the distinctive voltage (oxidation peak potential) indicative of AMR is at 1.05 V. Figure 3.19.(a) displays the proportional increase in I_p as the AMR concentration rises from 0.05µM to 100µM and the related two regression equations and calibration curves are found in Fig.3.19. (b). The first one, for the concentration range of 0.05µM -5µM, is (3.5).

$$I_{AMR} = 3.79C_{AMR} + 8.3;\ R^2 = 0.98 \quad (3.5)$$

The next linear region is within 5µM -100µM and holds the regression equation as (3.6).

$$I_{AMR} = 0.18C_{AMR} + 26.6;\ R^2 = 0.99 \quad (3.6)$$

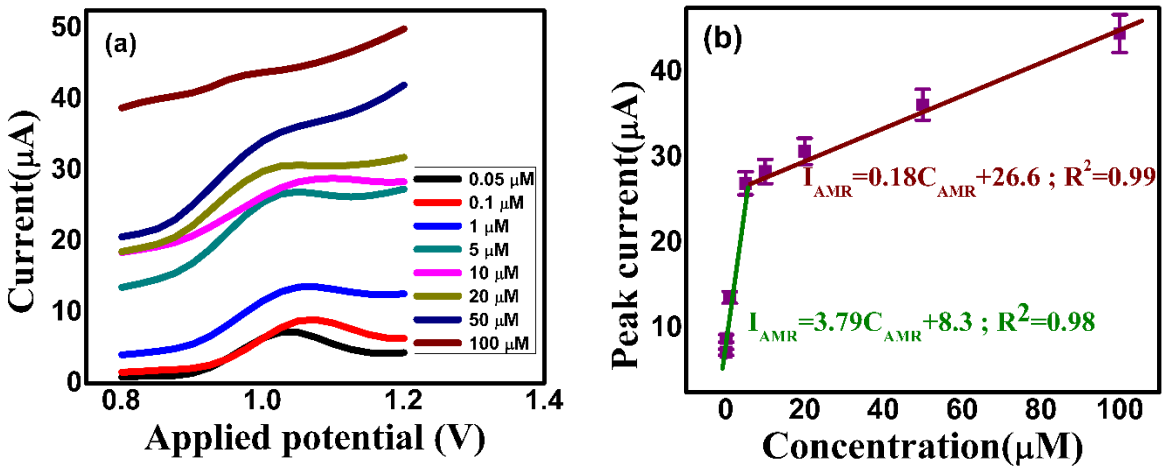

Fig.3.19. (a) DPV measurement plots for detecting AMR with Y_2O_3@GPE in 0.1 M PBS for various concentrations; (b) plot of linearity for peak current vs concentration.

Here, I_{AMR} and C_{AMR} stands for the peak current and corresponding concentration of AMR, respectively. The linear trend of response with increasing concentration of the AMR solution is indicative of the ability of the Y_2O_3@GPE to be applied for the quantitative AMR determination.

Table 3.4. Comparing proposed Y_2O_3@GPE for detecting AMR with past reports.

Electrode material	Linear range (µM)	LOD (nM)	Ref.
Ce^{3+}-doped CuO/CPE	0.05–240.00	10.20	[1]
Poly(L-arginine)–graphene modified glassy carbon electrode (GCE)	0.75-75	250	[14]
Co_3O_4-CeO_2/graphene composite modified electrode	2-96	159.1	[15]
PSS-GN/Co_3O_4/GCE	0.01–6.0	4	[32]
Fe_3O_4@rGO/GCE	0.05–50	50	[33]
CNTs-modified GCE	0.04–0.8	35	[34]
GQDs/ionic liquid/CPE	0.1–400.0	30	[35]
MWCNT	1.0–10.0	68	[36]
Pd/GO/SPE	0.08–360.0	30.0	[37]
Y_2O_3@GPE	**0.05-100**	**3.6**	**This work**

The appearance of two slopes in the calibration curve can be attributed to Langmuir adsorption isotherm behavior described in reference [31]. This behavior tells that there is an initial monolayer adsorption of analytes succeeded by subsequent multilayer adsorption. Because of the pronounced adsorption of Y_2O_3@GP, at lower concentrations, the initial layer of molecules

blankets the outermost accessible surface of the electrode. In the higher concentration range, the first layer of molecules screens the second layer of molecules resulting in the different interaction strength of the second layer of molecules from that of the first layer. Similar findings have previously been reported also in the analysis study of many small biomolecules [31]. The LOD for AMR was calculated as 3.6nM, considering the slope of the linear equation of the lower concentration range (0.05µM -5µM). The equation used here was equation (2.3) mentioned in the Section 2.3.4 of Chapter 2. This LOD is found better than the LOD of the maximum of the reported articles. Here, the movement of the oxidation potential after a certain AMR concentration can be justified as a result of the assertive adsorption property of AMR into the WE surface. The LOD and dynamic range of linearity are similar in nature and even excellently better compared to other reported works as briefed in Table 3.4.

3.5.9. Repeatability, reproducibility, and stability study

Repeatability, reproducibility, and stability are essential factors for assessing the performance of the electrochemical sensors. DPV method under carefully chosen experimental conditions is employed for the evaluation of these three indexes. The prepared sensor is subjected to repeated exposure to a 20µM solution of AMR in the presence of 0.1 M PBS 6 as the supporting medium (n = 4) for studying the repeatability, as found in Fig.3.20. (a-b). The results demonstrate a relative standard deviation (RSD) of 1.47% for four (1,2,3, and 4) repetitions, indicating the sensor's excellent repeatability. With same operational conditions, Fig.3.20. (c-d) demonstrate remarkably reproducible performance, as evidenced by the low RSD value of 1.99% across the four electrodes (1’,2’,3’,4’). Moreover, the electrode is preserved at room temperature for two months for reevaluating its performance in the identical analyte solution. The result is obtained at Day1, Day20, Day40, and Day60. No notable change in the peak current (RSD 2.1%) is observed, highlighting the outstanding stability of the electrode in Fig.3.20. (e-f).

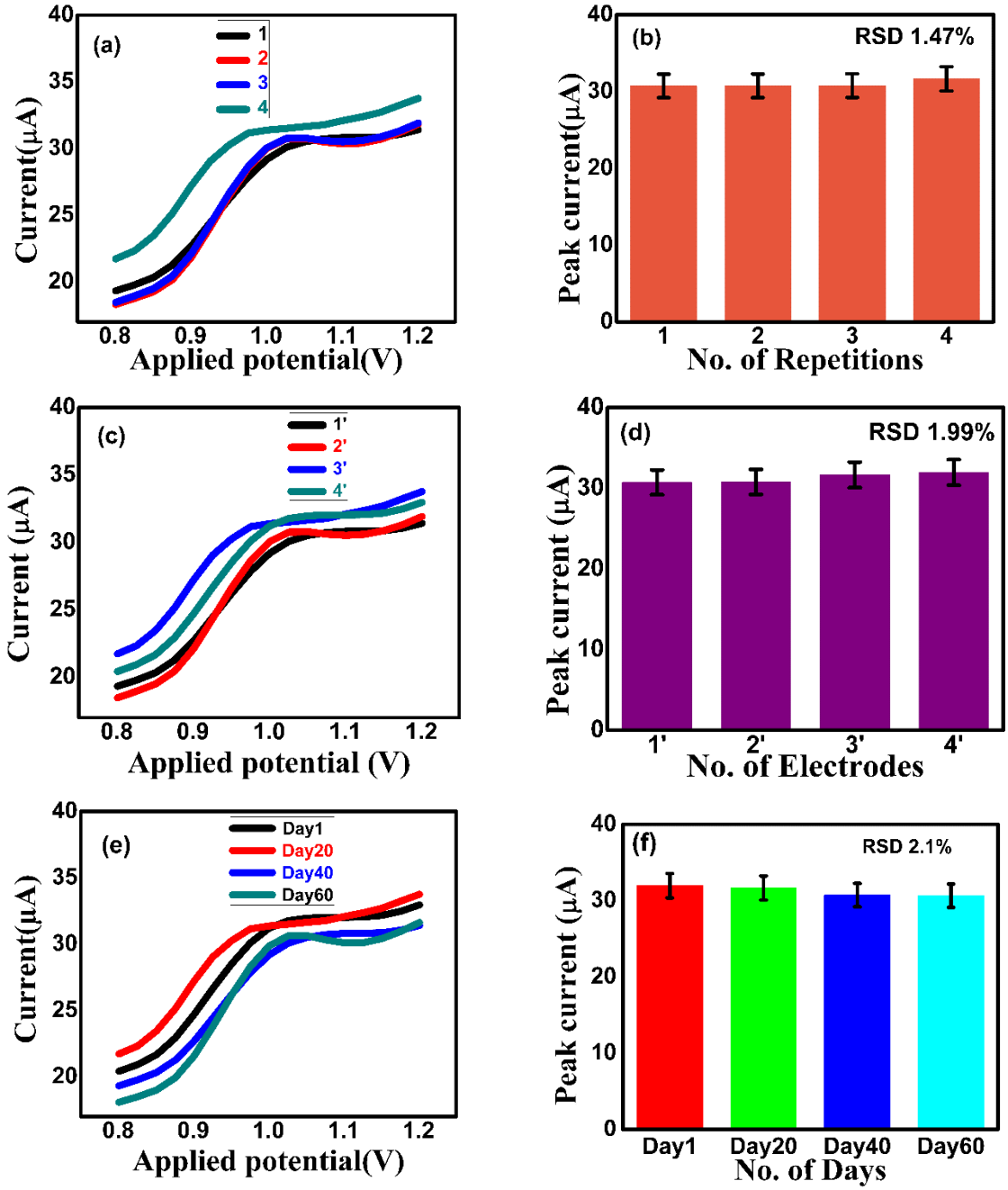

Fig.3.20. Analytical performance of Y_2O_3@GPE for AMR detection (a-b) DPV curve and related bar plot for repeatability; (c-d) DPV curve and related bar diagram of reproducibility; (e-f) DPV curve and related bar plot of stability.

3.5.10. Selectivity study

The Y_2O_3@GPE sensor undergoes exposure to various interferants, namely cations like Na^+, Ca^{2+}, Mg^{2+}, anion like Cl^-, and a synthetic food color named Rhodamine B (RhB), for assessing their effect on its electrochemical properties. Subsequent to the introduction of each interfering species followed by the introduction of the target analyte, corresponding CV responses are recorded.

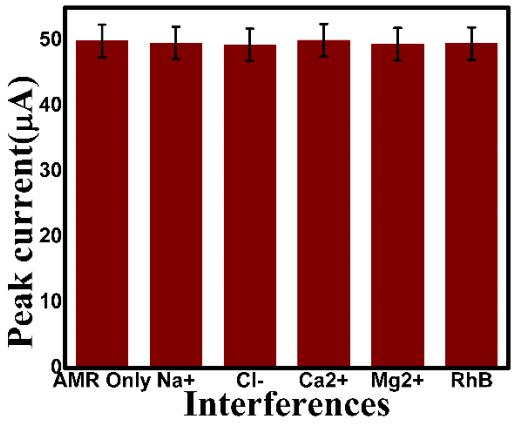

Fig.3.21. Influence of interfering agents to CV Ip responses of AMR at Y_2O_3@GPE.

Figure 3.21 illustrates the related bar diagram representation where the electrode is found to show the mere response to other interfering agents. Remarkably, the fluctuations in the relative signal did not surpass the permissible range of ±5%.

3.5.11. PCA for AMR concentrations using Y_2O_3@GPE

The PCA technique, described in the Section 2.3.6 of Chapter 2, has been applied here also for analyzing the Y_2O_3@GPE generated data of AMR solution. The DPV response curves for AMR concentrations (5μM, 10μM, 20μM, 50μM, and 100μM as C1, C2, C3, C4, and C5, respectively) using Y_2O_3@GPE are analyzed via this PCA tool.

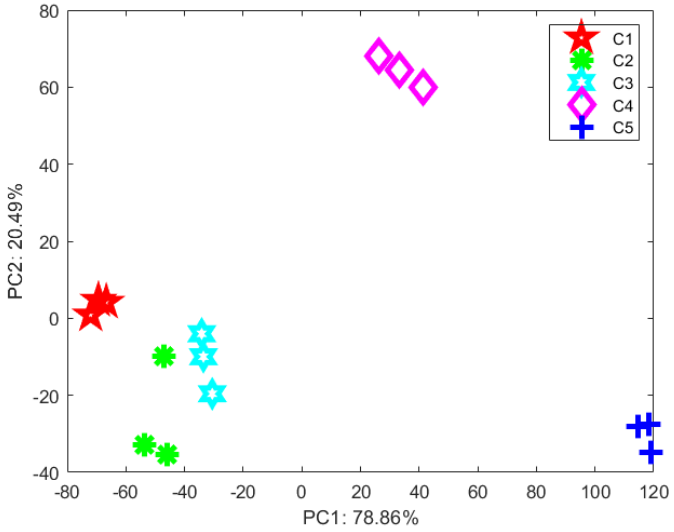

Fig.3.22 DPV data analysis of AMR obtained by Y_2O_3@GPE, using PCA-a graphical representation.

Three repetitions are considered for each concentration. The PCA plot with successful data clustering is shown in Fig.3.22., where all the different concentrations are found to be rightly discriminated. The PC1 and PC2 illustrate 78.86%, and 20.49% of total variances, respectively. A high S.I. value is found as 238.68, suggesting a clear separation of the classes in the dataset.

3.5.12. PLSR Analysis for AMR data

Different concentrations of AMR (C1-C5) have been assessed through PLSR analysis method, described before in the Section 2.3.7 of Chapter 2. For each concentration, the ratio between training data and testing data is 3:1. The prediction parameters are listed in Table 3.5. In Table 3.6, the correlation factor found after prediction denotes a well performing model in terms of accurate prediction of the response variable based on the predictor variables. Results in Table 3.5. show that the average prediction accuracy using the PLSR tool for voltametric detection of AMR using Y_2O_3@GPE is highly satisfactory as 99.58%. The root means square error of prediction (RMSEP) has a very good value of 0.4, lower than the RMSEP obtained in case of CPE based AMR detection, indicating the reduction in error of the system after incorporating the Y_2O_3 nanoparticles into the carbon paste.

Table 3.5. Comparison of actual and predicted AMR contents achieved via PLSR for Y_2O_3@GPE.

No. of samples	Actual AMR contents (µM)	Predicted AMR contents (µM)	Prediction accuracy (%)
1	5	4.72	94.48
2	10	10.5	104.97
3	20	19.47	97.33
4	50	50.36	100.71
5	100	100.41	100.41
Average prediction accuracy 99.58%			

Table 3.6. PLSR related parameters for Y_2O_3@GPE for voltammetric AMR detection.

C.F. (training)	C.F. (prediction)	RMSEP
1	0.99	0.4

3.5.13. Investigation of AMR in real application

As mentioned earlier, different candies are examined using this Y_2O_3@GPE for the validation of its application in case of real-life samples. Based on our survey of the existing literature, it can be inferred that majority of the works are focused on tap water samples, soft drinks, and various fruit juices such as orange and apple juice. Therefore, in our work, we have concentrated on detecting AMR in real samples of different candies which are primarily consumed by children. The idea is to prevent the high risk of fatal food borne diseases which can occur due to the adulteration and excessive consumption of azo-dye beyond the daily safe limit which can have an adverse effect on children's health. Three types of popular candies are bought from the local market places in India. After grinding them using mixer and grinder, 40ml of water was added separately to 1 gm of each of these candies and three different homogeneous solutions were made after around 30mins of sonication. Whatman UNIFLO

disposable sterile syringe filters (diameter 25 mm, pore size 0. 22µM) were used for the required filtration of those solutions. These samples were then sent through DPV analysis and the Standard Addition Method was undertaken. The results, listed in Table 3.7, were found pretty satisfactory with nice recovery rates of 102.2%-124% and RSD of 1.11%-2.57%. These results confirmed that the developed Y_2O_3@GPE sensor is full of potential for practical life application.

Table 3.7. Determination of AMR In different candy samples.

Sample	Spiking (µM)	Detected (µM)	Recovery [A] (%)	RSD [B] (%) (N=2)
Candy1	0	0	-	-
	1	1.24	124	1.15
	20	23.33	116.65	1.11
Candy2	0	4	-	1.75
	1	5.15	115	1.67
	20	24.44	102.2	1.6
Candy3	0	6	-	2.32
	1	7.04	104	1.2
	20	28	110	2.57

[a] Recovery = [(Detected-Diluted) (µM)]/Spiking (µM)
[b] R.S.D (%) = [100x Standard deviation]/ Mean

3.5.14. Comparative study for basic CPE and Y_2O_3@GPE: their performance parameters for detecting AMR

Table 3.8 is presented here to summarize the performance indices of CPE and Y_2O_3@GPE for the voltametric detection of AMR. Different parameter values clearly indicate that the modification of CPE with the Y_2O_3 nanoparticles unquestionably improves its efficiency for the voltametric detection of AMR. Though the RSD of repeatability value increases little bit in case of the Y_2O_3@GPE, but it has been allowed considering all other improvements in efficiency in case of Y_2O_3@GPE with respect to CPE performance.

Table 3.8. Comparison between CPE and Y_2O_3@GPE performance to detect AMR.

Sl. No.	Parameter	CPE	Y_2O_3@GPE
1	Maximum peak current	8.51µA	49.89µA
2	R^2 (Scan rate)	0.96	0.99
3	R^2 (Concentration)	0.98	0.98, 0.99
4	RSD(Repeatability)	1.3%	1.47%
5	RSD(Reproducibility)	2.8%	1.99%

6	RSD(Stability)	2.6%	2.1%
7	Stability span	21 Days	60 Days
8	Separability index (S.I.)	34.89	238.68
9	Prediction accuracy	93.73%	99.58%
10	LOD	0.17µM	3.6nM
11	RMSEP	0.76	0.4

3.6. Conclusion

This study deals with the synthesis of Y_2O_3 nanoparticles using a simple sol-gel method and thereafter applying it as a novel modifier for increasing the efficiency of CPE to be applied for the voltammetric detection of AMR. This modified combination exhibited a synergistic effect, increasing both sensitivity and selectivity of the AMR sensor. In an ideal scenario, the sensor demonstrated a good linearity (0.05–100µM) along with an outstandingly lower LOD (3.6 nM) in comparison with different electrodes reported in the literature, assuring its exceptional sensitivity. This LOD value is even much lower than the LOD of CPE based detection of AMR (0.17µM), reported earlier in this chapter. The presented electrode exhibited remarkable selectivity, reproducibility, repeatability, and stability for approximately a pair of months. Moreover, the proposed sensor was utilised for the detection of AMR in real specimens like different candies, consumed mainly by the infants, unveiling no noticeable interference in the matrix of real samples for AMR detection.

References

[1] H. A. Javar, H. M.-Moghaddam, A. Rajabizadeh, S. Hamzeh, and E. Akbari, "Development of an electrochemical sensor based on Ce^{3+} and CuO for the determination of amaranth in soft drinks," *Microchemical Journal*, vol. 183, no. September, p. 108081, 2022, doi: 10.1016/j.microc.2022.108081.

[2] J. A. Buledi *et al.*, "Selective oxidation of amaranth dye in soft drinks through tin oxide decorated reduced graphene oxide nanocomposite based electrochemical sensor," *Food and Chemical Toxicology*, vol. 165, no. May, p. 113177, 2022, doi: 10.1016/j.fct.2022.113177.

[3] M. Bijad, H. K.-Maleh, M. Farsi, and S. A. Shahidi, "Simultaneous determination of amaranth and nitrite in foodstuffs via electrochemical sensor based on carbon paste electrode modified with CuO/SWCNTs and room temperature ionic liquid," *Food*

Analytical Methods, vol. 10, no. 11, pp. 3773–3780, 2017, doi: 10.1007/s12161-017-0933-z.

[4] G. Zhang and Y. Ma, "Mechanistic and conformational studies on the interaction of food dye amaranth with human serum albumin by multispectroscopic methods," *Food Chemistry*, vol. 136, no. 2, pp. 442–449, 2013, doi: 10.1016/j.foodchem.2012.09.026.

[5] M. Iammarino, A. Mentana, D. Centonze, C. Palermo, M. Mangiacotti, and A. E. Chiaravalle, "Simultaneous determination of twelve dyes in meat products: development and validation of an analytical method based on HPLC-UV-diode array detection," *Food Chemistry*, vol. 285, no. March 2018, pp. 1–9, 2019, doi: 10.1016/j.foodchem.2019.01.133.

[6] N. Pourreza and S. Elhami, "Cloud point extraction and spectrophotometric determination of amaranth in food samples using nonionic surfactant Triton X-100 and tetrabutylammonium hydrogen sulfate," *Journal of the Iranian Chemical Society*, vol. 6, no. 4, pp. 784–788, 2009, doi: 10.1007/BF03246170.

[7] H. Oka *et al.*, "Identification of unlawful food dyes by thin-layer chromatography-fast atom bombardment mass spectrometry," *Journal of Chromatography A*, vol. 674, no. 1–2, pp. 301–307, 1994, doi: 10.1016/0021-9673(94)85235-9.

[8] M. Ryvolová, P. Táborský, P. Vrábel, P. Krásenský, and J. Preisler, "Sensitive determination of erythrosine and other red food colorants using capillary electrophoresis with laser-induced fluorescence detection," *Journal of Chromatography A*, vol. 1141, no. 2, pp. 206–211, 2007, doi: 10.1016/j.chroma.2006.12.018.

[9] R. Yemmi, B. E. Kumara Swamy, S. C. Sharma, C. Sridhar, and B. Kar, "Voltammetric sensor for amaranth at zinc oxide nanoparticle modified carbon paste electrode," *Inorganic Chemistry Communications*, vol. 161, no. January, p. 112133, 2024, doi: 10.1016/j.inoche.2024.112133.

[10] H. Beitollahi, F. Garkani Nejad, Z. Dourandish, and S. Tajik, "A novel voltammetric amaranth sensor based on screen printed electrode modified with polypyrrole nanotubes," *Environmental Research*, vol. 214, no. P1, p. 113725, 2022, doi: 10.1016/j.envres.2022.113725.

[11] F. Pogacean *et al.*, "Graphene/TiO_2 -Ag based composites used as sensitive electrode materials for amaranth electrochemical detection and degradation," *Journal of the Electrochemical Society*, vol. 165, no. 8, pp. B3054–B3059, 2018, doi: 10.1149/2.0101808jes.

[12] J. L. He, W. Kou, C. Li, J. J. Cai, F. Y. Kong, and W. Wang, "Electrochemical sensor based on single-walled carbon nanotube-TiN nanocomposites for detecting Amaranth," *International Journal of Electrochemical Science*, vol. 10, no. 12, pp. 10074–10082, 2015, doi: 10.1016/S1452-3981(23)11243-0.

[13] R. Zaimbashi, A. Mostafavi, and T. Shamspur, "Synthesis of vanadium oxide nanoplate for electrochemical detection of amaranth in food samples," *Journal of Electrochemical Science and Engineering*, vol. 12, no. 6, pp. 1153–1163, 2022, doi: 10.5599/jese.1394.

[14] Q. Q. Hu, H. Gao, Y. M. Wang, W. Ma, and D. M. Sun, "Simultaneous determination of carmine and amaranth based on a poly(L-arginine)–graphene modified electrode," *Journal of Analytical Chemistry*, vol. 73, no. 8, pp. 817–823, 2018, doi: 10.1134/S1061934818080051.

[15] H. Wang *et al.*, "Co_3O_4 -CeO_2 /Graphene Composite as a Novel Sensor for Amaranth Detection," *Journal of the Electrochemical Society*, vol. 168, no. 2, p. 027513, 2021, doi: 10.1149/1945-7111/abe3a3.

[16] H. Naskar, B. Ghatak, S. Biswas, B. Tudu, R. Bandyopadhay, and P. Pramanik, "Electrochemical detection of capsaicin using yttrium oxide nanoparticles modified graphite paste electrode (Y_2O_3/GPE)," *ISOEN 2019 - 18th International Symposium on Olfaction and Electronic Nose, Proceedings*, pp. 1–3, 2019, doi: 10.1109/ISOEN.2019.8823183.

[17] K. Jayasankar, A. Pandey, B. K. Mishra, and S. Das, "Evaluation of microstructural parameters of nanocrystalline Y_2O_3 by X-ray diffraction peak broadening analysis," *Materials Chemistry and Physics*, vol. 171, pp. 195–200, 2016, doi: 10.1016/j.matchemphys.2016.01.005.

[18] L. Smrčok, "Rietveld refinement of Y_2O_3 using the Pearson VII profile shape function," *Crystal Research and Technology*, vol. 24, no. 6, pp. 607–611, 1989, doi: 10.1002/crat.2170240609.

[19] B. Zhao, F. Mattelaer, G. Rampelberg, J. Dendooven, and C. Detavernier, "Thermal and plasma-enhanced atomic layer deposition of yttrium oxide films and the properties of water wettability," *ACS Applied Materials and Interfaces*, vol. 12, no. 2, pp. 3179–3187, 2020, doi: 10.1021/acsami.9b18412.

[20] M. Hajizadeh-Oghaz, R. S. Razavi, M. Barekat, M. Naderi, S. Malekzadeh, and M. Rezazadeh, "Synthesis and characterization of Y_2O_3 nanoparticles by sol–gel process for transparent ceramics applications," *Journal of Sol-Gel Science and Technology*, vol. 78, no. 3, pp. 682–691, 2016, doi: 10.1007/s10971-016-3986-3.

[21] R. Srinivasan, R. Yogamalar, and A. C. Bose, "Structural and optical studies of yttrium oxide nanoparticles synthesized by co-precipitation method," *Materials Research Bulletin*, vol. 45, no. 9, pp. 1165–1170, 2010, doi: 10.1016/j.materresbull.2010.05.020.

[22] L. Zhang *et al.*, "High sinterability nano-Y_2O_3 powders prepared via decomposition of hydroxyl-carbonate precursors for transparent ceramics," *Journal of Materials Science*, vol. 52, no. 14, pp. 8556–8567, 2017, doi: 10.1007/s10853-017-1071-0.

[23] S. Nag, S. Pradhan, D. Das, B. Tudu, R. Bandyopadhyay, and R. Banerjee Roy, "Fabrication of a molecular imprinted polyacrylonitrile engraved graphite electrode for detection of formalin in food extracts," *IEEE Sensors Journal*, vol. 22, no. 1, pp. 42–49, 2022, doi: 10.1109/JSEN.2021.3128520.

[24] S. Nag, D. Das, H. Naskar, B. Tudu, R. Bandyopadhyay, and R. Banerjee Roy, "Detection of metanil yellow adulteration in turmeric powder using nano nickel cobalt oxide modified graphite electrode," *IEEE Sensors Journal*, vol. 22, no. 13, pp. 12515–12521, 2022, doi: 10.1109/JSEN.2022.3178768.

[25] A. H. M. T. Ahmed *et al.*, "Electrochemical sensor based on molecularly imprinted polymer embedded graphite electrode for detecting curcumin," *Sensors and Actuators A: Physical*, vol. 344, no. June, p. 113748, 2022, doi: 10.1016/j.sna.2022.113748.

[26] E. Laviron, "General expression of the linear potential sweep voltammogram in the case of diffusionless electrochemical systems," *Journal of Electroanalytical Chemistry*, vol. 101, no. 1, pp. 19–28, 1979, doi: 10.1016/S0022-0728(79)80075-3.

[27] E. Laviron, "Adsorption, autoinhibition and autocatalysis in polarography and in linear potential sweep voltammetry," *Journal of Electroanalytical Chemistry*, vol. 52, no. 3, pp. 355–393, 1974, doi: 10.1016/S0022-0728(74)80448-1.

[28] H. Naskar, S. Pradhan, B. Ghatak, S. Biswas, B. Tudu, and R. Bandyopadhyay, "Electrochemical detection of capsaicin in chili pepper using molecular imprinted poly β-cyclodextrin embedded graphite (MIP-β-CD@G) electrode," *IEEE Sensors Journal*, vol. 21, no. 16, pp. 17657–17664, 2021, doi: 10.1109/JSEN.2021.3083527.

[29] T. Nandy Chatterjee *et al.*, "Detection of theaflavins in black tea using a molecular imprinted polyacrylamide-graphite nanocomposite electrode," *Sensors and Actuators B: Chemical*, vol. 246, pp. 840–847, 2017, doi: 10.1016/j.snb.2017.02.139.

[30] T. N. Chatterjee *et al.*, "Molecular imprinted polymer based electrode for sensing catechin (+C) in green tea," *IEEE Sensors Journal*, vol. 18, no. 6, pp. 2236–2244, 2018, doi: 10.1109/JSEN.2018.2791661.

[31] H. Naskar, S. Biswas, B. Tudu, R. Bandyopadhyay, and P. Pramanik, "Voltammetric detection of thymol (THY) using polyacrylamide embedded graphite molecular imprinted polymer (PAM@G-MIP) electrode," *IEEE Sensors Journal*, vol. 19, no. 19, pp. 8583–8589, 2019, doi: 10.1109/JSEN.2019.2922045.

[32] S. Jing, H. Zheng, L. Zhao, L. Qu, and L. Yu, "Electrochemical sensor based on poly (sodium 4-styrenesulfonate) functionalized graphene and Co_3O_4 nanoparticle clusters for detection of amaranth in soft drinks," *Food Analytical Methods*, vol. 10, no. 9, pp. 3149–3157, 2017, doi: 10.1007/s12161-017-0889-z.

[33] Q. Han, X. Wang, Z. Yang, W. Zhu, X. Zhou, and H. Jiang, "Fe_3O_4@rGO doped molecularly imprinted polymer membrane based on magnetic field directed self-assembly for the determination of amaranth," *Talanta*, vol. 123, pp. 101–108, 2014, doi: 10.1016/j.talanta.2014.01.060.

[34] P. Wang, X. Hu, Q. Cheng, X. Zhao, X. Fu, and K. Wu, "Electrochemical detection of amaranth in food based on the enhancement effect of carbon nanotube film," *Journal of Agricultural and Food Chemistry*, vol. 58, no. 23, pp. 12112–12116, 2010, doi: 10.1021/jf103263p.

[35] S. Akbari, "A new voltammetric sensor according to graphene quantum dots/ionic liquid modified carbon paste electrode for amaranth sensitive determination," *International Journal of Environmental Analytical Chemistry*, vol. 102, no. 3, pp. 789–803, 2022, doi: 10.1080/03067319.2020.1726338.

[36] S. Chandran, L. A. Lonappan, D. Thomas, T. Jos, and K. Girish Kumar, "Development of an electrochemical sensor for the determination of amaranth: a synthetic dye in soft drinks," *Food Analytical Methods*, vol. 7, no. 4, pp. 741–746, 2014, doi: 10.1007/s12161-013-9676-7.

[37] S. Tajik, H. Beitollahi, H. W. Jang, and M. Shokouhimehr, "A simple and sensitive approach for the electrochemical determination of amaranth by a Pd/GO nanomaterial-modified screen-printed electrode," *RSC Advances*, vol. 11, no. 1, pp. 278–287, 2020, doi: 10.1039/d0ra08723h.

Chapter 4

Detection of Indigo Carmine (ICN) using Carbon Paste Electrode (CPE), and Y_2O_3 Nanoparticles modified Graphite Paste Electrode (Y_2O_3@GPE)

This chapter elucidates the creation and application of a carbon paste electrode (CPE), followed by the enhancement of a graphite electrode with Y_2O_3 nanoparticles for the precise detection of Indigo Carmine (ICN) in candy products. It incorporates an intricate comparative examination of ICN detection, juxtaposed with prior research. In-depth discussion is provided on the electrochemical attributes of the developed electrode, experimental variables crucial to ICN detection, and a thorough scrutiny of real sample results.

List of Sections

Contents of this chapter are based on mentioned publication:

Samhita Dasgupta, A.H.M. Toufique Ahmed, Ipshita Bhattacharjee, Shreya Firdoushi, Don Biswas, Sumani Mukherjee, Bidya Mondal, Rajib Bandyopadhyay, Bipan Tudu, "Electrochemical detection of indigo carmine in candies using Y_2O_3 nanoparticles infused graphite electrode," *Journal of Food Composition and Analysis*, vol. 135, 106626, pp. 1-9, 2024. [DOI: https://doi.org/10.1016/j.jfca.2024.106626]

4.1. Introduction

Indigo carmine (ICN) (Disodium [2(2′) E]-3,3′-dioxo-1,1′,3,3′-tetrahydro[2,2′-biindolylidene]-5,5′-disulfonate) is a blue artificial food dye, widely known as a coloring object in beverages, foods, cosmetics industries and in the dyeing sectors [1], [2]. ICN is used also in pharmacies and medicines for diagnosis purpose [3], [4]. The chemical structure of ICN can be found in Fig. 4.1.

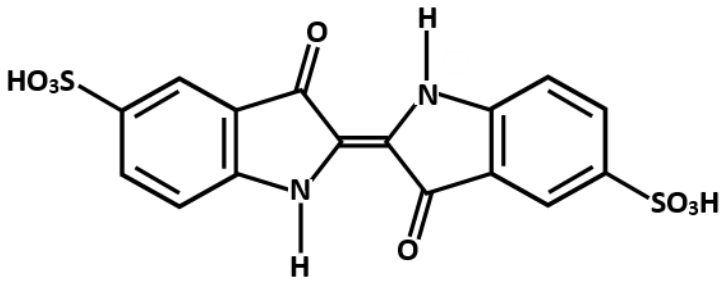

Fig. 4.1. Chemical structure of ICN.

Numerous conventional methods like high-performance liquid chromatography [5], spectrophotometry [6], liquid chromatography/tandem mass spectrometry [7] and thin-layer chromatography [8] have been used for the detection purpose of ICN so far. In contrast to these alternative way outs, electrochemical methods are one step forward because of being portable, simple, budget friendly, and swift in analysis [9], [10]. However, though ICN has electroactive properties, its electrochemical analysis makes the electrode surface face fouling. Hence, very few literatures are available on the electrochemical detection of ICN [11], [12], [13] as developing an electrode for ICN detection with little adsorption of ICN is a challenging task. Still, a few published literatures regarding ICN have already been discussed in Chapter 1, Section 1.1 and Section 1.4. A voltametric sensor has been developed for detecting ICN using glassy carbon electrode (GCE) modified with SeO_2 nanoparticles and surfactants [3]. However, still there exists a field for improvement in both the LOD and the detection range of all sensors. This study finds a budgetary route by developing a simple CPE for detecting ICN electrochemically in the laboratory. Different CV and DPV responses are noted for the electrochemical study of this electrode. Next, Y_2O_3 nanoparticles are incorporated in the carbon paste for better efficiency. Reasons behind the use of Graphite and Y_2O_3 nanoparticles for the electrode fabrication have already been discussed in the Section 2.1 of Chapter 2.

4.2. Experimentation with CPE to detect ICN

4.2.1. Components and molecules

Loba Chemie Pvt. Ltd. (India) is the source of ultra-pure ICN. Graphite powder is bought from Sigma Aldrich, USA while Y_2O_3, paraffin oil, PEG-400, and ammonia are purchased from Merck India. Being of analytical grade, all chemicals obtained are used without further refinement. The required supporting electrolytes, including phosphate buffered saline (PBS), citrate buffered saline (CBS), and acetate buffered saline (ABS), each at a concentration of 0.1 M, are prepared in the research lab. Millipore water (18 MΩ cm^{-1}) derived from a Merck Millipore system is employed for the making of all aqueous solutions and electrode cleaning. Each and every experiment are done at an ambient temperature of approximately 23°C-27°C.

4.2.2. Apparatus and instrumentation

Electrochemical analysis is performed employing a three-electrode setup alongside a potentiostat PGSTAT101 (Metrohom Autolab, Netherlands). The system comprises a reference electrode (Ag/AgCl), a platinum counter electrode, and a custom carbon paste electrode (CPE) serving as the working electrode. NOVA software from Metrohom Autolab is utilized to visualize cyclic voltammetry (CV) and differential pulse voltammetry (DPV) responses. Additionally, Labman Scientific Instruments', India ultrasonicator facilitates proper blending of solutes and solvents.

4.2.3. Experimental setup

The experimental setup is same as mentioned earlier, in the Section 2.2.3 of Chapter 2. The only change is that here the target analyte is the aqueous solution of ICN.

4.2.4. The working electrode WE-CPE

The CPE development is already described in Section 2.2.4 of Chapter 2, and in 3.2.4 of Chapter 3 also.

4.3. Results and discussions for CPE to detect ICN

4.3.1. Electrochemical behaviour of CPE for detecting ICN

The electrochemical behaviour of the CPE is studied by monitoring the cyclic voltammogram (CV). For aqueous solution of ICN, the CV response of CPE within the 0-1 V range is primarily recorded with only 0.1M PBS-6 solutions, at a scan rate of 50mV/sec. Next, 100µM of the ICN solution is added to the PBS solution, and the CV response is monitored once again,

maintaining same potential range and scan rate. Figure 4.2. (a) depicts that an oxidation peak and a reduction peak develop in the presence of the target analyte, whereas no peak is found in the absence of the same. The electrochemical reaction is thus clearly occurring at the CPE surface as the oxidation peak and reduction peak are achieved at near 0.54 V with a peak current of 4.94µA, and at near 0.49 V with a peak current of -1.72µA, respectively, in the presence of the target molecule only. The reasons behind selecting a scan rate of 50mV/sec and 100µM concentration have already been discussed in the Section 2.3.1 of Chapter 2.

4.3.2. Influence of buffer variation

To determine the optimal buffer solution, an extensive investigation is conducted using different buffered saline solutions (pH 6), namely ABS, PBS, and CBS, respectively. From Fig.4.2. (b), it can be noticed that the oxidation and reduction Peak currents (Ip) for CPE are the utmost (4.94µA and -1.72µA, respectively) for PBS. Besides, it can be observed that this maximum current in case of PBS is obtained applying the lowest voltage value. Therefore, PBS is ultimately selected to achieve the optimal response using CPE for the detection of ICN. Subsequently, PBS solutions with pH values of 5, 6, and 7 are considered to determine the ideal pH. The maximum current, mentioned already, is attained for PBS-6 (Fig.4.2. (c)); thus, pH is taken as 6 in this experiment.

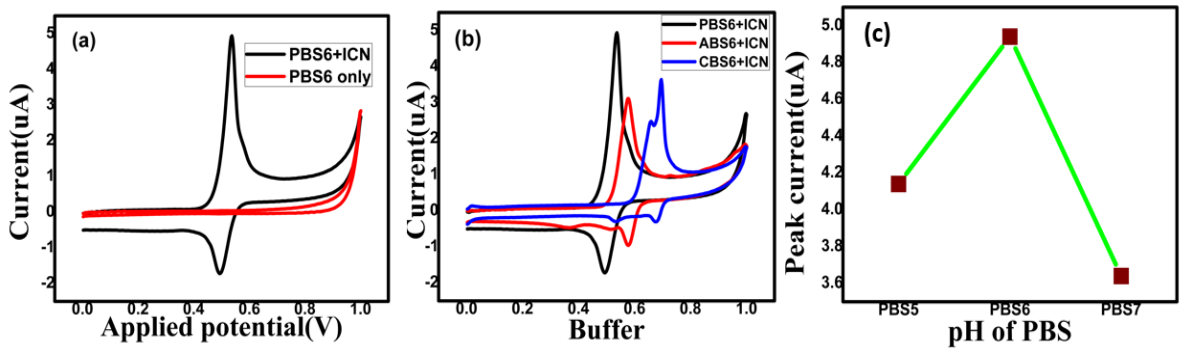

Fig. 4.2. CV data (a) of CPE in presence and absence of ICN molecule; (b) plot for 100µM ICN in PBS, ABS, CBS solutions each with pH 6; (c) pH optimization of PBS for CPE for ICN.

4.3.3. Scan rate variation study

The electrode's performance is assessed through CV analysis over a voltage range of 0-1 V, for studying the impact of scan rate variation. Figure 4.3.(a) depicts the CV data, demonstrating that the peak current (I_p) increases proportionally with scan rates ranging from 5 to 300 mV/s. Figure 4.3. (b) illustrates the corresponding linearity plot, exhibiting a twofold linearity

attributed to oxidation and reduction processes. Equations (4.1) and (4.2) represent the linear equations for oxidation and reduction, respectively

$$I_{ICN} = 0.1v + 1.17;\ R^2 = 0.98 \quad (4.1)$$

$$I_{ICN} = -0.06v + 1.02;\ R^2 = 0.97 \quad (4.2)$$

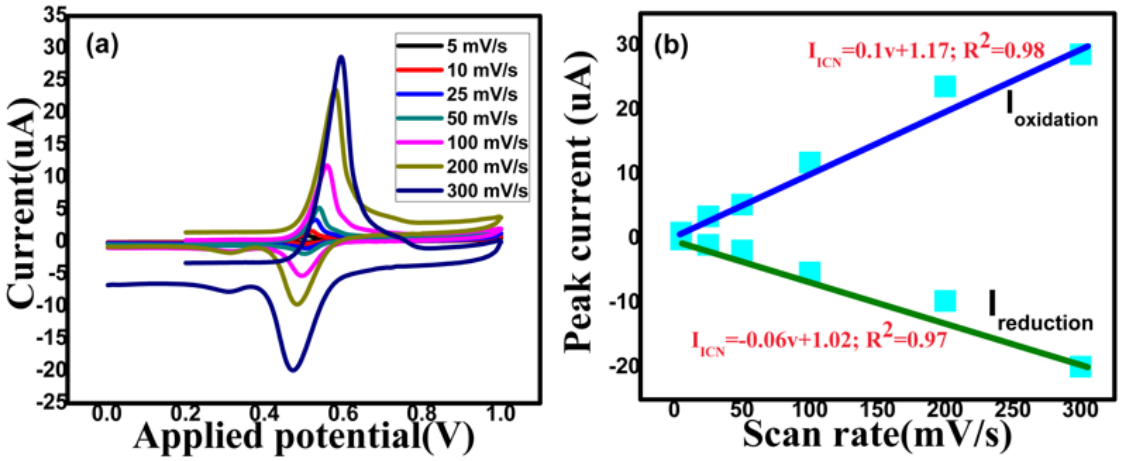

Fig. 4.3. (a) CV responses of Ip variation with scan rate (5-300 mV/sec;) (b) Linear plot for Ip vs scan rate in 0.1 M PBS for detecting ICN.

4.3.4. Concentration variation study

The DPV responses are closely monitored to investigate the impact of various ICN concentrations on the surface of the CPE electrode, spanning a potential range from 0.35 V to 0.8 V (buffer 0.1M PBS). In Fig. 4.4. (a), a systematic increase in peak current is evident with the gradual elevation of ICN concentrations (5µM, 10µM, 20µM, and 100µM).

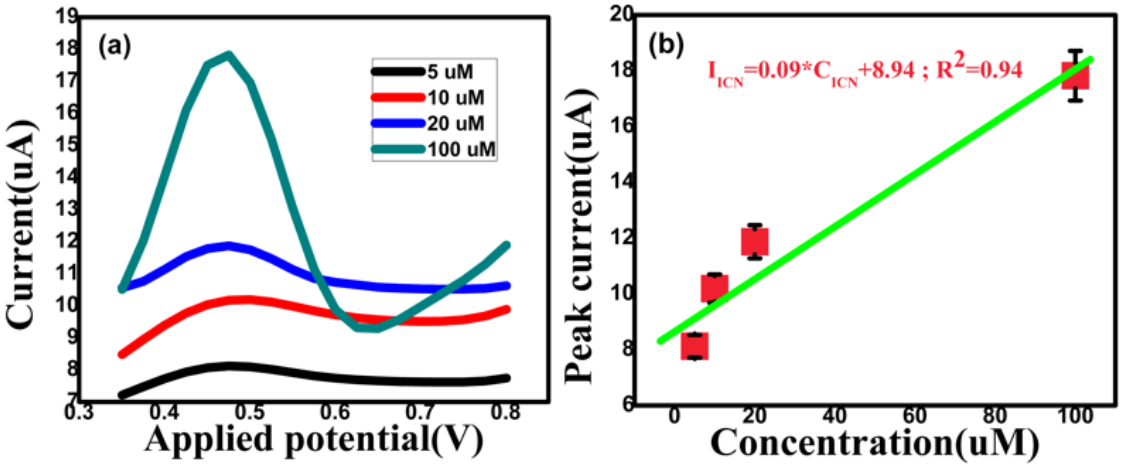

Fig. 4.4. (a) DPV responses for ICN by CPE in 0.1 M PBS (a) concentration of 5-100µM; (b) Linear plot of Ip vs concentration.

Figure 4.4. (b) illustrates the calibration plot, displaying a linear trend described by regression equation (4.3):

$$I_{ICN} = 0.09C_{ICN} + 8.94;\ R^2 = 0.94 \quad (4.3)$$

The Limit of Detection (LOD) is determined as 0.83µM using equation (2.3), mentioned in the Section 2.3.4 of Chapter 2.

4.3.5. Repeatability, reproducibility, and stability study for ICN with CPE

A study on repeatability involves three consecutive DPV responses, designated as Rp1, Rp2, and Rp3, revealing the nice consistency of the CPE, with a mere 2.97% Relative Standard Deviation (%RSD) as depicted in Fig. 4.5. (a). Moreover, an assessment of reproducibility is conducted by examining the DPV responses of three identical CPEs, labelled Rd1, Rd2, and Rd3, yielding a commendable result with an RSD of 4.2%, as illustrated in Fig. 4.5. (b). Additionally, a stability analysis was carried out by storing the same CPE at ambient temperature and conducting tests at 16-day intervals over a span of 30 days. The observed behaviour indicates satisfactory stability, with an RSD of 3.6% as shown in Fig. 4.5. (c).

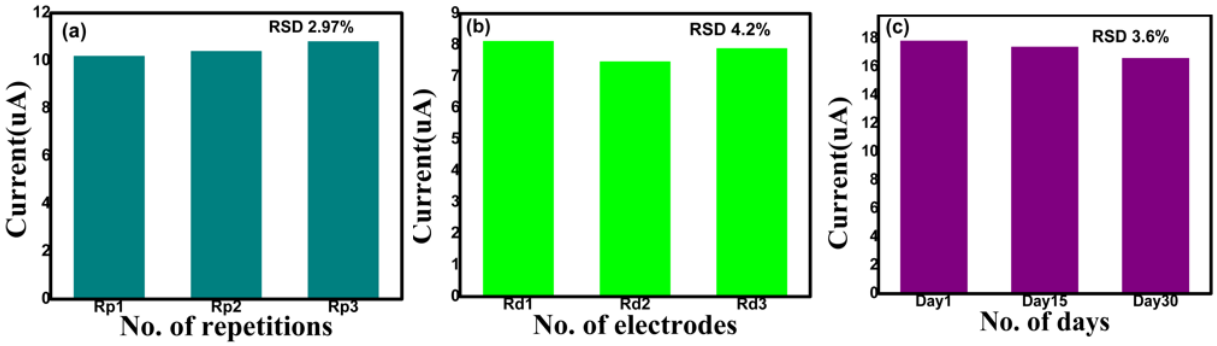

Fig. 4.5. For aqueous solution of ICN using CPE(a) Repeatability graph; (b) Reproducibility study; (c) Stability plot.

4.3.6. PCA for ICN concentrations

Incorporating the PCA methodology, as outlined in Section 2.3.6 of Chapter 2, it has been employed here also to analyse the CPE-generated data for ICN solution. The DPV response curves corresponding to ICN concentrations (5µM, 10µM, 20µM, and 100µM designated as C1, C2, C3, C4, respectively) utilizing CPE were subjected to this PCA analysis. Each concentration underwent three repetitions. The resulting PCA plot, exhibiting successful data clustering, is elegantly showcased in Fig.4.6., where each concentration is accurately distinguished. PC1 and PC2 encapsulate 83.19% and 11.09% of the total variances, respectively. The computed S.I. stands at 40.57, indicative of a pronounced separation among the dataset's classes.

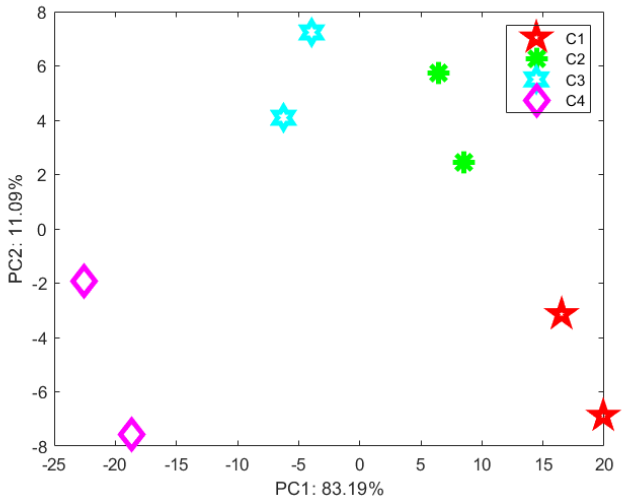

Fig. 4.6. The graph for DPV data (by CPE for ICN) analysis using PCA.

4.3.7. PLSR for ICN concentrations

Four distinct concentrations of ICN (C1-C4) have been sent through PLSR analysis method, narrated earlier in the Section 2.3.7 of Chapter 2. For each concentration, the training data and testing data are selected in a ratio of 3:1. The prediction parameters listed in Table 4.1. show that the average prediction accuracy using the PLSR tool for voltametric detection of ICN using CPE is 83.65%. The root means square error of prediction (RMSEP) is 0.98.

Table 4.1. Comparison of actual and predicted ICN contents achieved via PLSR for CPE.

No. of samples	Actual ICN contents (µM)	Predicted ICN contents (µM)	Prediction accuracy (%)
1	5	4.13	117.4
2	10	11	90
3	20	29	55
4	100	127.8	72.2
Average prediction accuracy 83.65%			

4.3.8. Discussions

The essence of this investigation revolves around the fast electrochemical detection of Indigo Carmine facilitated by an optimized CPE. Exhibiting an expansive operational spectrum, the system demonstrates a linearity spanning from 5µM to 100µM, with a LOD at 0.83µM. Through meticulous analysis utilizing the PCA tool, the DPV responses garnered from this CPE for ICN were thoroughly scrutinized, yielding a noteworthy SI value of 40.57. Regrettably, actual sample data has not been documented within this particular study. However, such data acquisition has been diligently conducted in the subsequent investigation, wherein

various types of candies served as the subject matter. There, an exhaustive exploration unfolds, elucidating the utilization of Y_2O_3 nanoparticles modified GPE, showcasing its efficacy in real-world scenarios.

4.4. Experimentation with Y_2O_3 nanoparticles modified graphite paste electrode (Y_2O_3@GPE) for detecting ICN

4.4.1. Reagents

All reagents used are detailed earlier in the Section 4.2.1 of this Chapter.

4.4.2. Formation of Y_2O_3 nanoparticles

Y_2O_3 nanoparticles development has been discussed in the Section 3.4.2 of Chapter 3.

4.4.3. Required characterization techniques

XRD, XPS, SEM, EDS, and FTIR methods have been used for the characterization of the developed Y_2O_3 nanoparticles. All of them are detailed in the Section 3.4.3, and Sections 3.5.1 to 3.5.4 of Chapter 3.

4.4.4. Y_2O_3@GPE fabrication

Y_2O_3@GPE fabrication method is detailed in the Section 3.4.4 of Chapter 3.

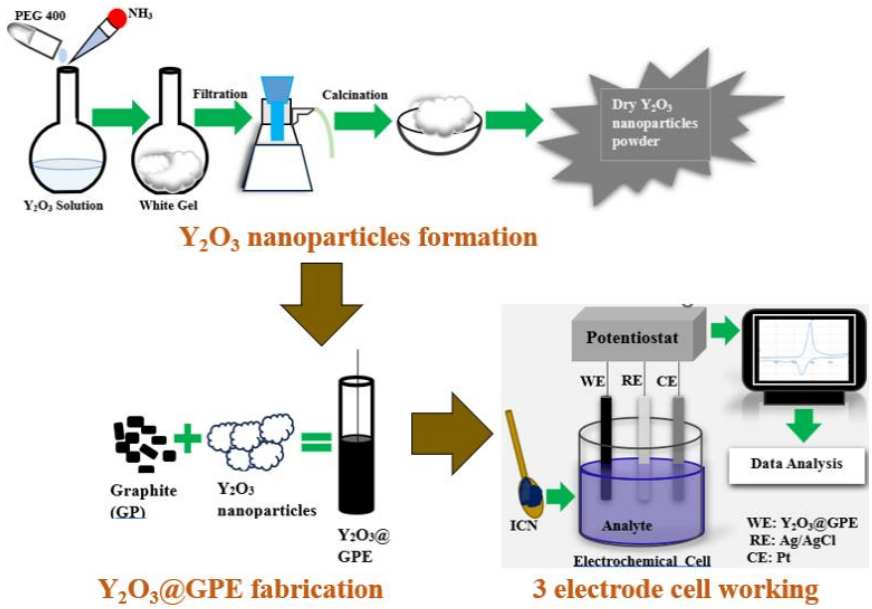

Fig. 4.7. Steps of measurement procedure for voltametric ICN detection using Y_2O_3@GPE.

The nanoparticles preparation followed by their application in forming the electrode and then data recording using this electrode are combined in a single picture shown in Fig.4.7.

4.5. Results and discussions for Y_2O_3@GPE for detecting ICN

4.5.1. Investigation of optimum modifier

At the very beginning of this study, three types of metal oxides like CuO, Y_2O_3, and Sm_2O_3 are examined to prepare the modified GPE with the equal quantity of graphite powder. The CVs of the CuO@GPE, Y_2O_3@GPE, and Sm_2O_3@GPE, developed afresh, in the presence of 100 µM of ICN with 0.1 M PBS6 as supporting buffer medium, are shown in Fig.4.8. (a).

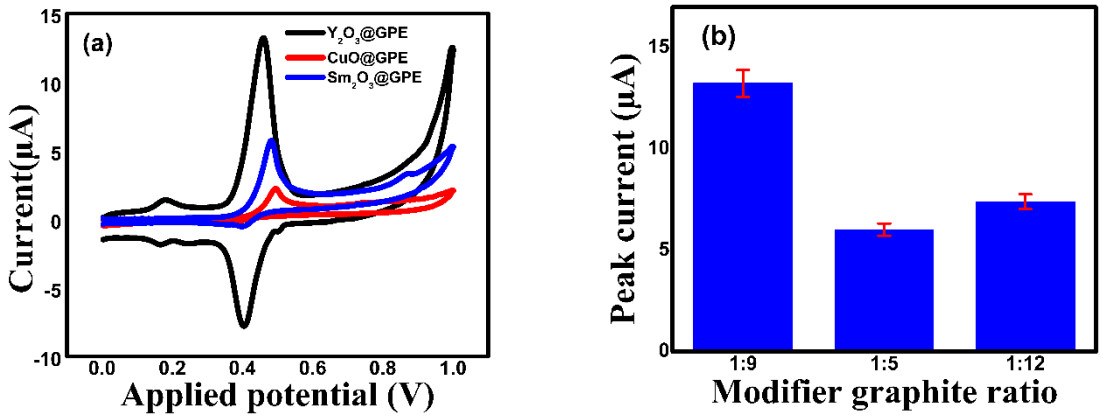

Fig. 4.8. (a) CVs of Sm_2O_3@GPE, CuO@GPE, and Y_2O_3@GPE in 100µM ICN solution in 0.1 M PBS6 for optimum modifier selection; (b) Bar plot for modifier: graphite vs peak current.

In the absence of ICN, none of them shows any response. Comparison among these curves provide the fact that the anodic and cathodic peak currents for Y_2O_3@GPE are much greater than those of the remaining two. As can be seen in Fig.4.8. (a), among all the modified electrodes, Y_2O_3@GPE notably increases the effectiveness of the process. The highest peak current for ICN were obtained on Y_2O_3@GPE, and therefore it is chosen as the modifier for next steps.

4.5.2. Impact of amount of the modifier Y_2O_3

Deciding the proper amount of the modifier plays a vital role behind the sensing properties of the Y_2O_3@GPE. Here three Y_2O_3@GPE were developed with different weight ratio of Y_2O_3 nanoparticles to graphite (1:9, 1:12, and 1:5) for determining 100µM ICN, respectively. The experimental data presented in Fig.4.8. (b) is indicative of the maximum current response of ICN in case of the 1:9 ratio combination. Lower current output of the sensor in case of 1:12 ratio may be because of the too little amount of Y_2O_3 nanoparticles to enhance the required electron transfer of ICN. Y_2O_3 generally is nonconductive in nature. The reason behind getting lower current response in case of 1:5 ratio may be too much covering of the surface area by Y_2O_3 nanoparticles and reduced conductivity of the CPE as a result. Thus, the optimum

modified GPE is prepared by mixing the Y_2O_3 nanoparticles with graphite powder in a ratio of 1:9.

4.5.3. Y_2O_3@GPE electrocatalytic performance

The electrochemical behaviour was studied via CV response monitoring for this Y_2O_3@GPE. CV responses for both the bare CPE and this Y_2O_3@GPE, in Fig.4.9. (a), show that the later one goes through a redox process with the oxidation peak current Ipa at 0.46 V and reduction peak current Ipc around 0.4 V. The Y_2O_3@GPE provided a higher oxidation peak current Ipa (13.2 µA) while compared to the Ip provided by the CPE (4.94 µA), mentioned in the section 4.3.1 of this chapter. This positive jump in Ip may be presented as a result of the acceleration in the electron kinetics because of the modification by nanoparticles.

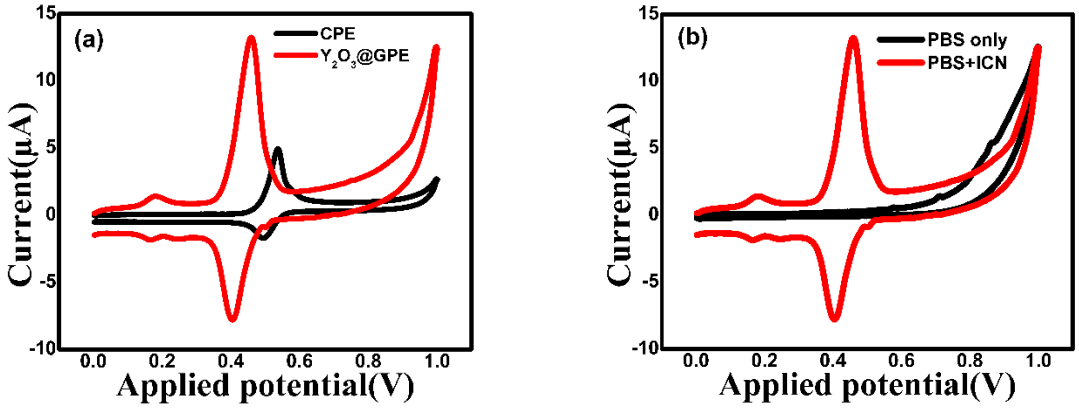

Fig. 4.9. (a)Performance comparison-bare CPE and Y_2O_3@GPE; (b)Role of ICN on CV plot.

For this modification, the surface area of the electrode increases improving the electrochemical performance. Moreover, Fig.4.9. (b) shows that no peak arises when there is the buffer solution only. It is a proof for the occurrence of the peaks resulted by the ICN molecules found in the 100µM ICN stock solution.

4.5.4. Buffer and pH variation

The used buffer solution and the medium pH have eminent role on the CV responses of Y_2O_3@GPE. Y_2O_3@GPE was dipped in ICN solution using three distinct supporting buffers separately, namely PBS, ABS, and CBS, each of pH 6. Figure 4.10. (a) provides the CV diagrams for optimum buffer selection. The ICN solution with PBS6 was found reaching the highest I_p, thus leading to the selection of PBS6 as optimum buffer. For the best-tuning of the medium pH, the redox processes were conducted in PBS of pH-5,6, and 7 (Fig.4.10. (b)). The results in Fig.4.10. (b) are indicative of the optimization of pH at 6 giving the highest I_p. The I_p reduces at PBS-5 and also as it reaches 7, probably as a result of poor ICN adsorption. The

plots for peak potential (E_p) and pH are there in Fig.4.10. (c), and Fig.4.10. (d), as E_{pa}, the anodic peak potential and E_{pc}, the cathodic peak potential, respectively. Two linearities are noticed which are mentioned below in (4.4) and (4.5) respectively.

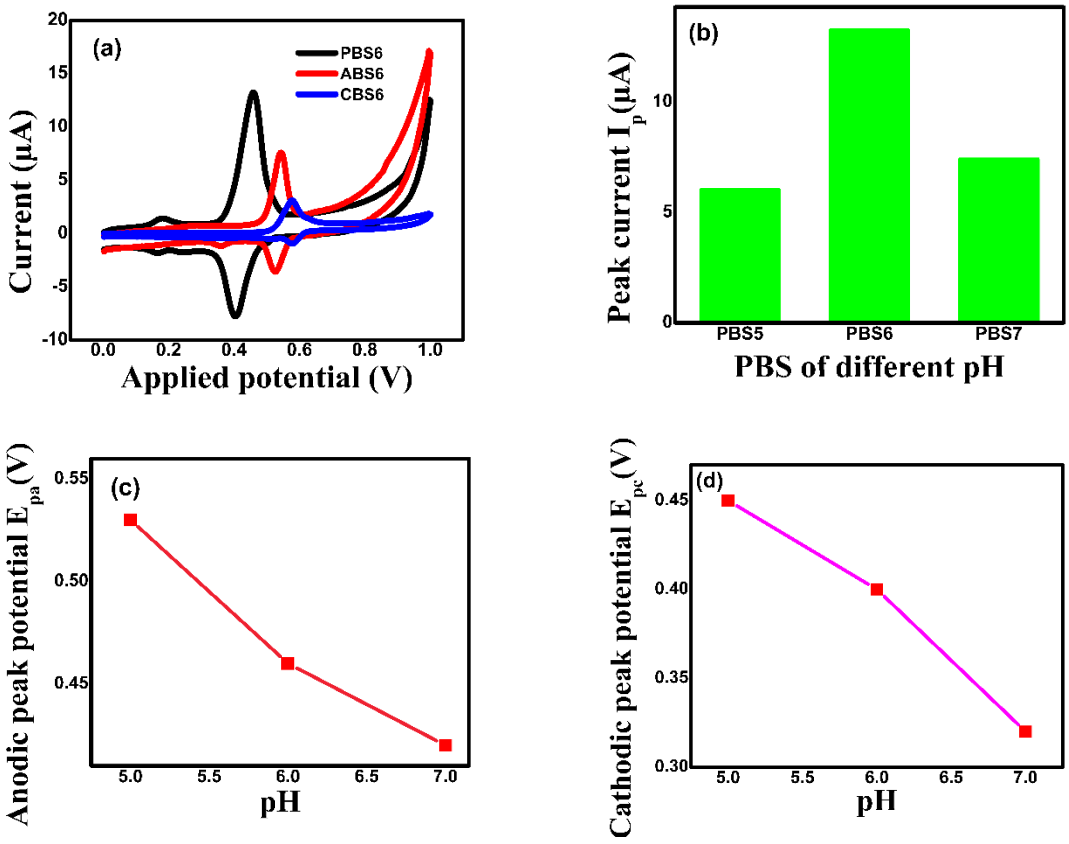

Fig. 4.10. (a) Optimum buffer selection for Y_2O_3@GPE; (b) Bar diagram for I_p and pH; (c) Plot showing linear relationship between E_{pa} and pH; (d) Plot for linearity between E_{pc} and pH.

$$E_{Pa} = -0.055pH + 0.8;\ R^2 = 0.98 \quad (4.4)$$

$$E_{Pc} = -0.06pH + 0.75;\ R^2 = 0.99 \quad (4.5)$$

These equations lead to the conclusion that E_p depends on pH with the slope values of -0.055 and -0.06, close to the theoretical value provided by Nernst [14], indicating equal number of protons and electrons engagement in the reaction mechanisms.

4.5.5. Scan rate variation

The performance of this electrode in face of scan rate variation is studied via CV analysis within 0-1 V voltage. Figure 4.11. (a) displays the CV data where I_p increases following a proportional manner with the rise in scan rates (5-300 mV/s) whereas the corresponding linearity plot is shown in Fig.4.11. (b). The linearity achieved is two by number, one because of oxidation and

the other for reduction. These two linear equations, for oxidation and reduction respectively, are found in (4.6) and (4.7).

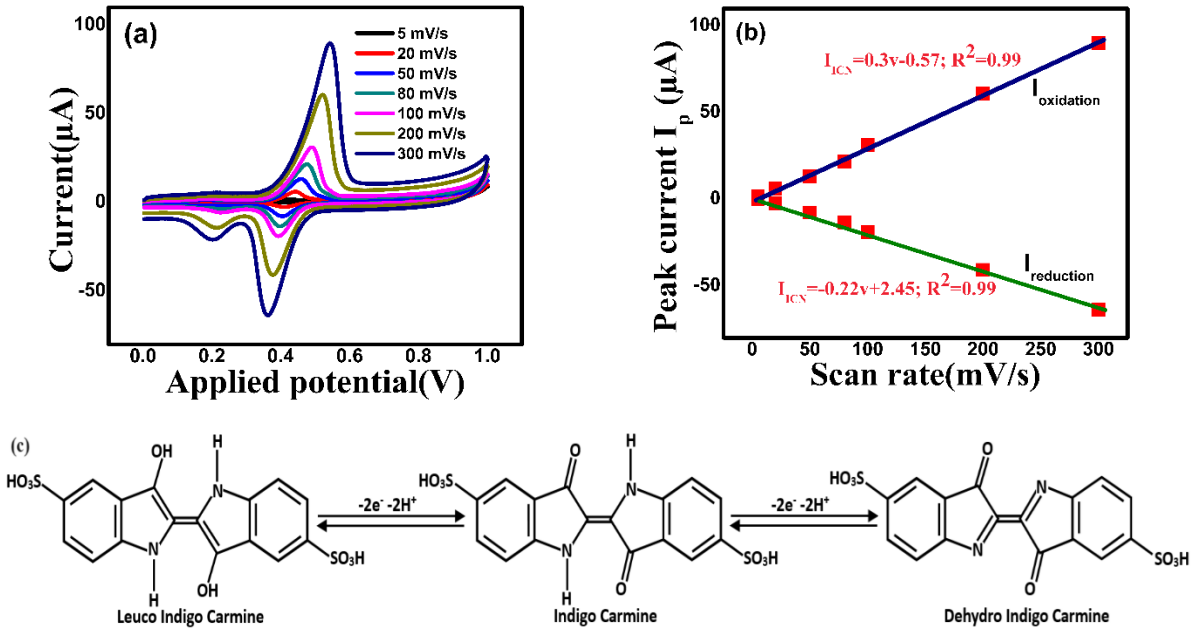

Fig. 4.11. (a) CV plots related to the detection of ICN with Y_2O_3@GPE in 0.1 M PBS for scan rate variation; (b) Linearity plot for I_p vs scan rate; (c) ICN redox behaviour.

$$I_{ICN} = 0.3v - 0.57;\ R^2 = 0.99 \tag{4.6}$$

$$I_{ICN} = -0.22v + 2.45;\ R^2 = 0.99 \tag{4.7}$$

It is found in Fig. 4.11. (a) that the gap between the Epa and Epc increases with the increasing scan rate, denoting a quasi-reversible reaction of the oxidation reduction pairs [14]. The reaction mechanism related to the ICN molecule upon the electrode surface may be something like one presented in Fig.4.11. (c). Being an electroactive colorant, ICN performs the reduction at the electrode surface to form Leuco indigo carmine and the oxidation to Dehydro indigo carmine [3]. Both of these processes happen via transfer of two electrons and two protons. The equation utilized to compute the quantity of electrons conveyed during the oxidation process [15], [16] is (2.7), as previously indicated in Section 2.5.6 of Chapter 2. The significance of every symbol employed therein is also elucidated in section 2.5.6. n was found to be 1.7251, and estimated as 2 later, which matches with the number of transferred electrons found from the reaction mechanism. It is comparable to the reports [14], [17]. The coefficient of charge transfer, α , was calculated to be 0.5. The surface concentration of ICN was calculated as 0.35 × 10^{-8} mole /cm^2, using (2.7) again. In addition, heterogeneous rate constant K_s of the reaction

was found to be 1.48 s^{-1}, applying Laviron's equation [18], [19], expressed in Eq. (2.9) in the Section 2.5.6 of Chapter 2.

4.5.6. Concentration variation

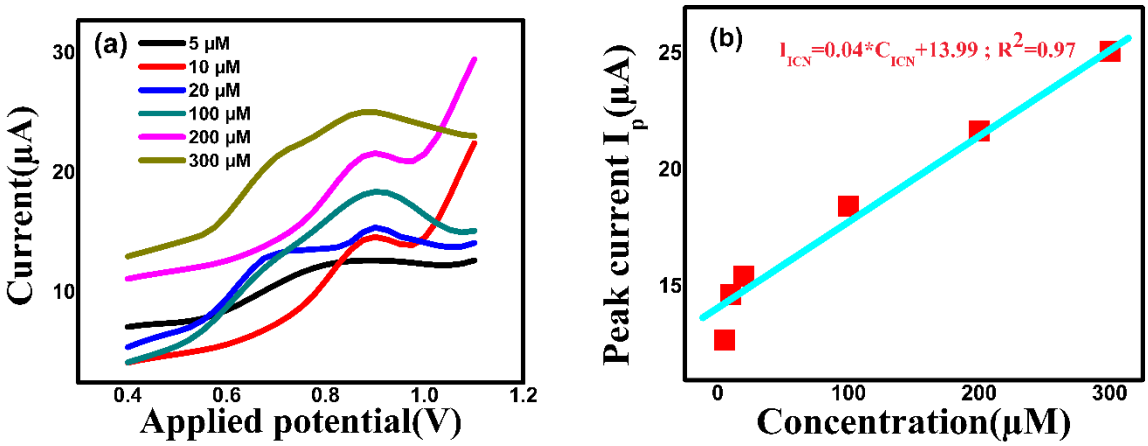

Fig. 4.12.(a) DPV plots related to the detection of ICN with Y_2O_3@GPE in 0.1 M PBS for varying concentrations; (b) Linearity plot for Ip vs concentration.

DPV provides better sensitivity than CV and yields clear peaks at lower concentration levels also [20], [21], [22]. In case of the DPV response of Y_2O_3@GPE for ICN detection, the proportional rise in Ip with the ICN concentration rise from 5µM to 300µM is depicted in Fig.4.12. (a). The regression equation associated to this feature is in (4.8). The corresponding calibration line is presented in Fig.4.12. (b).

$$I_{ICN} = 0.04C_{ICN} + 13.99;\ R^2 = 0.97 \tag{4.8}$$

I_{ICN} and C_{ICN} are representative of the highest current and corresponding concentration of ICN, respectively. The linear response pattern with rising ICN concentration proves the Y_2O_3@GPE to be capable for the quantitative ICN determination. The LOD and LOQ for ICN detection using this method were found 0.11 µM and 0.35 µM, respectively, considering (4.9) and (4.10).

$$LOD = 3\sigma/m \tag{4.9}$$

$$LOQ = 10\sigma/m \tag{4.10}$$

σ being the standard deviation of the I_p values for the lowest detected concentration and m being the slope of the calibration curve [14], [23], [24]. This LOD is found superior to the LOD of most of the reported articles. The LOD and the linear dynamic range having natural similarity are actually better with respect to other narrated works as found in Table 4.2.

4.5.7. Repeatability, reproducibility, and stability features

Repeatability, reproducibility, and stability are some key features considered for the judgement of an electrochemical sensor performance. DPV method under specific conditions were employed here for this purpose. The sensor underwent four periodic exposures named S1, S2,

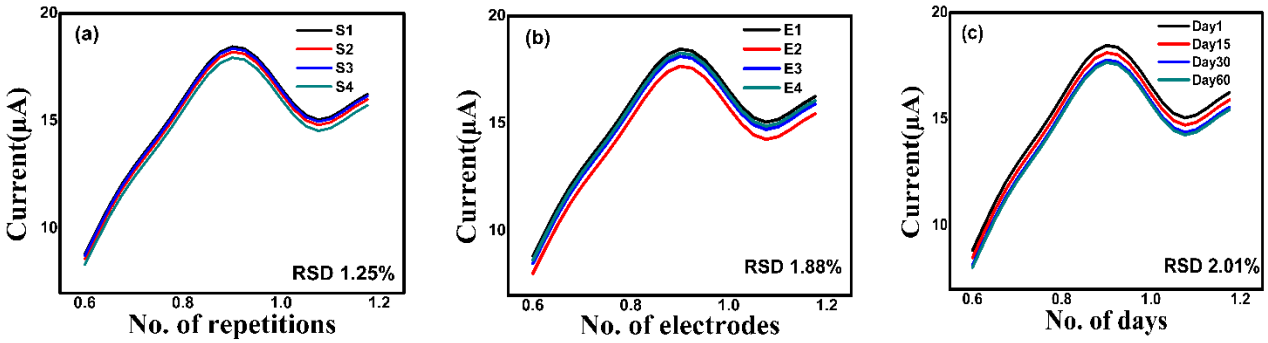

Fig. 4.13. Performance analysis DPV plots of Y_2O_3@GPE for ICN detection-(a) Repeatability; (b) Reproducibility; (c) Stability.

S3, and S4 to a 100µM ICN solution in 0.1 M PBS6, demonstrating splendid repeatability (RSD = 1.25%) in Fig.4.13. (a) . Under the same conditions, reproducibility was achieved with a low RSD of 1.88% over four electrodes (E1, E2, E3, and E4) as shown in Fig. 4.13. (b). The sensor maintained its stability for two months at room temperature, with not much significant loss in Ip (RSD 2.01%) on Day1, Day15, Day30, and Day60, which is visible in Fig.4.13. (c).

Table 4.2. Proposed Y_2O_3@GPE for detecting ICN compared to previous reports.

Methodology	Electrode material	Linear range (µM)	LOD (µM)	Ref.
CV	SPCE	0.5-100	0.19	[12]
DPV	SPCE	0.2-20	0.17	[12]
SWV	SPCE	0.7-10	0.34	[12]
CV	SPE	0.5-100	0.20	[13]
DPV	NBE/CPE	1-100	0.36	[14]
DPV	Poly (glutamic acid)/MWNT based paste electrode	5-50	0.36	[17]
DPV	**Y_2O_3@GPE**	**5-300**	**0.11**	**[This Work]**

4.5.8. Interference study

For selectivity testing purpose, the impacts of a number of interferents on the I_{pa} were monitored. Ions like K^+, Na^+, Cl^-, and some food colorants like Tartrazine (TZ), and Erythrosine were considered in this case. Introducing one interfering agent followed by the introduction of ICN, corresponding CV response were recorded and the same process was

followed for each interferent. The associated Bar diagram plot is illustrated in Fig. 4.14., where Y_2O_3@GPE responds negligibly to other interferents. These little fluctuations did not make the response cross the tolerance range of ±5%. A probable reason behind it may be the fact that ICN has a lower Epa where the oxidation of these interferants does not yet take place.

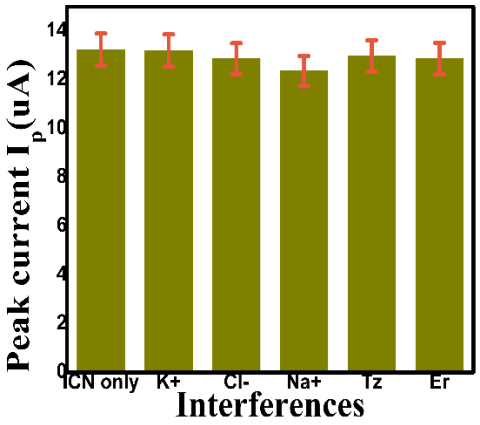

Fig. 4.14. Impact of interfering agents upon CV Ip responses of ICN at Y_2O_3@GPE.

4.5.9. PCA for ICN concentrations using Y_2O_3@GPE

The PCA machine learning technique, as delineated in Section 2.3.6 of Chapter 2, has been employed herein to analyse the Y_2O_3@GPE generated data of ICN solution.

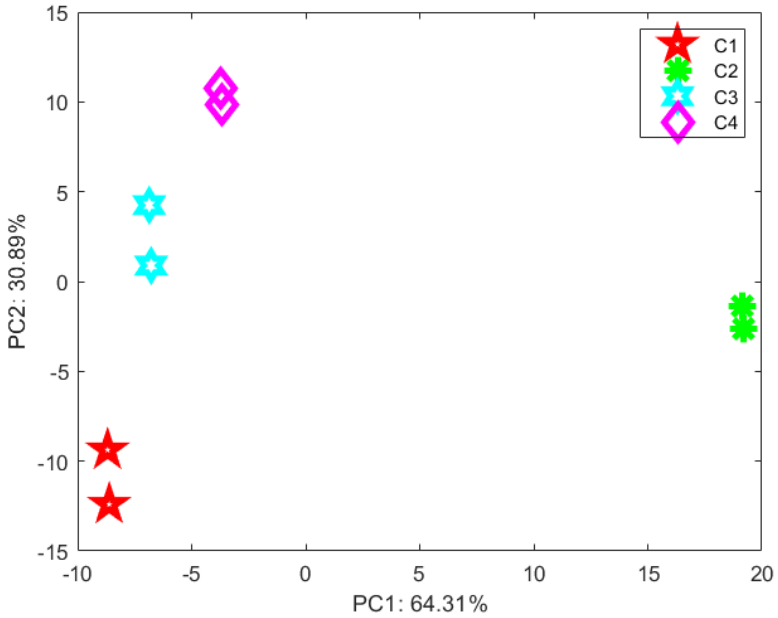

Fig. 4.15. PCA-a graphical representation to analyse the DPV data of ICN achieved by Y_2O_3@GPE.

Utilizing the DPV response curves for ICN concentrations (5µM, 10µM, 20µM, and 100µM denoted as C1, C2, C3, and C4, respectively) with Y_2O_3@GPE, this PCA tool is applied. Each

concentration undergoes three repetitions. The PCA plot, exhibiting successful data clustering, is depicted in Fig. 4.15, wherein all distinct concentrations are accurately distinguished. PC1 and PC2 account for 64.31% and 30.89% of the total variances, respectively. A notably high S.I. value of 71.31 is observed, indicating a distinct separation of classes within the dataset.

4.5.10. PLSR analysis for ICN using Y_2O_3@GPE

Four discrete concentrations of ICN (denoted as C1-C4) have undergone analysis via the PLSR method, elucidated previously in Section 2.3.7 of Chapter 2. For each concentration, the training and testing data are allocated in a ratio of 3:1. The prediction parameters outlined in Table 4.3 reveal that the average prediction accuracy for voltametric detection of ICN utilizing Y_2O_3@GPE stands at an impressive 100.15% using the PLSR tool. Additionally, the root mean square error of prediction (RMSEP) is recorded at 0.59, which is lower than the value of RMSEP obtained in case of CPE (0.98). This indicates that the modification via nanoparticles helps in reducing the RMSEP value and increases the efficiency.

Table 4.3. Comparison of actual and predicted ICN contents achieved via PLSR for Y_2O_3@GPE.

No. of samples	Actual ICN contents (µM)	Predicted ICN contents (µM)	Prediction accuracy (%)
1	5	5.2	96
2	10	9.8	102
3	20	19.7	101.5
4	100	98.9	101.1
Average prediction accuracy 100.15%			

4.5.11. Practical data analysis

As previously mentioned, practical application of the Y_2O_3@GPE was validated by employing it for the analysis of two types of candies popular in Indian market. Once purchased, these candies were ground using a mixer and grinder. 30ml of water was separately poured to 1 gm of each candy dust leading to the formation of three different homogeneous solutions after 30 minutes of sonication. After filtering these solutions using Whatman UNIFLO disposable sterile syringe filters (12.5 mm in radius, pore size 0.22µM), the filtered samples were sent through DPV analysis, applying the Standard Addition Method. The obtained results in Table 4.4, offered trustworthy outcomes, having the recovery rates of 96.25%-117.5% and Relative Standard Deviation (RSD) values of 1.49%-1.9%. These findings are the assurance that the developed Y_2O_3@GPE sensor is full of potentials for real-life practical applications.

Table 4.4. Determination of ICN in candies.

Sample	Spiking (µM)	Detected (µM)	Recovery [a] (%)	RSD [b] (%) (N=2)
Candy1	0	0	-	-
	10	11.75	117.5	1.49
	20	20.75	103.75	1.85
Candy2	0	2	-	
	10	13.5	115	1.55
	20	21.25	96.25	1.9

[a] Recovery = [(Detected-Diluted) (µM)]/Spiking (µM)

[b] R.S.D (%) = [100x Standard deviation]/ Mean

4.5.12. Comparative study for basic CPE and Y_2O_3@GPE: their performance parameters for detecting ICN

Table 4.5. presented here brief the performance indices of CPE and Y_2O_3@GPE for the voltametric ICN detection. Different parameter values clearly indicate that the modification of CPE with the Y_2O_3 nanoparticles increases its efficiency for detecting ICN.

Table 4.5. Comparison between CPE and Y_2O_3@GPE Performance to detect ICN.

Sl. No.	Parameter	CPE	Y_2O_3@GPE
1	Maximum oxidation peak current	4.94µA	13.2µA
2	R^2 (Scan rate)	0.98, 0.97	0.99, 0.99
3	R^2 (Concentration)	0.94	0.97
4	RSD(Repeatability)	2.97%	1.25%
5	RSD(Reproducibility)	4.2%	1.88%
6	RSD(Stability)	3.6%	2.01%
7	Stability span	30days	60days
8	Separability index (S.I.)	40.57	71.31
9	Prediction accuracy	83.65%	100.15%
10	LOD	0.83 µM	0.11µM
11	RMSEP	0.98	0.59

4.5.13. Reasons behind individual Detection of AMR and ICN, Though the Modifier Material (Y_2O_3 Nanoparticles) is Same

The Sections 3.4 and 3.5 of Chapter 3, and the Sections 4.4 and 4.5 of this chapter show that the same Y_2O_3 nanoparticle has been used in both cases for the modification of carbon paste

material to increase the efficiency of basic CPE. The lack of simultaneous detection of AMR and ICN on a Y_2O_3@GPE may be attributed to several factors. Here are some possible reasons:

a) Differential oxidation potentials: AMR and ICN are found having different oxidation potentials like 0.84V and 0.46V, respectively. If the electrochemical detection method employed is tailored to a specific potential range, it could singularly identify one of the artificial food colors, disregarding the other.

b) Electrode modification: The Y_2O_3 nanoparticles ingrained in the graphite paste electrode might selectively enhance the electrochemical response of one analyte over the other due to differences in their interaction with the modified electrode surface.

c) Interference from matrix components: The presence of other components in the food sample matrix might interfere with the simultaneous detection of AMR and ICN. It's essential to consider the complexity of the food matrix and optimize the electrochemical conditions to minimize interference from other substances.

d) Optimization of experimental parameters: Parameters such as scan rate, potential range, and electrolyte composition can significantly influence the electrochemical behaviour of analytes. The experimental conditions need to be carefully optimized to ensure the simultaneous detection of both artificial food colors.

e) Cross-contamination: If the electrode is not properly cleaned between measurements or if there is any carryover from one analysis to the next, it can lead to cross-contamination and affect the specificity of the detection.

f) Instrumental limitations: The instrumentation used for electrochemical detection may have limitations in terms of sensitivity or selectivity.

However, still some data were recorded considering the aqueous solution where AMR and ICN were in 1:1 ratio. Different potential ranges were studied and the responses obtained are shown below in Fig.4.16. (a-b).

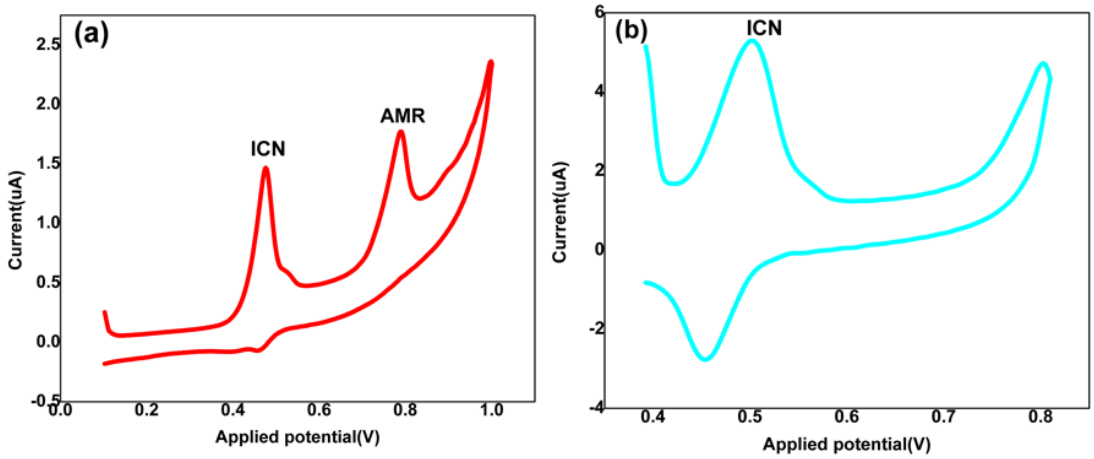

Fig. 4.16. Simultaneous detection of AMR and ICN using Y_2O_3@GPE (a) 0.1V-1V applied voltage range; (b) 0.38V-0.82V applied voltage.

The plot in Fig.4.16. (a) shows the appearance of both the oxidation peak currents, though both the peak current is seemed lower than the peak current obtained for individual oxidation. A potential ranging from 0.1V to 1V has been applied here. In case of Fig.4.16. (b), where the applied potential is 0.38-0.82 V, oxidation of ICN takes place at some increased potential of 0.51V, whereas no peak for AMR is got. These may be because of some reasons:

a) Incomplete detection: The oxidation potential of AMR is 0.84V, which is close to the upper limit of the selected voltage range (1V) for Fig.4.16. (a). This may result in incomplete detection or saturation of the signal for amaranth, making it difficult to accurately quantify higher concentrations.

b) Limited sensitivity for ICN: The oxidation potential of ICN is 0.46V, and if the lower limit of the voltage range (0.38V for Fig.4.16. (b)) is not sufficiently low, the sensitivity for detecting ICN may be compromised. Lowering the potential range may enhance the sensitivity for analytes with lower oxidation potentials.

c***) Overlap and interference:*** Interference between two molecules may make it challenging to distinguish and quantify each analyte separately.

d) Background current and noise: Operating at higher potentials may lead to increased background current and noise, affecting the signal-to-noise ratio and the overall sensitivity of the electrochemical detection method.

e) Signal saturation: The oxidation potential of amaranth is 0.8V. Operating within a 0.38-0.82V range might lead to signal saturation for amaranth, making it challenging to accurately measure higher concentrations. Saturation can result in a plateau in the current response, making it difficult to differentiate between different concentrations.

4.6 Conclusion

The current study focuses on synthesizing Y_2O_3 nanoparticles using a straightforward sol-gel method and subsequently utilizing them as a novel modifier to enhance the efficiency of Carbon Paste Electrode (CPE) for the voltammetric detection of ICN. This modified combination showed a synergistic effect for the ICN sensor. Under ideal conditions, the sensor exhibited excellent linearity (5–300µM) and an exceptionally low Limit of Detection (LOD) of 0.11µM, surpassing those reported for various electrodes in existing literature, thus ensuring outstanding sensitivity. This LOD value is significantly lower than the previously reported LOD of CPE-based ICN detection (0.83µM) in this chapter. The presented electrode demonstrated remarkable selectivity, reproducibility, repeatability, and stability for approximately two months. Furthermore, the proposed sensor was applied for detecting ICN in real samples such as various candies, commonly consumed by infants, revealing no significant interference in the matrix of real samples for ICN detection.

References

[1] E. G.-Segura, M. S.-Ríos, and A. C.-Cruz, “Sorption of indigo carmine by a fe-zeolitic tuff and carbonaceous material from pyrolyzed sewage sludge,” *Journal of Hazardous Materials*, vol. 170, no. 2–3, pp. 1227–1235, 2009, doi: 10.1016/j.jhazmat.2009.05.102.

[2] U. R. Lakshmi, V. C. Srivastava, I. D. Mall, and D. H. Lataye, “Rice husk ash as an effective adsorbent: Evaluation of adsorptive characteristics for Indigo Carmine dye,” *Journal of Environmental Management*, vol. 90, no. 2, pp. 710–720, 2009, doi: 10.1016/j.jenvman.2008.01.002.

[3] L. Kavieva and G. Ziyatdinova, “Voltammetric sensor based on SeO_2 nanoparticles and surfactants for indigo carmine determination,” *Sensors*, vol. 22, pp. 3224,2022.

[4] “Scientific Opinion on the re-evaluation of Indigo Carmine (E 132) as a food additive,” *European Food Safety Authority Journal*, vol. 12, no. 7. 2014. doi: 10.2903/j.efsa.2014.3768.

[5] K. S. Minioti, C. F. Sakellariou, and N. S. Thomaidis, "Determination of 13 synthetic food colorants in water-soluble foods by reversed-phase high-performance liquid chromatography coupled with diode-array detector," *Analytica Chimica Acta*, vol. 583, no. 1, pp. 103–110, 2007, doi: 10.1016/j.aca.2006.10.002.

[6] J. J. Berzas, J. Rodríguez Flores, M. J. Villaseñor Llerena, and N. Rodríguez Fariñas, "Spectrophotometric resolution of ternary mixtures of Tartrazine, Patent Blue V and Indigo Carmine in commercial products," *Analytica Chimica Acta*, vol. 391, no. 3, pp. 353–364, 1999, doi: 10.1016/S0003-2670(99)00215-9.

[7] C. F. Tsai, C. H. Kuo, and D. Y. C. Shih, "Determination of 20 synthetic dyes in chili powders and syrup-preserved fruits by liquid chromatography/tandem mass spectrometry," *Journal of Food and Drug Analysis*, vol. 23, no. 3, pp. 453–462, 2015, doi: 10.1016/j.jfda.2014.09.003.

[8] S. Publishers, "of Cl~ron~ufo~rupl~~~, 4," *Science (1979)*, vol. 1, no. I 987, pp. 437–444, 1987.

[9] H. M. Abu Shawish, N. A. Ghalwa, S. M. Saadeh, and H. El Harazeen, "Development of novel potentiometric sensors for determination of tartrazine dye concentration in foodstuff products," *Food Chemistry*, vol. 138, no. 1, pp. 126–132, 2013, doi: 10.1016/j.foodchem.2012.10.048.

[10] M. Arvand and N. Ghodsi, "Electrospun TiO_2 nanofiber/graphite oxide modified electrode for electrochemical detection of l-DOPA in human cerebrospinal fluid," *Sensors and Actuators B: Chemical*, vol. 204, pp. 393–401, 2014, doi: 10.1016/j.snb.2014.07.110.

[11] T. A. Silva, G. F. Pereira, O. Fatibello-Filho, K. I. B. Eguiluz, and G. R. Salazar-Banda, "Electroanalytical sensing of indigo carmine dye in water samples using a cathodically pretreated boron-doped diamond electrode," *Journal of Electroanalytical Chemistry*, vol. 769, pp. 28–34, 2016, doi: 10.1016/j.jelechem.2016.03.015.

[12] M. Díaz-González, C. Fernández-Sánchez, and A. Costa-García, "Comparative voltammetric behavior of indigo carmine at screenprinted carbon electrodes," *Electroanalysis*, vol. 14, no. 10, pp. 665–670, 2002, doi: 10.1002/1521-4109(200205)14:10<665::AID-ELAN665>3.0.CO;2-C.

[13] M. J. Bengoechea Álvarez, M. T. Fernández Abedul, and A. Costa García, "Flow amperometric detection of indigo for enzyme-linked immunosorbent assays with use of screen-printed electrodes," *Analytica Chimica Acta*, vol. 462, no. 1, pp. 31–37, 2002, doi: 10.1016/S0003-2670(02)00310-0.

[14] M. Arvand, M. Saberi, M. S. Ardaki, and A. Mohammadi, "Mediated electrochemical method for the determination of indigo carmine levels in food products," *Talanta*, vol. 173, no. February, pp. 60–68, 2017, doi: 10.1016/j.talanta.2017.05.062.

[15] S. Nag, D. Das, H. Naskar, B. Tudu, R. Bandyopadhyay, and R. Banerjee Roy, "Detection of metanil yellow adulteration in turmeric powder using nano nickel cobalt oxide modified graphite electrode," *IEEE Sensors Journal*, vol. 22, no. 13, pp. 12515–12521, 2022, doi: 10.1109/JSEN.2022.3178768.

[16] A. H. M. T. Ahmed *et al.*, "Electrochemical sensor based on molecularly imprinted polymer embedded graphite electrode for detecting curcumin," *Sensors and Actuators A: Physical*, vol. 344, no. June, p. 113748, 2022, doi: 10.1016/j.sna.2022.113748.

[17] N. Hareesha, J. G. Manjunatha, B. M. Amrutha, P. A. Pushpanjali, M. M. Charithra, and N. Prinith Subbaiah, "Electrochemical Analysis of Indigo Carmine in Food and Water Samples Using a Poly(Glutamic Acid) Layered Multi-walled Carbon Nanotube Paste Electrode," *Journal of Electronic Materials*, vol. 50, no. 3, pp. 1230–1238, 2021, doi: 10.1007/s11664-020-08616-7.

[18] E. Laviron, "General expression of the linear potential sweep voltammogram in the case of diffusionless electrochemical systems," *Journal of Electroanalytical Chemistry*, vol. 101, no. 1, pp. 19–28, 1979, doi: 10.1016/S0022-0728(79)80075-3.

[19] E. Laviron, "Adsorption, autoinhibition and autocatalysis in polarography and in linear potential sweep voltammetry," *Journal of Electroanalytical Chemistry*, vol. 52, no. 3, pp. 355–393, 1974, doi: 10.1016/S0022-0728(74)80448-1.

[20] H. Naskar, S. Pradhan, B. Ghatak, S. Biswas, B. Tudu, and R. Bandyopadhyay, "Electrochemical detection of capsaicin in chili pepper using molecular imprinted poly β-cyclodextrin embedded graphite (MIP-β-CD@G) electrode," *IEEE Sensors Journal*, vol. 21, no. 16, pp. 17657–17664, 2021, doi: 10.1109/JSEN.2021.3083527.

[21] T. Nandy Chatterjee *et al.*, "Detection of theaflavins in black tea using a molecular imprinted polyacrylamide-graphite nanocomposite electrode," *Sensors and Actuators B: Chemical*, vol. 246, pp. 840–847, 2017, doi: 10.1016/j.snb.2017.02.139.

[22] T. N. Chatterjee *et al.*, "Molecular imprinted polymer based electrode for sensing catechin (+C) in green tea," *IEEE Sensors Journal*, vol. 18, no. 6, pp. 2236–2244, 2018, doi: 10.1109/JSEN.2018.2791661.

[23] S. Biswas, R. Das, M. Basu, R. Bandyopadhyay, and P. Pramanik, "Synthesis of carbon nanoparticle embedded graphene for sensitive and selective determination of dopamine and ascorbic acid in biological fluids," *RSC Advances*, vol. 6, no. 103, pp. 100723–100731, 2016, doi: 10.1039/c6ra16774h.

[24] D. Das *et al.*, "Titanium Oxide nanocubes embedded molecularly imprinted polymer-based electrode for selective detection of caffeine in green tea," *IEEE Sensors Journal*, vol. 20, no. 12, pp. 6240–6247, 2020, doi: 10.1109/JSEN.2020.2972773.

Chapter 5

Conclusion and Future Scopes

This chapter elucidates the creation and application of a carbon paste electrode (CPE), followed by the enhancement of a graphite electrode with CuO nanoparticles, and Y_2O_3 nanoparticles for the precise detections of malachite green (MG), in fish fillets and pond water; amaranth (AMR), and indigo carmine (ICN) in candy products, respectively. The summary of findings along with recommendation and future scopes have been presented.

List of Sections

5.1. Introduction

First and foremost, the thesis presents a unique paradigm for detecting various artificial food colors through their voltammetric responses. The synthetic food colors are a powerful substitute for the natural sources of coloring agents. As the over dose of these artificial colors cause a number of diseases in human bodies, the proper monitoring of the quantity of daily intake of these colors are much needed. It is in this background; this thesis work has been taken up to develop a few electrodes specific for a few artificial food colorants. Some metal oxide modified electrodes are developed and studied in the previous chapters.

This dissertation encapsulates the journey undertaken in the development of some budget friendly electrochemical sensors for the detection of artificial food colorants. It synthesizes the key findings, throws light on the innovative contributions made to the field, and discusses the broader implications of these advancements. Revisiting the research objectives and examining how they have been achieved, this chapter underscores the significance of the developed sensors in enhancing food safety and quality assurance. Moreover, it prepares the stage for future research directions also, highlighting the potential for these technologies to revolutionize food monitoring practises.

5.2. Summary of findings

Our limited literature survey yielded a number of studies in which the individual electrochemical detection of malachite green (MG), amaranth (AMR), and indigo carmine (ICN) have been pursued. The results obtained in this thesis work are briefed in Table 5.1. The detection limit has considerably been improved in each case when compared to the reports obtained earlier. It may be observed that the modification of CPE with nanoparticles for the development of all the three electrodes resulted in a lower value of LOD than some of the previous electrochemical methods.

The findings of the thesis work are summarized below.

a) CPE is modified with CuO nanoparticles for the detection of MG molecule. Sol-gel method is applied for this synthesis of nanoparticles. The electrochemical characteristics of this electrode with the results in real samples have been presented in Chapter 2 of this thesis.

b) For the sensitive and selective determination of AMR in children's consumable candies, Y_2O_3 nanoparticles have been ingrained in CPE. Y_2O_3 nanoparticles also have been synthesised

in-house using sol-gel method. Overall analytical performance of this electrode has been presented in Chapter 3 of this thesis.

c) A Y_2O_3 embedded graphite paste electrode is developed for the determination of ICN in candies. The materials synthesis, characterization and electrochemical responses are discussed in chapter 4 of this thesis. Besides, the reasons behind the individual detection of AMR and ICN using the same nanoparticles modified graphite paste electrode (Y_2O_3@GPE) are also discussed.

Table 5.1. Brief outline of the developed electrodes performance.

Molecule	Electrode	Method	Linearity (µM)	LOD	Repeatability (% RSD)	Reproducibility (%RSD)	Refs.
Malachite Green (MG)	CuO@GPE	DPV	1-1000	0.18 µM	2.09%-2.18%	2.03%-2.21%	[1]
Amaranth (AMR)	Y_2O_3@GPE	DPV	0.05-100	3.6 nM	1.47%	1.99%	[2]
Indigo Carmine (ICN)	Y_2O_3@GPE	DPV	5-300	0.11 µM	1.25%	1.88%	[3]

5.3. Recommendations

This approach can be useful for the food and beverage industry, quality control laboratories, healthcare, educational institutions, and research laboratories because of the following points:

a) The developed electrodes will be of great help in order to replace the costly existing instruments. All the materials used are easily accessible and budget friendly.

b) The simple process of synthesis and the ease of response- recovery property of the electrodes makes them very convenient and useful for real-time applications.

c) Three different sensors have been designed and fabricated as a part of this thesis work to assess the presence and level of significant artificial food colors -Malachite Green in fish fillets and Amaranth and Indigo Carmine in different candies.

5.4. Future scopes

Further improvements on the proposed sensing methodologies are briefed below for extending the research in the same domain. These are listed as follows:

- Further improvement of these electrodes: may be implementation of the molecularly imprinted polymer (MIP) technology.

- Chance of probable cost cutting if the data collection and processing system is designed in-house, replacing the costly Autolab instrument.
- HPLC reference data may be taken up for correlation study.
- In order to design the prediction model in order to quantify respective synthetic food colorants, advanced algorithms like deep learning, convolution neural networks can be applied for better accuracy.
- In this thesis, sensors specific only to MG, AMR, and ICN have been designed. Other different significant food colors contributing to the maximum health hazards can be developed in a similar way.

5.5. Conclusion

In conclusion, this research has successfully developed and validated novel electrochemical sensors for the precise detection of a few artificial food colorants. Through rigorous experimentation and analysis, these sensors have demonstrated high sensitivity, selectivity, and reproducibility, proving them as valuable tools for ensuring food safety and quality. The innovative approaches and methodologies introduced in this study not only enhance our understanding of voltammetric responses of food dyes, but also pave the way for future advancements in food monitoring technologies. The practical applications of these findings are large, promising notable contributions to public health and regulatory standards.

References

[1] S. Dasgupta *et al.*, "Electrochemical sensor based on CuO nanoparticles-modified graphite electrode for the detection of malachite green," *Nano Life*, vol. 14, no. 1, pp. 1–12, 2024, doi: 10.1142/S1793984423500150.

[2] S. Dasgupta, A. H. M. T. Ahmed, I. Bhattacharjee, S. Firdoushi, and D. Biswas, "Crafting a graphite electrode with embedded Y_2O_3 nanoparticles for the electrochemical detection of amaranth in candies," *IEEE Sensors Journal*, vol. 24, no.13, pp. 20750-20757, 2024. [DOI: 10.1109/JSEN.2024.3400317].

[3] S. Dasgupta et al., "Electrochemical detection of indigo carmine in candies using Y_2O_3 nanoparticles infused graphite electrode," *Journal of Food Composition and Analysis*, vol. 135, 106626, pp. 1-9, 2024. [DOI: https://doi.org/10.1016/j.jfca.2024.106626]

Sambita Dasgupta
22/05/2024

Chapter 5: Conclusion and Future Scopes